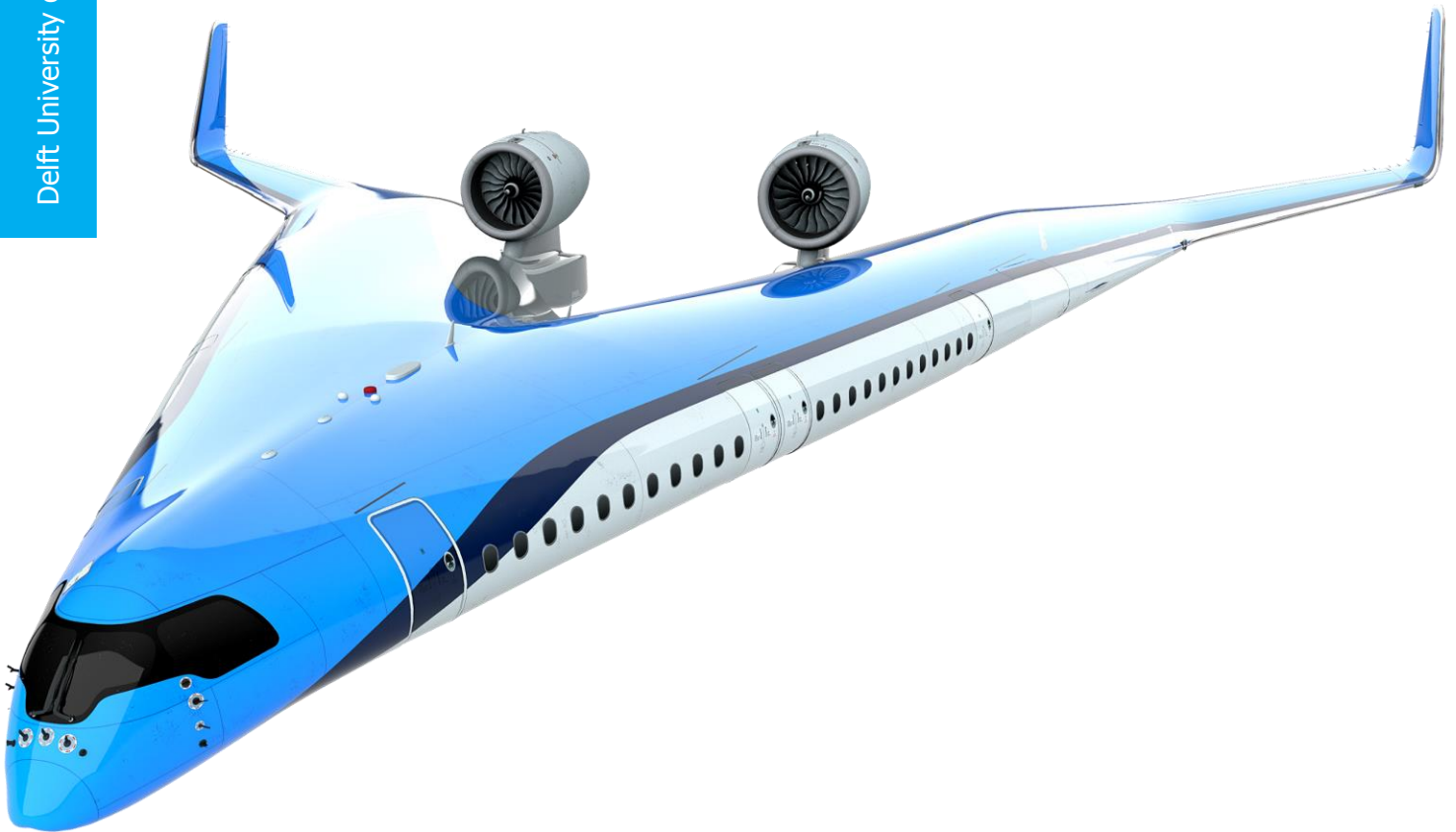


Improving the Flying V Directional Control Power by the Implementation of Split Flaps

Thesis Report

S. Nolet

Delft University of Technology



Improving the Flying V Directional Control Power by the Implementation of Split Flaps

Thesis Report

by

S. Nolet

to obtain the degree of Master of Science
at the Delft University of Technology,
to be defended publicly on Thursday April 7, 2022 at 9:00 AM.

Student number:	4535677	
Project duration:	May 18, 2021 – April 7, 2022	
Thesis committee:	Dr. ir. R. Vos,	TU Delft, supervisor
	Prof. dr. ir. L. L. M. Veldhuis,	TU Delft
	Ir. O. Stroosma,	TU Delft
	Ir. M. T. H. Brown,	TU Delft

*An electronic version of this thesis is available at <http://repository.tudelft.nl/>
Front page figure is taken from <https://www.tudelft.nl/lr/flying-v>*

Preface

This thesis report discusses the experimental investigation in adding split flaps onto the Flying V. The study aims to identify the aerodynamic behaviour of such flaps for improving the directional control of the Flying V. It comprises explanation of the performed wind tunnel tests and post-processing calculations.

The thesis is in fulfilment of my Master's degree at the faculty of Aerospace Engineering, at the Delft University of Technology. I would like to thank my supervisor Roelof Vos for this thesis opportunity, as well as for his insights and feedback. I would additionally like to thank Malcom Brown, for his valuable help during the preparation and setup of the wind tunnel experiments. Finally, I would like to thank my girlfriend, my family and my friends for their unlimited support.

*S. Nolet
Delft, March 2022*

Executive summary

This thesis is performed with the aim to investigate whether split flaps can be a feasible solution for increasing the Flying V directional control power. In order to do so, a set of wind tunnel experiments have been concluded with a 4.6% half wing model in the Open-Jet-Facility at the Delft University of Technology. Here, several split flap geometries have been tested to fully establish their behaviour in terms of yaw and other parameters of interest. Additionally, calculations have been performed to provide an adequate split flap design for certification of the lateral-directional specifications from CS-25.

From the wind tunnel experiments, it was found that split flaps on the outboard wing section can effectively increase the directional control power over angles of attack between 0° and 30° . However, yaw control is lost when $\alpha \leq -5^\circ$ due to lower wing stall. This makes the lower split flap lose pressure, while the upper split flap produces a negative sideforce, negating yaw creation. The maximum decrease in split flap effectiveness is found around $\alpha = 17.5^\circ$, where a leading edge vortex is present over the outboard wing. This decreases pressure over the upper split flap, resulting in a effectiveness decrease of around 41%. As the effectiveness does not decrease further, split flaps can be continuously effective at higher angles of attack when compared to the winglet rudders. The low pressure on the upper flap also causes large adverse coupled moments in pitch and roll. The effect of split flaps on the yawing moment is found to be linear with deflection angle, where their effect on other aerodynamic properties is found to be more non-linear.

The deflection of outboard split flaps do not have a significant interference effect on rudder yaw power, but can have some interference effects on adjacent main wing control surfaces. Differential deflection between the upper and lower flap has been shown to potentially decrease coupling in pitch and roll, while maintaining a certain level of yaw power, which is especially applicable for $\alpha < 15$. In this region, the split flaps can also be globally rotated trailing edge down to mitigate adverse coupled moments while beneficially increasing the total created yaw. With global rotation, the split flaps can be used in a dual functionality as both yaw effector and roll/pitch effector. A combination of low to moderate split deflection angles and trailing edge down rotations are required to do this effectively.

It was found that sustaining a steady heading sideslip during crosswind conditions, as well as a 30° coordinated turn into the operative engine, were the most demanding certification specification in terms of directional control. A maximum additional yaw coefficient of $2.4113e-3$ has to be provided by the split flaps. Designs with a maximum deflection angle above 30° are deemed feasible, as this would maximally require only the replacement of the current CS3 surfaces. When a maximum deflection of 60° is set by the designer, a sub-scale split flap width of 111.87 mm is needed, which translates to a full-scale split flap of 2.431 m. Based on the sensitivity analysis and projected Reynolds effects, this is considered a conservative design for the full-scale Flying V. At $\alpha = 0^\circ$, the recommended geometry is projected to increase the maximum directional control power of the Flying V by 38.1%. At $\alpha = 27.5^\circ$, the maximum directional control power can even be increased by 85.5%. Both increases come at the cost of a significant drag increase.

Contents

Executive Summary	ii
List of Figures	v
List of Tables	viii
Nomenclature	ix
1 Introduction	1
2 Background	3
2.1 Flying V	3
2.2 Split flaps	4
2.3 Lateral-Directional Control Requirements	6
2.3.1 Sign convention	6
2.3.2 CS 25.143: Controllability and Manoeuvrability	7
2.3.3 CS 25.147: Directional and lateral control	8
2.3.4 CS 25.161: Trim	9
2.4 Research objective and questions.	10
3 Research Methodology	11
3.1 Split flap design	11
3.1.1 Split flap model design rules	11
3.1.2 Estimation of split flap performance	13
3.1.3 Preliminary split flap sizing	14
3.2 Wind tunnel model and measurements	15
3.2.1 Open Jet Facility	15
3.2.2 Flying V model and setup	16
3.2.3 Measurements and processing	17
3.2.4 Test matrix	18
3.2.5 Corrections	19
3.2.6 Uncertainty analysis.	19
3.3 Split flap conceptual sizing procedure.	20
3.3.1 Flight mechanics model.	20
3.3.2 Reynolds number scaling.	24
3.3.3 Sizing calculations	24
3.3.4 Sensitivity analysis.	25
4 Verification and Validation	27
4.1 Short term repeatability	27
4.2 Long term repeatability	28
4.3 Tuft photographs	30
4.4 Verification of the preliminary design calculations.	30
4.5 Validity of split flap model placement	31
4.6 Validation of the flight mechanics model	32

5	Results and Discussion	35
5.1	General effect of split flaps on aerodynamics	35
5.1.1	Effect on aerodynamic forces	35
5.1.2	Effect on aerodynamic moments	41
5.1.3	Coupling effects and linearity of split flap deflection	43
5.2	Effect of split flaps on directional control in detail	45
5.2.1	Comparison with winglet rudders	45
5.2.2	Effect of split flap size	45
5.2.3	Split flap yaw control derivatives	47
5.3	Effect of split flaps on surrounding control surfaces	49
5.3.1	Effect of split flaps on rudder effectiveness	49
5.3.2	Effect of split flaps on CS2 effectiveness	50
5.4	Mitigating adverse split flap effects	51
5.4.1	Differential deflection between upper and lower flap	52
5.4.2	Global rotation of mutual deflected split flaps	54
6	Split flap conceptual sizing	57
6.1	Required split flap yawing moment.	57
6.1.1	Trim calculations	57
6.1.2	Linear simulations	59
6.1.3	Sensitivity analysis.	61
6.2	Split flap sizing.	63
6.2.1	Recommended split flap geometry	63
6.2.2	Varying maximum split flap deflection	64
6.2.3	Projected final split flap performance	66
7	Conclusion and Recommendations	67
7.1	Conclusions.	67
7.2	Recommendations.	68
	Bibliography	70
A	Test matrix summary	73

List of Figures

2.1	Isometric view of the current Flying V design [8]	3
2.2	Sketch of the Flying V planform by Faggiano [9]	4
2.3	Northrop Grumman B-2 Spirit during landing [12]	5
2.4	Illustration of a split flap cross section [14]	6
2.5	Directional sign convention	7
2.6	Sideslip sign convention	7
2.7	Lateral sign convention	7
2.8	Illustration of a OEI situation	8
3.1	Top view of the left wing wind tunnel model including highlighted detail on the outboard wing section.	12
3.2	Section cut B-B from figure 3.1, including visualisation of the split flap design	13
3.3	Frontal area drag coefficients of wedges and cones as a function of their half-vertex angle [21].	14
3.4	Decrease of coefficient with their height to span ratio [21].	14
3.5	Illustration of the created forces by a split flap on the outboard wing	15
3.6	Top-view of the Flying V model including outboard detail view highlighting the areas of SF10, SF15, SF20 and SF22.	16
3.7	Schematic of the OJF facility [25]	16
3.8	Side and back view of the wind tunnel test setup	17
3.9	Example of the trim input of δ_{CS3} per iteration i .	23
4.1	Errorbar plot of the measurement uncertainty for a clean wing and a wing including split flap. Uncertainty is calculated using a 95% confidence interval.	27
4.2	Lift coefficient repeatability. Errorbars are included with a 95% confidence interval.	28
4.3	Drag polar repeatability. Errorbars are included with a 95% confidence interval.	28
4.4	Illustration of difference in setup mounting angle	29
4.5	Repeatability of the calculated absolute C_n between the current research and the research by Johnson. Errorbars are included with a 95% confidence interval.	29
4.6	Repeatability of the calculated ΔC_n between the current research and the research by Johnson. Errorbars are included with a 95% confidence interval.	29
4.7	Repeatability of ΔC_n between wind tunnel campaigns. Errorbars are included with a 95% confidence interval.	30
4.8	Comparison of the half-wing aerodynamic coefficients, with and without the implementation of yarn tufts.	31
4.9	Comparison of ΔC_n calculations (according to section 3.1.2) versus test measurements. All results are shown for $\alpha = 0^\circ$. Errorbars are included with a 95% confidence interval.	31
4.10	Top-side visualisation of split flap cross section in normal condition	32
4.11	Top-side visualisation of split flap cross section for verification	32
4.12	Errorbar plot of the measurement uncertainty for the regular and verification runs. Uncertainty is calculated using a 95% confidence interval.	33

4.13 Comparison of the roll simulation for regulation CS 25.147(d)	34
5.1 Lift coefficient behaviour of SF15	36
5.2 Tuft image of the outboard wing lower surface at $\alpha = 0^\circ$, including SF15 with $\delta_{sf} = 40^\circ$ outlined in green.	37
5.3 Tuft image of the outboard wing lower surface at $\alpha = -5^\circ$, including SF15 with $\delta_{sf} = 40^\circ$ outlined in green.	37
5.4 Depiction of vortex separation line at $\alpha = 15^\circ$. Adapted from Viet [26].	37
5.5 Tuft image of the outboard wing upper surface at $\alpha = 10^\circ$, including SF15 with $\delta_{sf} = 40^\circ$ outlined in green.	38
5.6 Tuft image of the outboard wing upper surface at $\alpha = 15^\circ$, including SF15 with $\delta_{sf} = 40^\circ$ outlined in green.	38
5.7 Tuft image of the outboard wing upper surface at $\alpha = 25^\circ$, including SF15 with $\delta_{sf} = 40^\circ$ outlined in green.	39
5.8 Drag coefficient behaviour of SF15	39
5.9 Tuft image of the outboard wing lower surface at $\alpha = -10^\circ$, including SF15 with $\delta_{sf} = 40^\circ$ outlined in green.	40
5.10 Total drag coefficient increase for several SF15 deflections	40
5.11 Sideforce coefficient behaviour of SF15	41
5.12 Pitching moment coefficient behaviour of SF15	42
5.13 Rolling moment coefficient behaviour of SF15	42
5.14 Yawing moment coefficient behaviour of SF15	43
5.15 δ_{sf} vs ΔC_L	44
5.16 δ_{sf} vs ΔC_D	44
5.17 δ_{sf} vs ΔC_Y	44
5.18 δ_{sf} vs ΔC_m	44
5.19 δ_{sf} vs ΔC_l	45
5.20 δ_{sf} vs ΔC_n	45
5.21 Yawing moment comparison of SF15 and winglet rudders	46
5.22 ΔC_n behaviour of SF10	46
5.23 ΔC_n behaviour of SF20	46
5.24 Normalised yawing moment $\Delta C_n/S_{sf}$, including 99% confidence error bars.	47
5.25 Normalised drag force $\Delta C_D/S_{sf}$, including 99% confidence error bars.	47
5.26 Example of yaw effectiveness of SF20 including linear fit. Error bars are included with a 99% confidence interval.	48
5.27 Linear split flap yaw control derivatives	48
5.28 R^2 values of the linear split flap yaw control derivatives from figure 5.27.	48
5.29 Isolated ΔC_n due to varying rudder deflection for several configurations at $\alpha = 0, 5, 10, 15, 20$ and 25 degrees.	50
5.30 Isolated ΔC_m due to varying CS2 deflection for several configurations at $\alpha = 0, 5, 10, 15, 20$ and 25 degrees.	51
5.31 Isolated ΔC_l due to varying CS2 deflection for several configurations at $\alpha = 0, 5, 10, 15, 20$ and 25 degrees.	52
5.32 Aerodynamic moment coefficients behaviour for SF15 with several differential deflection angles between the upper and lower split flap.	53
5.33 Pitch-to-yaw and roll-to-yaw behaviour for SF15 with several differential deflection angles between the upper and lower split flap.	54
5.34 Aerodynamic moment coefficients behaviour for SF22 at $\delta_{sf} = 40$ for several global CS3 deflection angles.	55

5.35 Isolated CS3 influence on C_l for SF22 configuration at $\delta_{sf} = 20^\circ$, compared to the clean wing configuration.	56
5.36 Isolated CS3 influence on C_l for SF22 configuration at $\delta_{sf} = 40^\circ$, compared to the clean wing configuration.	56
5.37 Isolated CS3 influence on C_l for SF22 configuration at $\delta_{sf} = 60^\circ$, compared to the clean wing configuration.	56
6.1 OEI bank to bank manoeuvre with full aileron input	60
6.2 OEI bank to bank manoeuvre with full aileron input and split flap input	60
6.3 OEI bank to bank manoeuvre with 60% aileron input and no split flap input	60
6.4 OEI yaw manoeuvre with the operative engine	61
6.5 OEI yaw manoeuvre with the operative engine, including split flap input	61
6.6 OEI yaw manoeuvre against the operative engine	62
6.7 OEI yaw manoeuvre against the operative engine, including split flap	62
6.8 Sensitivity of stability derivatives for the coordinated turn design case	63
6.9 Sensitivity of control derivatives for the coordinated turn design case	63
6.10 Sensitivity of stability derivatives for the steady heading sideslip design case	63
6.11 Sensitivity of control derivatives for the steady heading sideslip design case	63
6.12 Graphic of the final split flap geometry ($b_{sf} = 111.87\text{mm}$) on the Flying V model, including an outboard detail. The surfaces in red represent the split flaps. The left wing split flap has been deflected to $\delta_{sf} = 60^\circ$	65
6.13 Maximum split flap deflection angle versus required (sub-scale) split flap width, for a required $C_{n_{sf}}$ of $2.4113\text{e-}3$ at $\alpha = 11.54^\circ$	65
6.14 Projected final split flap yaw power in comparison with the winglet rudders	66
6.15 Projected final split flap drag penalty in comparison with the winglet rudders	66

List of Tables

2.1	CS 25.143(h) manoeuvre specifications [20]	7
3.1	Summary of each tested requirement, including way of testing and settings.	25
4.1	Maximum uncertainty values found from figure 4.1.	28
4.2	Verification of trim calculations for regulation CS 25.147(c)	33
5.1	Total surface areas of the split flaps (summation of upper and lower surface area) in mm ² .	46
5.2	$C_{n_{\delta_{sf}}}$ per configuration and its maximum decrease	48
6.1	CS 25.143(h): 30° coordinated turn	57
6.2	CS 25.147(c): 20° banked turn	58
6.3	CS 25.161(b): lateral and directional trim in steady heading sideslip	58
6.4	CS 25.161(d): lateral and directional trim in OEI situation	59
6.5	Final sizing summary for $\delta_{sf_{max}} = 60^\circ$	64
A.1	Summary of the test matrix used throughout the wind tunnel campaigns	74

Nomenclature

Symbols

A	=	wing aspect ratio [-]
b_{ref}	=	aircraft reference span [m]
b_{sf}	=	split flap width [m]
\bar{c}	=	mean aerodynamic chord [m]
C_D	=	drag coefficient [-]
$C_{D\cdot}$	=	drag coefficient with respect to frontal area [-]
C_L	=	lift coefficient [-]
$C_{L\alpha}$	=	lift curve slope [deg^{-1}]
C_l	=	rolling moment coefficient [-]
C_{lp}	=	derivative of rolling moment coefficient with respect to roll rate [-]
C_{lr}	=	derivative of rolling moment coefficient with respect to yaw rate [-]
$C_{l\beta}$	=	derivative of rolling moment coefficient with respect to sideslip angle [-]
$C_{l\delta_{CS1}}$	=	derivative of rolling moment coefficient with respect to CS1 deflection [-]
$C_{l\delta_{CS2}}$	=	derivative of rolling moment coefficient with respect to CS2 deflection [-]
$C_{l\delta_{CS3}}$	=	derivative of rolling moment coefficient with respect to CS3 deflection [-]
$C_{l\delta_r}$	=	derivative of rolling moment coefficient with respect to rudder deflection [-]
C_m	=	pitching moment coefficient [-]
C_n	=	yawing moment coefficient [-]
$C_{n_{asym}}$	=	yawing moment coefficient due to asymmetric thrust [-]
$C_{n_{OEI}}$	=	yawing moment coefficient due to One-Engine-Inoperative [-]
C_{np}	=	derivative of yawing moment coefficient with respect to roll rate [-]
C_{nr}	=	derivative of yawing moment coefficient with respect to yaw rate [-]
$C_{n_{sf}}$	=	yawing moment coefficient due to split flaps [-]
$C_{n\beta}$	=	derivative of yawing moment coefficient with respect to sideslip angle [-]
$C_{n\delta_{CS1}}$	=	derivative of yawing moment coefficient with respect to CS1 deflection [-]
$C_{n\delta_{CS2}}$	=	derivative of yawing moment coefficient with respect to CS2 deflection [-]
$C_{n\delta_{CS3}}$	=	derivative of yawing moment coefficient with respect to CS3 deflection [-]
$C_{n\delta_r}$	=	derivative of yawing moment coefficient with respect to rudder deflection [-]
$C_{n\delta_{sf}}$	=	derivative of yawing moment coefficient with respect to split flap deflection [-]
C_Y	=	sideforce coefficient [-]
C_{Yp}	=	derivative of sideforce moment coefficient with respect to roll rate [-]
C_{Yr}	=	derivative of sideforce moment coefficient with respect to yaw rate [-]
$C_{Y\beta}$	=	derivative of sideforce moment coefficient with respect to sideslip angle [-]
$C_{Y\delta_{CS1}}$	=	derivative of sideforce moment coefficient with respect to CS1 deflection [-]
$C_{Y\delta_{CS2}}$	=	derivative of sideforce moment coefficient with respect to CS2 deflection [-]
$C_{Y\delta_{CS3}}$	=	derivative of sideforce moment coefficient with respect to CS3 deflection [-]
$C_{Y\delta_r}$	=	derivative of sideforce moment coefficient with respect to rudder deflection [-]
D	=	drag force [N]
D_b	=	non-dimensional differential operator for asymmetric motions [-]

F_x	=	force in x direction [N]
F_y	=	force in y direction [N]
F_z	=	force in z direction [N]
g_0	=	gravitational acceleration [m/s ²]
K_x	=	non-dimensional radius of gyration about the X-axis [-]
K_z	=	non-dimensional radius of gyration about the Z-axis [-]
K_{xz}	=	non-dimensional product of inertia [-]
I	=	rolling moment [Nm]
L	=	lift force [N]
m	=	pitching moment [Nm]
M_x	=	moment in x direction [Nm]
M_y	=	moment in y direction [Nm]
M_z	=	moment in z direction [Nm]
n	=	sample size [-]
n	=	yawing moment [Nm]
p	=	roll rate [s ⁻¹]
q	=	dynamic pressure [Pa]
r	=	yaw rate [s ⁻¹]
R^2	=	coefficient of determination [-]
S_{ref}	=	aircraft reference area [m ²]
S_{sf}	=	split flap surface area [m ²]
S_f	=	frontal area [m ²]
t_{n-1}	=	t-factor related to sample size n [-]
T	=	thrust force [N]
u	=	velocity in x direction [m/s]
v	=	velocity in y direction [m/s]
V	=	velocity [m/s]
V_{SR_1}	=	reference stall speed in a certain configuration [m/s]
V_2	=	take-off safety speed [m/s]
w	=	velocity in z direction [m/s]
W	=	weight [N]
x_{sf}	=	split flap lever arm to centre of gravity in the x direction [m]
x_b	=	aircraft body axis in x direction
y_{engine}	=	engine lever arm to centre of gravity in the y direction [m]
y_{sf}	=	split flap lever arm to centre of gravity in the y direction [m]
Y	=	sideforce [N]
Y_b	=	aircraft body axis in y direction
Z_b	=	aircraft body axis in z direction
α	=	angle of attack [deg]
β	=	angle of sideslip [deg]
δ	=	control surface deflection angle [deg]
θ	=	angle of pitch [deg]
θ_0	=	angle of pitch in steady flight [deg]
ϕ	=	bank angle [deg]
μ	=	mean [-]
μ_b	=	relative density in asymmetric motions [-]
λ	=	sweep angle [deg]
λ_{sf}	=	split flap hingeline sweep angle [deg]
σ	=	standard deviation [-]
ψ	=	yaw angle [deg]

Subscripts

<i>asym</i>	=	asymmetric
<i>clean</i>	=	clean configuration
<i>CS1</i>	=	control surface 1
<i>CS2</i>	=	control surface 2
<i>CS3</i>	=	control surface 3
<i>EB</i>	=	external balance
<i>OEI</i>	=	one-engine-inoperative
<i>r</i>	=	rudder
<i>sf</i>	=	split flap
<i>sf,u</i>	=	upper split flap
<i>sf,l</i>	=	lower split flap
<i>WTM</i>	=	wind tunnel model

1

Introduction

Over the past 50 years, the conventional cylindrical-fuselage and fixed-wing aircraft have dominated the aviation design space [1]. A good example of this is the Boeing 747 series, which came into service in 1969 and is still being produced to this day [2]. The conventional design can also be seen in newer aircraft designs, such as the Boeing 787 or Airbus A350. The wing-fuselage configuration is thus not very innovative, yet the aircraft have to become progressively efficient. Sustainability and efficiency are becoming more and more important in the aviation industry. Increasing air traffic and public awareness have made aircraft emissions one of the most pressing criteria for the growth of commercial aviation [3]. As the room for improvements is finite and is getting smaller, the aviation industry has to further evolve to keep up with this increasing need for low-emissions.

In an effort to improve aircraft efficiency, some designers have turned towards the flying wing concept. Such an aircraft does not have a conventional wing-fuselage body, but rather combines these parts for aerodynamic or structural benefits. The flying wing concept is not new, but it has been revamped by aircraft designers in the search for out-of-the-box sustainability improvements. The Flying V is such a flying wing concept, originally thought of by J. Benad during an internship at Airbus [4]. His aim was to design a highly efficient commercial passenger aircraft, which could compete with the likes of an Airbus A350-900. He came up with a configuration which interconnected the fuselage and the wing, creating a flying wing aircraft with the shape of a 'V', hence its name. This new design had the potential of a 10% higher lift-over-drag ratio while having a 2% lower mass compared to the A350-900, meaning less emissions for the same mission. Research on the Flying V has been done at Delft University of Technology since 2016. During this time, the design by Benad has been further developed and optimised. Several experimental and computational studies have been performed on the aerodynamic properties and the handling qualities of the aircraft.

Stability and control issues were (and still are) one of the major hurdles for the development of flying wing designs [5]. For the Flying V, this is no different. In terms of directional control, the aircraft makes use of a set of rudders incorporated in its winglets. It has been found during experimental wind tunnel testing that these rudders have a large efficiency falloff with increasing angle of attack [6]. A preliminary investigation into handling characteristics of the Flying V showed that due to this efficiency falloff, insufficient yaw control was available in certain critical operational situations [7]. The present study was therefore proposed to find a feasible solution for creating more directional yaw authority for the Flying V. During a preceding literature study it has been found that the addition of split flaps provides a promising solution.

This thesis will thoroughly evaluate the characterisation of implementing split flaps on the Flying V through experimental investigation. First, valuable background information on the Flying V and split flaps in general, as well as lateral-directional aircraft requirements, will be presented in chapter 2. This will also reflect on the research objective and questions.

Next, the methodology used throughout the research is explained in chapter 3. Following the methodology, chapter 4 discusses the verification and validation performed during the research. The wind tunnel results are then extensively presented and discussed in chapter 5, after which a split flap conceptual sizing procedure is performed in chapter 6. This leaves the conclusions and recommendations, which are presented in chapter 7.

2

Background

In order to give the reader more introductory knowledge about the thesis subject, this chapter briefly presents the background of the research. It consists mostly of established information from a literature study preceding the thesis work. First, it gives information about the Flying V and some previous work on this novel aircraft. Next, the characteristics of split flaps are elaborated and the required directional control requirements of CS-25 are discussed. Lastly, the research objective and research questions are established, after which the thesis outline is presented.

2.1. Flying V

As explained in the introduction, the Flying V is a novel flying wing design which fuses the wing and fuselage to make a distinctive 'V'-shaped aircraft. The Flying V is a rather young concept, created in 2015 by J. Benad [4]. The main reason for the radical design was to get a higher aerodynamic efficiency than direct competitors such as the Airbus A350-900. The Flying V project has been researched at Delft University of Technology since 2016. A render of the current design of the Flying V is presented in figure 2.1.



Figure 2.1: Isometric view of the current Flying V design [8]

The design of Benad was first put through a multidisciplinary design iteration. This was performed by Faggiano, who redesigned the planform to be aerodynamically more efficient, while providing initial sizing of the aircraft systems [9]. A simple sketch of the more optimised wing planform is shown in comparison to the initial design in figure 2.2. Faggiano claims a maximum lift to drag ratio of 23.7 with a 12% reduction in subsonic drag. When comparing

to the NASA Common Research Model, which is a conventional configuration benchmark, the optimised Flying V design is 25% aerodynamically more efficient at its design cruise condition [9].

In terms of directional control, Faggiano set some driving requirements for the initial sizing of the winglet rudders. These included that for a One-Engine-Inoperative (OEI) situation, the aircraft should be able to balance the asymmetric thrust with rudder deflections below 20° . Additionally, the aircraft should be able to balance out a 11.5° sideslip for landing in maximum crosswind conditions, again for rudder deflections below 20° . This winglet rudder sizing was quite basic, as it was performed using some simple force and moment estimations.

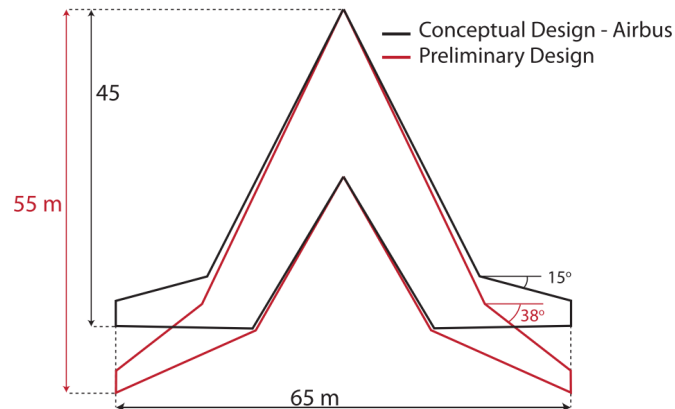


Figure 2.2: Sketch of the Flying V planform by Faggiano [9]

After the findings of Faggiano, the studies on the Flying V were mostly performed on systems level. Palermo and Johnson have contributed to the topic of stability and control of the Flying V [6, 10]. Palermo has investigated the longitudinal static stability and control parameters of the Flying V. In order to do so, he performed wind tunnel campaigns with a 4.6% Froude scaled half-wing model of the Flying V. Johnson analysed the effect of winglet integration on the aerodynamic properties, as well as the effect of winglet rudder deflections. In previous wind tunnel studies, the winglet was not taken into account. Their thesis is therefore a valuable benchmark for the present study, in terms of the aerodynamic properties of the model. Quantification of the aerodynamic influence of rudder deflections is given in this paper, however, no conclusions are drawn as to whether the control power is sufficient. Johnson's findings are important for the current research, as the directional control power in certain configurations can directly be compared.

In the context of the current thesis, the last notable study on the Flying V was the thesis by Cappuyns [7]. In their work, he investigated the stability and control properties of the Flying V. Based on several certification specifications of CS-25, it was concluded that the current directional control allocation is not sufficient for several flight situations, among which some specific OEI situations. From these conclusions, it was recommended to improve the directional control authority of the aircraft. This could possibly be done through the application of split flaps, which is the foundation of the current thesis.

2.2. Split flaps

As stated, the current research investigates the aerodynamic characteristics and feasibility of split flaps in order to increase the Flying V directional control power. Since split flaps are not common control effectors, this section will give the reader some background information on

such devices.

Split flaps are a common solution for yaw control of pure flying wings. Such control devices effectively consist of two flaps at the trailing edge of the wing which can be “split” apart. It thus consists of an upper flap which deflects upward and a lower flap which deflects downward. When the flaps on one wing half are split open, the flaps on the other wing are closed. This will create an intentional drag force which will yaw the aircraft towards the deflected side. The devices are therefore sometimes also described as ‘split drag rudders’. Split flaps have been implemented in many fighter and flying wing designs in the past [5, 11], of which the best known example is probably the Northrop Grumman B-2 Spirit. This aircraft is shown in figure 2.3, where the split flaps can be seen at the trailing edge near the wingtips. Here, the split flaps are used on both wings simultaneously for a secondary braking function.



Figure 2.3: Northrop Grumman B-2 Spirit during landing [12]

It is also possible that the upper and lower surface of the split flap are deflected together to work as an ordinary aileron or elevator. Such an approach is for instance implemented for the NASA X-48B BWB concept [13]. If the split flaps can both provide a rudder function and aileron/elevator functions, the devices are sometimes described as ‘split ailerons’. An illustration of a split flap cross section is presented in figure 2.4. Here it is shown how both aileron and rudder modes can be created by using such control surfaces. It can be observed that both modes have separate hinge lines. For the aileron mode, a central hinge line is used to pivot both surfaces simultaneously. For the rudder mode, both surfaces have their own hinge line. It is assumed in the present study that the split flaps to be implemented on the Flying V can both work in rudder function and aileron/elevator functions. However, as the aileron functionality of the outboard control surfaces is already investigated in previous theses, the focus of the present study purely lies on the split (rudder) functionality. It should always be kept in mind that when split flaps on one wing are used in split functionality, the flaps on the other wing can be used in aileron/elevator functionality.

By deflecting the upper and lower surface, split flaps mostly create pressure drag, which over a lever arm is converted to a yawing moment. The increase in pressure drag can be explained by the higher inclination of the surfaces and the flow separation at the trailing edges [15]. The pressure in front of the flaps is therefore high, while the pressure behind the flaps is low. The skin friction drag is not really affected by the addition of split flaps as the wetted area is generally not increased. The split control surfaces are usually placed as far

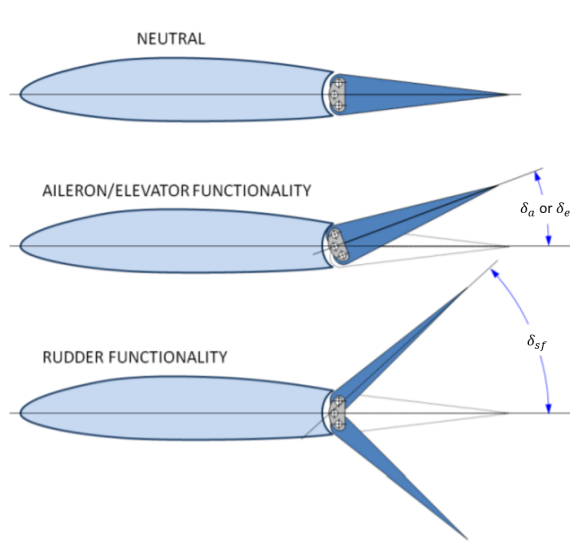


Figure 2.4: Illustration of a split flap cross section [14]

outboard as possible, such that the lever arm to the centre of gravity is as large as possible. This alleviates the need for very high drag forces, which could deteriorate proper performance of the aircraft [16].

On aerodynamic level, several notions are made from previous studies, which are incorporated in the current research. Dorsett and Mehl show in their study into innovative control concepts that split flaps can have a decrease in efficiency at higher angles of attack, due to separation of the main wing [11]. Decrease in efficiency can also occur due to interaction with leading edge vortices [17]. In terms of sideslip, the efficiency of the split flaps is not significantly altered for low to moderate angles [18]. The split flaps are generally found to be highly coupled. They do not only affect drag and yaw, but also lift, sideforce, pitch and roll [11]. Lochert et al. have investigated split flaps for yaw control of a tailless aircraft configuration [17]. They found that the adverse effects on roll and pitch could potentially be decreased by setting different upper and lower flap deflections. Additionally, split flaps might cause adverse interaction effects with other properties of the wing, such as the control surfaces near the split flaps. This can be through vortex interaction or through the pressure differences close to the split flaps [19].

2.3. Lateral-Directional Control Requirements

Ultimately, the point of adding split flaps to the Flying V is to ensure that the full scale aircraft has enough yaw power. As any other large aeroplane, the Flying V has to adhere to the rules and guidelines as stated in CS-25. This document lists the certification specifications and acceptable means of compliance for large aircraft, and is published by the European Union Aviation Safety Agency (EASA) [20]. Several requirements in terms of directional control are therefore retrieved from CS-25. The driving requirements in terms of lateral-directional control are described in this section. These are later used to identify a proper split flap configuration for the full-scale Flying V.

2.3.1. Sign convention

Before we get into the technical requirements, the sign convention for lateral-directional motions is shown. Throughout the report, the sign convention as presented by figures 2.5 to 2.7 is used.

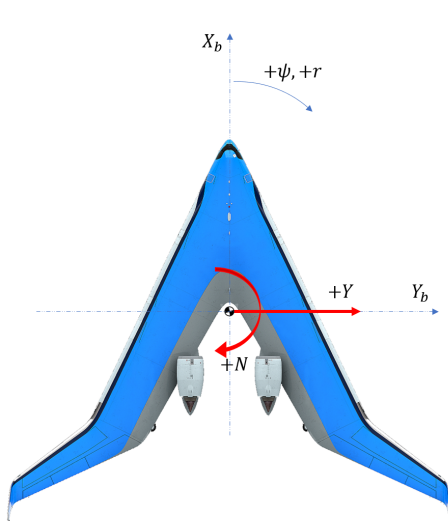


Figure 2.5: Directional sign convention

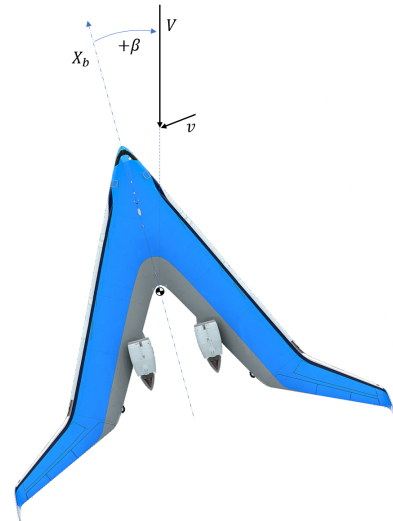


Figure 2.6: Sideslip sign convention

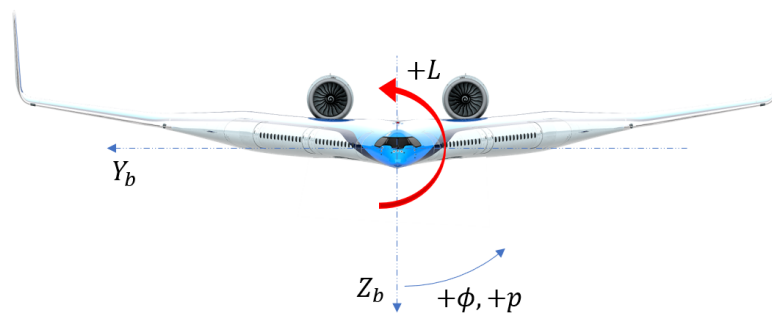


Figure 2.7: Lateral sign convention

2.3.2. CS 25.143: Controllability and Manoeuvrability

Several manoeuvring capabilities are specified in this section of CS-25. In terms of lateral-directional control, it is stated in subparagraph (h) that: *The manoeuvring capabilities in a constant speed coordinated turn at forward centre of gravity, as specified in the following table, must be free of stall warning or other characteristics that might interfere with normal manoeuvring.*

Table 2.1: CS 25.143(h) manoeuvre specifications [20]

Configuration	Speed	Manoeuvring bank angle in a coordinated turn	Thrust/power setting
Take-off	V_2	30°	Asymmetric WAT-limited
Take-off	$V_2 + xx$	40°	All engines operating climb
En-route	V_{FTO}	40°	Asymmetric WAT-limited
Landing	V_{ref}	40°	Symmetric for -3° flight path angle

In the investigation into the handling qualities of the Flying V, Cappuyns has also performed

calculations for this requirement [7]. He concluded that the first specified manoeuvre was difficult to be certified with the ordinary directional control allocation. This take-off manoeuvre will therefore be one of the requirements for the current research. As compliance was shown for the other three situations, these will not be handled.

2.3.3. CS 25.147: Directional and lateral control

This section of CS-25 is the most demanding in terms of lateral-directional control properties of large aircraft. It poses 4 requirements which will be assessed in the final sizing. First of all, subparagraph (a) on general directional control states: *It must be possible, with the wings level, to yaw into the operative engine and to safely make a reasonably sudden change in heading of up to 15° in the direction of the critical inoperative engine. This must be shown at $1.3 V_{SR1}$, for heading changes up to 15° , and with -*

1. *The critical engine inoperative and its propeller (if applicable) in the minimum drag position;*
2. *The power required for level flight at $1.3 V_{SR1}$, but not more than maximum continuous power;*
3. *The most unfavourable centre of gravity;*
4. *Landing gear retracted;*
5. *Wing-flaps in the approach position; and*
6. *Maximum landing weight.*

Figure 2.8 shows the yawing moment caused during a starboard OEI situation. The split flaps and winglet rudders thus have to create a counteractive yawing moment on top of the needed yawing moment to change the heading of the aircraft. It should be noted that this requirement might be ambiguous to assess, as 'reasonably sudden' is not specific. It is stated in the Acceptable Means of Compliance (AMC) that this requirement is mainly in place to show that the aircraft can yaw without further application of bank angle.

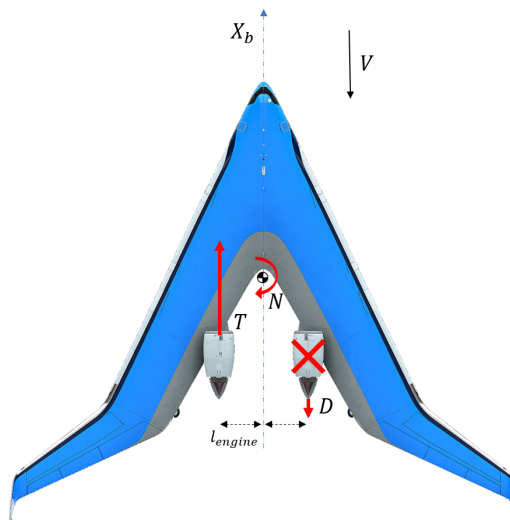


Figure 2.8: Illustration of a OEI situation

Next, subparagraphs (c) and (d) specify requirements regarding the lateral control of the aircraft. While the present study is not on the sizing of the ailerons, it is shown in Cappuyns that adequate yaw control is needed during turning flight with OEI [7]. Subparagraph (c) states: *It must be possible to make 20° banked turns, with and against the inoperative engine, from steady flight at a speed equal to 1.3 V_{SR1}, with –*

1. *The critical engine inoperative and its propeller (if applicable) in the minimum drag position;*
2. *The remaining engines at maximum continuous power;*
3. *The most unfavourable centre of gravity;*
4. *Landing gear both retracted and extended;*
5. *Wing-flaps in the most favourable climb position; and*
6. *Maximum take-off weight;*

In practise, this requirement looks a lot like CS 25.143(h), but with several other configuration settings.

Paragraph (d) of CS 25.147 states: *With the critical engine inoperative, roll response must allow normal manoeuvres. Lateral control must be sufficient, at the speeds likely to be used with one engine inoperative, to provide a roll rate necessary for safety without excessive control forces or travel.* More information is provided in the AMC, where it is explained that with a OEI situation, the aircraft should be able to roll from trim at 30° bank angle, to a bank angle of 30° in the other direction within 11 seconds. This has to be done for V₂ at maximum take-off weight.

2.3.4. CS 25.161: Trim

This section of CS-25 has some final demanding lateral-directional control situations for which certification testing should be performed. Subparagraph (b) on lateral and directional trim states the following: *The aeroplane must maintain lateral and directional trim with the most adverse lateral displacement of the centre of gravity within the relevant operating limitations, during normally expected conditions of operation (including operation at any speed from 1.3 V_{SR1} to V_{MO}/M_{MO}).*

This requirement is performed for one of the most directionally adverse condition of operation, which is during low speed crosswind conditions. From the AMC 25.177(c) it is found that the appropriate sideslip angles for normal operation can be calculated using equation (2.1). Here, the airspeed should be implemented in knots, as the calculation is performed with a theoretical 30 knot crosswind.

$$\beta = \arcsin 30/V \quad (2.1)$$

Figure 2.6 illustrates what the Flying V looks like in crosswind conditions, due to a crosswind v . The sideslip creates a restoring yawing moment N_β , mainly caused by the vertical tailplanes. In order to maintain straight, steady sideslipping flight, the value of N_β has to be counteracted by the winglet rudders and split flaps.

Additionally, subparagraph (d) of CS 25.161 states another situation where directional control has to be sufficient enough for trim: *The aeroplane must maintain longitudinal, directional, and lateral trim (and for lateral trim, the angle of bank may not exceed 5°) at 1.3 V_{SR1}, during the climbing flight with –*

1. *The critical engine inoperative;*
2. *The remaining engines at maximum continuous power; and*
3. *The landing gear and wing-flaps retracted.*

2.4. Research objective and questions

Based on the known information from previous Flying V and split flap studies, the research objective and research questions for the current thesis work are set up. The research objective can be summarised as:

“To identify the general aerodynamic behaviour of split flap implementation on the Flying V by performing wind tunnel tests and to improve the Flying V directional control power by carrying out a conceptual split flap sizing procedure based on certification requirements.”

In the context of this objective, several research questions are set up. The aerodynamic behaviour of the split flaps, and its performance in different configurations, is central for the research. For this, the investigation into the behaviour of the created yawing moment is the most important feature. Additionally, interaction effects should be investigated and mitigation of adverse split flap effects should be highlighted. Lastly, an effort for the conceptual sizing of the split flaps can be an important step for future investigation of these devices. The research questions are then as follows:

- What is the effect of split flaps on the directional control power of the Flying V?
- What is the effect of split flaps on the rest of the Flying V aerodynamic parameters?
- What is the effect of split flaps on the effectiveness of surrounding control surfaces?
- How are adverse split flap moments mitigated by the application of:
 - differential deflection between upper and lower flap?
 - global rotation of the split flaps?
- What would be an appropriate conceptual split flap geometry for the full size Flying V, such that the aircraft adheres to the lateral-directional control requirements of CS-25?

3

Research Methodology

This chapter discusses the methodology which has been implemented during the preparation and execution of the research. It will first discuss how the split flaps are designed, and how these are implemented on the Flying V wind tunnel model. The wind tunnel setup is presented next, including an explanation of the model measurements and calculations. Finally, this chapter extensively discusses the way that the conceptual split flap sizing is performed for the full-scale Flying V.

3.1. Split flap design

The way that the split flaps were designed for the wind tunnel model is explained in this section. As split flaps are generally unconventional, no real design or sizing methods could be found from literature. Their design methodology is therefore thought up on the fly, purposefully for the Flying V outboard wing section. This section evaluates the chosen design rules, explains the directional control design point and shows the way that the split flap performance is estimated. It concludes with the presentation of the tested split flap designs.

3.1.1. Split flap model design rules

No real design rules on split flap design can be found in literature. For this reason, the design rules in the present study are adapted from previous split flap research and the Flying V half-wing geometry. As split flaps are best suited on the outboard wing sections, it is chosen to investigate replacing part of the current outboard control surfaces by split flaps. This has several implications on the design space of the split flaps. These implications, and other design choices are explained below. Figures 3.1 and 3.2 are included to help visualise the design rules. The first figure highlights the outboard section of the wing, while the second figure presents a cross section along this outboard section. The design rules are as follows:

1. The split flaps will replace part of the current outboard control surfaces. The upper and lower flaps are also envisioned to be able to work together, to act as elevon, similar as the part of the control surfaces that they replace. The replacement provides that the central hinge line of the total device is similar as the current control surface hinge line, ultimately meaning less difficulty in split flap integration.
2. The split flaps are located as far outboard as possible, as this increases the effectiveness of the flap and thus alleviates the amount of drag that is needed. As the split flaps will replace part of the current control surfaces, the most outboard location of the third control surface (CS3) is chosen as the begin point of the split flaps. This is highlighted in figure 3.1 with the blue line.

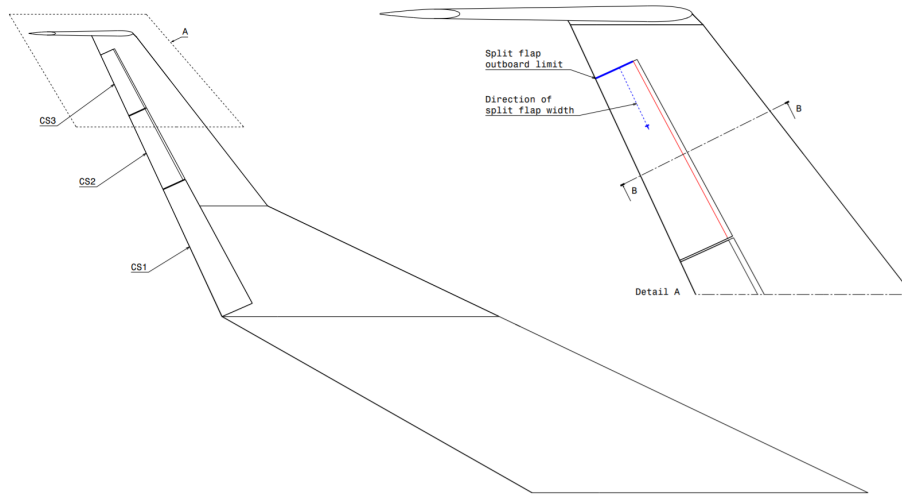


Figure 3.1: Top view of the left wing wind tunnel model including highlighted detail on the outboard wing section.

3. The width of the split flap (b_{sf}) is a free design parameter. It is defined as the length from the start points towards the inboard direction of the wing, parallel to the control surface leading edge. This is indicated in figure 3.1 with the dotted blue line.
4. The separate hingelines of both the upper and lower split flap are located at the thickest point of the control surface geometry. This is true for each point along the split flap width. This rule effectively restrains the sweep of the split flap λ_{sf} . The thickest point of the control surface is indicated in figure 3.1 with a red line and in figure 3.2 with a black dotted line.
5. The outer curvature of the split flaps have the same curvature as the current control surfaces. This is true for each point along the split flap width. This is done to make sure that the non-deflected split flaps have the same geometry as the current outboard control surfaces, so operation in elevon configuration would not be changed. This process is visualised in figure 3.2, where the second cross section shows the red line for the upper surface curvature and the blue line for the lower surface curvature.
6. Both curvatures rotated over an angle δ_{sf} , which is visualised in figure 3.2 in the third cross section. This process creates the split. The deflection angle δ_{sf} is therefore also a free parameter. If not specified otherwise, the deflection angle of the upper flap $\delta_{sf,u}$ is equal to the deflection angle of the lower flap $\delta_{sf,l}$.
7. Lastly, the split flaps are given some inside thickness for 3D-printing and stiffness purposes. It is assumed that this does not affect the aerodynamics of the split flaps. This step is visualised in figure 3.2 in the last cross section.

In the early design stage, also more inboard split flap placements were considered. A more inboard starting point placement could result in a slightly smaller required width due to the taper of the control surface planform. While investigating a variable split flap placement, it was found that the width could maximally be decreased by about 10%, by placing the split flaps at the most inboard location of CS1. However, this would require a drag increase of about 42% in order to get the same amount of yawing moment. It was therefore deemed that the decrease in b_{sf} would not outweigh the needed increase in drag, hence resulting in the second design rule.

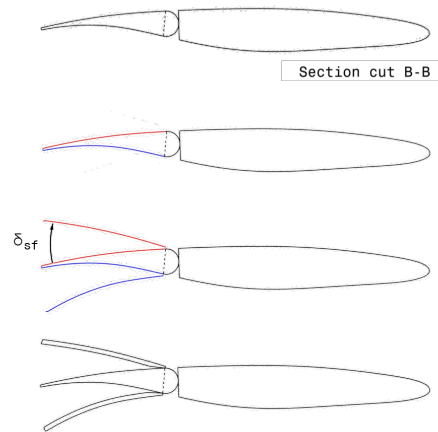


Figure 3.2: Section cut B-B from figure 3.1, including visualisation of the split flap design

Throughout the report it is presumed that if the flaps on one wing are split open, the flaps on the other wing are closed. The split deflections δ_{sf} are created by placing 2 small brackets between the split flap and underlying control surface. These brackets are also 3D printed and fit accurately between the outer geometry of the control surface and the inner geometry of the split flaps. Brackets have been created for both the upper and lower split flaps to create deflection angles of 10, 20, 30, 40, 50 and 60 degrees. The brackets are attached to both surfaces with double sided tape and provide additional stiffness to the flaps. It is assumed that the brackets, as well as the part of the control surface on which the split flaps are attached, do not interfere with the aerodynamic results as they are located in the wake of the split flap.

3.1.2. Estimation of split flap performance

Yasim et al. include a small discussion on the initial sizing process for a split flap in their paper [15]. It is stated that before high-fidelity testing can confirm the exact split flap geometry, a simplified sizing approach is necessary. It was thus decided to perform an initial sizing process such that split flaps of roughly the correct geometry could be tested in the wind tunnel. For this, an estimation of the split flap performance had to be performed. As already stated, the split flaps create yaw by exerting an increase in drag and sideforce on the outboard sections of the aircraft. So in order to estimate the amount of yaw that is created by a particular split flap, the amount of created force had to be estimated.

First, the case where the airflow is normal to the split flap height is considered. The 2D normal drag force coefficient (C_{D_n}) based on the frontal area of several shapes is found in the work by Hoerner [21]. Figure 3.3 represents the 2D C_{D_n} for wedges per half-vertex angle. This coefficient is based on the area of the wake of the wedge S_w . It is assumed that split flaps work in a similar fashion as such wedges, in the analogy that δ_{sf} equals the half-vertex angle. In addition, figure 3.4 was found in the work by Hoerner. This figure shows the decrease of 2D coefficients to 3D coefficients, based on the height to span ratio of the frontal area. The properties in figure 3.3 and figure 3.4 are therefore combined to estimate the total 3D C_{D_n} value for the split flaps, at a certain b_{sf} and δ_{sf} . Note that as the outboard wing section is tapered, the chord (and thus height) of the split flap along its width is not constant. For this reason the average height of the split flap frontal area is used in the computations of its 3D C_{D_n} .

It is further discussed by Hoerner that C_{D_n} remains approximately constant for small to medium sweep angles (below 45°) [21]. The total normal force is decoupled into a sideforce

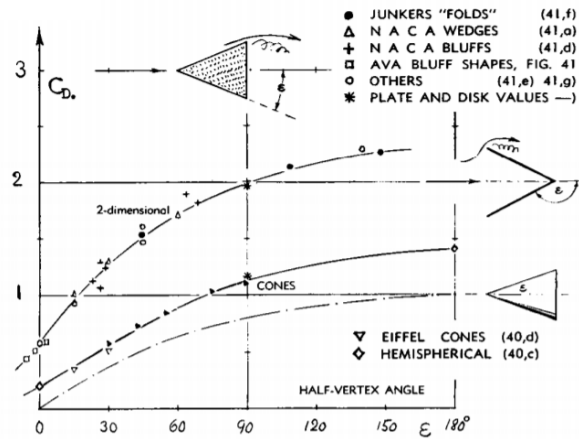


Figure 3.3: Frontal area drag coefficients of wedges and cones as a function of their half-vertex angle [21].

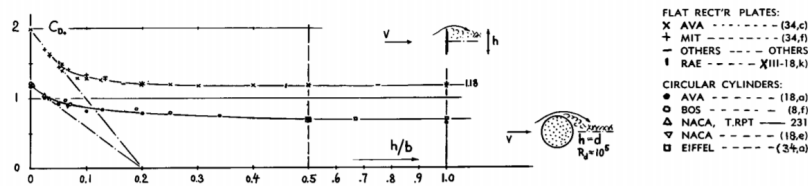


Figure 3.4: Decrease of coefficient with their height to span ratio [21].

and drag force using the split flap sweep λ_{sf} . This is also shown in figure 3.5, where the created yaw due to split flaps is visualised. For a split flap with a certain b_{sf} and δ_{sf} , the amount of created yawing moment could now be estimated by translating the drag and sideforce over their lever arm distances x_{sf} and y_{sf} .

3.1.3. Preliminary split flap sizing

The chosen preliminary design point is trim in a low-speed One-Engine-Inoperative (OEI) situation, where the directional control allocation has to balance out the asymmetric moments while leaving some control power for manoeuvring. Situations with OEI usually require a lot of directional control power and can be demanding for the available directional control power [22]. This design point could be quickly determined at this stage of the research, with the unknown behaviour of split flaps with angle of attack and the little time available for preparation of the wind tunnel tests. Later in the research, reported in section 3.3, a more appropriate design point based on the rules and regulations of CS-25 is defined for the full-scale Flying V, after which a conceptual sizing is performed by making use of the wind tunnel data.

In a OEI situation for a twin-engine aircraft, one of the engines is defective, while the other engine has to produce high thrust to keep the aircraft from losing velocity. Additionally, the defective engine will produce extra drag due to windmilling [23]. This asymmetric condition will therefore produce a lot of yawing moment, which has to be balanced by the directional control devices. The produced OEI yawing moment coefficient due to the engines is defined in equation (3.1). Here, ΔT encapsulates both the increase in thrust of the working engine and increase in drag of the defective engine. It is assumed both engines are distanced equally far from the aircraft centre of gravity, which is represented by the moment arm y_{engine} .

$$C_{n_{OEI}} = \frac{\Delta T \cdot y_{engine}}{q S_{ref} b_{ref}} \quad (3.1)$$

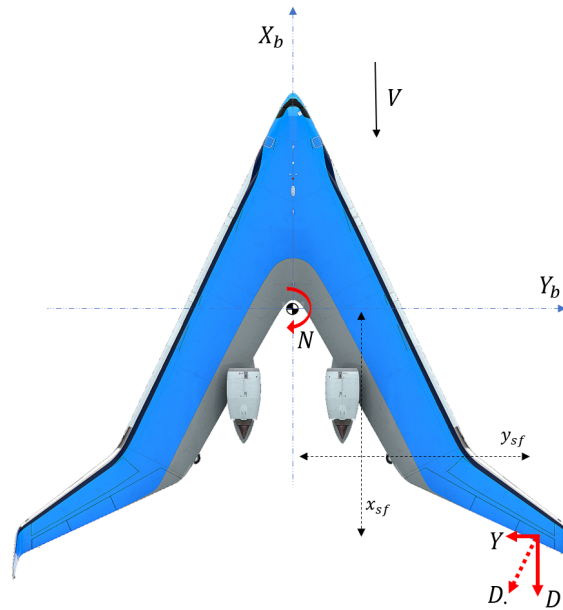


Figure 3.5: Illustration of the created forces by a split flap on the outboard wing

ΔT is taken as the equivalent bare engine take-off thrust of the Trent XWB-84 engine [24], a similar approach as taken by Cappuyns [7]. It is assumed that this maximum thrust value is a decent overestimation in order to also account for the additional drag of the defective engine. The dynamic pressure is taken at sea-level conditions, at a velocity of 80 m/s.

The winglet rudders work together with the split flaps in order to create the required yawing moment to oppose the OEI yawing moment. Here, any possible interaction effects between the two control surfaces are neglected. The yawing control power of the winglet rudders is found from the work by Johnson [6]. A winglet rudder deflection of 20 degrees is set, as suggested by Faggiano [9]. This seems like a low maximum rudder deflection, but this would leave room for manoeuvrability of the aircraft.

Assuming the split flaps will have a δ_{sfmax} of 60° , the required split flap width can now be calculated. At $\alpha = 0^\circ$, where the split flap yaw estimation is deemed most accurate, a split flap of approximately $b_{sf} = 150\text{mm}$ is needed. Due to the varying effectiveness of the winglet rudders with increasing incidence angle [6], and the simplifications in the preliminary sizing procedure, it is chosen to also test a smaller and larger size split flap. This also allows the investigation of possible size effects.

Three split flap configurations are created for the wind tunnel model, with widths of 100mm, 150mm and 200mm. Additionally, a fourth configuration of roughly 220mm is created. This fourth configuration spans the whole width of CS3 and can be used for several research questions. A top-view of the 4 split flap configurations is presented in figure 3.6.

3.2. Wind tunnel model and measurements

In order to give the reader more context on the experiments that have been conducted during the research, this section will present the wind tunnel setup and the type of measurements that were performed.

3.2.1. Open Jet Facility

During the thesis work, wind tunnel campaigns were to be performed in the Open Jet Facility (OJF). This is a low speed, closed circuit wind tunnel, located at the Delft University of

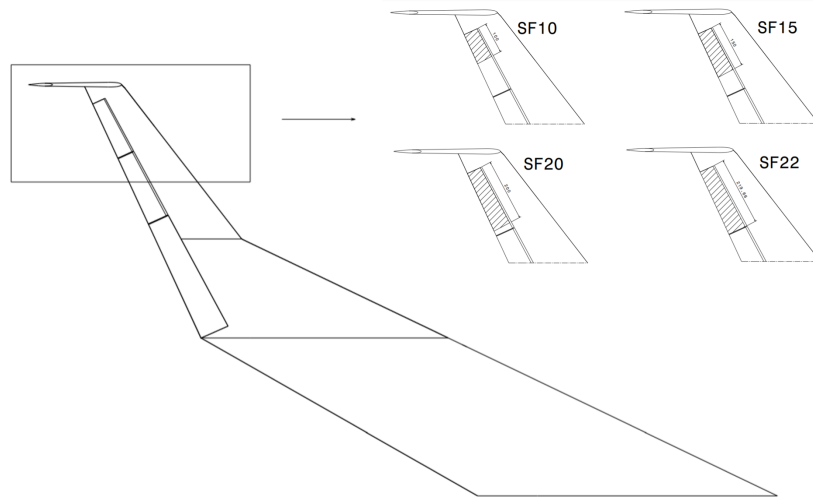


Figure 3.6: Top-view of the Flying V model including outboard detail view highlighting the areas of SF10, SF15, SF20 and SF22.

Technology. It has an octagonal jet, with both width and height equal to 2.85 meters, which introduces the flow into a larger open test section. The maximum test section velocity is about 35 m/s. A schematic of the wind tunnel facility is presented in figure 3.7.

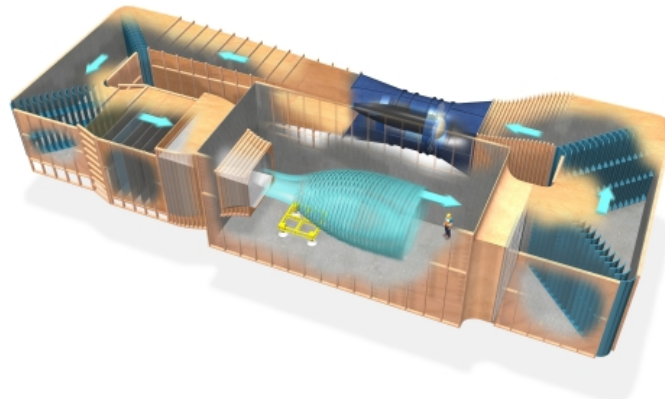


Figure 3.7: Schematic of the OJF facility [25]

3.2.2. Flying V model and setup

In the OJF, use is made of a half-wing model of the Flying V. This model is created by applying geometric Froude scaling laws to the full-scale concept geometry, as described by Palermo and Viet [10, 26]. The resulting model is a 4.6% scaled half-wing model which can be used on a turntable in the wind tunnel facility. As a result of the scaling, the model has a half-span of 1.495 meters. A detailed summary of the model dimensions can be found in the work of Palermo or Johnson [6, 10]. The model has a set of four adjustable control surfaces: 3 trailing edge control surfaces on the outboard section (CS1, CS2 and CS3), and 1 control surface in the winglet which acts as a rudder (CSR). The outboard wing section is fitted with a carborundum trip strip, as recommended by van Uiter [27].

The major disadvantage of using a half-wing model is that only the case of zero sideslip can be investigated in the wind tunnel. No asymmetric flight conditions can be correctly experimented, while such flight conditions can be of major interest for investigating directional control power. It is assumed for now that this is not detrimental for predicting the split flap effectiveness, as Lochert et al. show that low to medium sideslip angles do not have a significant effect on their split flaps performance [17]. This assumption might however not hold, due to the sweep angle of the split flap hinge lines in the current research.

The half-wing model is mounted on an external balance, which is connected to a turntable. This way, the aerodynamic forces and moments subjected on the model can directly be measured for varying angles of attack. A three view schematic of this model is presented in figure 3.8. In this picture, also the octagonal jet, the turntable and external balance are projected.

3.2.3. Measurements and processing

The raw forces and moments are measured in the x -, y - and z -direction of the external balance reference system, subscript EB in figure 3.8. Each measurement is a time averaged result of a 10 second period in which data is taken at a 2000Hz frequency. This is done to mitigate the random error caused by turbulence, vibrations in the model and the high sensitivity of the external balance. The measurements on their own do not provide valuable information for the research, as they have to be transformed to the reference system of the wind tunnel model (subscript WTM). Both the orientation and origin of the EB reference system have to be transformed to represent the WTM reference system. The transformation from the external balance system to the wind tunnel model system is given by the matrix multiplications in equation (3.2) and equation (3.3).

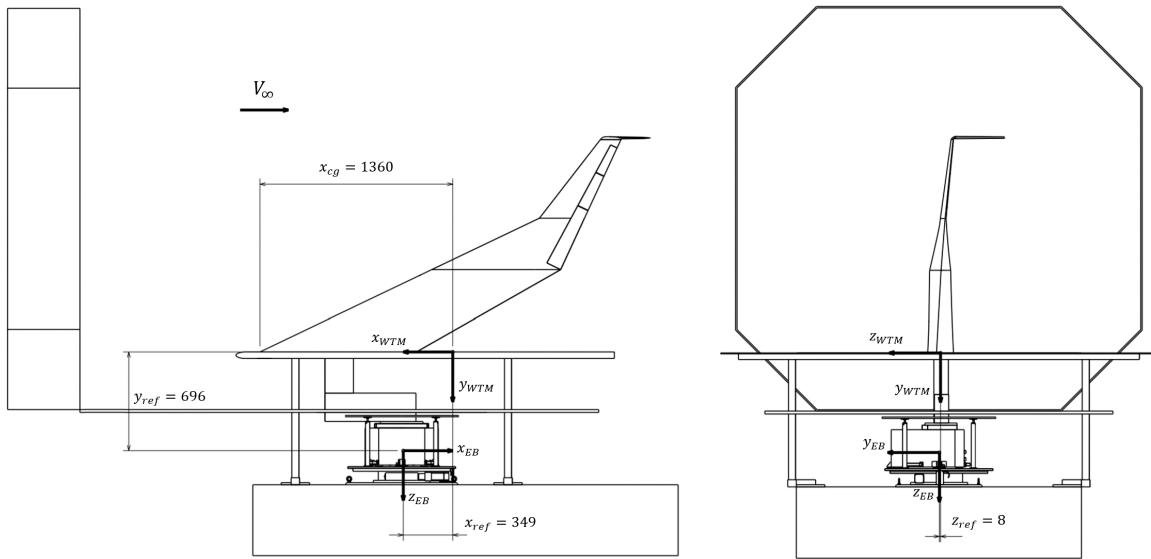


Figure 3.8: Side and back view of the wind tunnel test setup

$$\vec{F}_{WTM} = \mathbf{R}_{EB-WTM} \vec{F}_{EB} \quad (3.2)$$

$$\vec{M}_{WTM} = \mathbf{R}_{EB-WTM} \vec{M}_{EB} + \vec{r}_{EB-WTM} \times \mathbf{R}_{EB-WTM} \vec{F}_{EB} \quad (3.3)$$

$$\mathbf{R}_{EB-WTM} = \begin{bmatrix} -1 & 0 & 0 \\ 0 & 0 & 1 \\ 0 & 1 & 0 \end{bmatrix} \quad (3.4)$$

$$\vec{r}_{EB-WTM} = [x_{ref} \ y_{ref} \ z_{ref}] = [0.349 \ 0.696 \ 0.008] \quad (3.5)$$

Both the external balance and the wind tunnel model are connected on the turntable, meaning that both reference frames rotate with angle of attack α . The pitch, roll and yawing moment are related to the aircraft body system, while the lift, drag and sideforce are related to the aerodynamic reference system. The latter system is defined by the rotation of the aircraft with the airspeed vector. The reason for choosing two different systems is to stay in line with previous Flying V wind tunnel experiments, to allow direct comparison with previous results. When following these definitions, the aircraft aerodynamic parameters can then directly be related to the external balance forces and moments as follows:

$$\begin{aligned} L &= -F_{x_{EB}} \sin(\alpha) - F_{y_{EB}} \cos(\alpha) & m &= M_{z_{EB}} + F_{x_{EB}} y_{ref} - F_{y_{EB}} x_{ref} \\ D &= F_{x_{EB}} \cos(\alpha) - F_{y_{EB}} \sin(\alpha) & l &= -M_{x_{EB}} + F_{y_{EB}} z_{ref} + F_{z_{EB}} y_{ref} \\ Y &= F_{z_{EB}} & n &= M_{y_{EB}} + F_{x_{EB}} z_{ref} + F_{z_{EB}} x_{ref} \end{aligned}$$

The model aerodynamic coefficients can consequently be set up by normalisation as:

$$\begin{aligned} C_L &= \frac{L}{qS} & C_m &= \frac{m}{qS\bar{c}} \\ C_D &= \frac{D}{qS} & C_l &= \frac{l}{qSb} \\ C_Y &= \frac{Y}{qS} & C_n &= \frac{n}{qSb} \end{aligned}$$

The influence of split flaps is evaluated by taking the delta between the clean wing and the wing including deflected split flaps. When for instance looking at the influence of split flaps on the drag coefficient, the split flap influence is isolated as: $\Delta C_D = C_{D_{sf}} - C_{D_{clean}}$. Most of the results in this paper refer to ΔC values instead of the absolute values of C .

In order to support several findings in the data, and to investigate possible flow field changes due to the split flaps, also several tuft photographs have been taken. For this, yarn tufts of about 4 to 5 cm were taped to the model outboard wing surface, with a spacing of about 2 cm between the tufts.

3.2.4. Test matrix

It has been shown in previous researches that the Flying V has an unstable pitch brake between 15 and 20 degrees angle of attack. Additionally, the stall lift coefficient due to control surface limitations has been estimated to occur around 28.5 degrees angle of attack [26]. In order to get a full view of the split flap behaviour and range of applicability, it is chosen to apply an angle of attack range from -10 to 30 degrees. For some cases, such as higher tunnel velocities and high deflection angles, the load limit of the external balance was reached or large vibrations of the model were found. This resulted in a smaller maximum angle of attack range for certain runs. A summary of the test matrix can be found in appendix A.

3.2.5. Corrections

It is common in wind tunnel testing to apply several post-processing corrections to the acquired data. This is for instance to correct for the enclosing walls of the wind tunnel, which can interfere with the behaviour of the air around the model. Ewald [28], Garner et al. [29] and Barlow et al. [30] describe various open jet wind tunnel corrections which could be applied to the measurements in the OJF. The corrections mostly consist of factors concerning lift interference corrections and blockage corrections. The first has to do with discrepancies in inflow angle, while the latter concerns differences in the flow velocity.

In an investigation of the free flight Flying V sub-scale model, it was shown by Ruiz Garcia et al. that the wind tunnel experiments have discrepancies with the free flight data, which could be resolved by applying wind tunnel corrections [31]. However, Garcia [32] and Viet [26] have discussed the application of such corrections for the half-wing model of the Flying V in the OJF. They both conclude that it is best to not apply such corrections to the measured data. The assumptions for the corrections are not guaranteed to hold during the experiments, and non-linear or asymmetric portions of the data are not deemed correctable with the suggested corrections from literature. It is therefore chosen to not apply any flow corrections in this research.

A source of error which has been corrected for in this study is the measurement bias of the external balance. Over time, the bias of the external balance was found to drift, which can cause a systematic error in the measurements. It is assumed that this bias is build up linearly over time. Zero-velocity runs were taken before and after each run, in order to measure the initial and final bias of the external balance. The corrected forces and moments were then linearly deducted at each timestamp during the run.

The split flaps are manually attached to the wind tunnel model and interchanged between each of the runs. Although special care was taken to ensure correct placement and orientation, alignment was done by eye. It is thus inevitable that some small systematic errors could be present in some of the measurements.

3.2.6. Uncertainty analysis

The outcome of the wind tunnel experiments are not constant. This is due to random error caused by aerodynamic disturbances or model vibrations. In order to establish the confidence in the results, the uncertainty of each datapoint has been evaluated. Previous researches have commonly repeated datapoints three times to raise the confidence in the results [6, 33, 34]. This low number of repetitions is however deemed too small, as one outlier would be too influential on the certainty of your measurement. Therefore, each model configuration and angle of attack setting has been repeated 5 times. This would raise the level of certainty of the results, at the cost of a longer test time per configuration.

It is assumed that the aerodynamic measurements are normally distributed, but as the sample size is still relatively low and the standard deviation is not readily known, it is chosen to model the probability as a t-distribution [35]. The mean and standard deviation for a set of samples x_i with sample size n is then presented as equation (3.6) and equation (3.7). The lower and upper bound of the error in the measurements can consequently be calculated using equation (3.8). In this equation, the t-factor t_{n-1} is related to the sample size and the used confidence interval.

$$\mu = \frac{\sum_1^n x_i}{n} \quad (3.6)$$

$$\sigma = \sqrt{\frac{\sum_1^n (x_i - \mu)^2}{n - 1}} \quad (3.7)$$

$$(x_l, x_u) = \mu \pm t_{n-1} \frac{\sigma}{\sqrt{n}} \quad (3.8)$$

3.3. Split flap conceptual sizing procedure

As explained in section 2.3, the Flying V has to adhere to several lateral-directional requirements for the certification according to CS-25. This includes the demonstration of several directionally challenging situations. This section describes the methodology on the conceptual sizing procedure of the split flaps, by making use of the captured wind tunnel data. Showing compliance with the regulations specified by CS-25 for the full-scale Flying V is central for the sizing methodology. First, the calculation approach of how much yaw power is required from the split flaps is explained. This includes the explanation of a simple linear flight mechanics model and additional assumptions that are made for the calculations. After this, it is shown how the required split flap size can be extrapolated from the wind tunnel data.

3.3.1. Flight mechanics model

Previously, during the preliminary sizing of the split flaps, the design point was taken as a simple OEI situation where the directional instabilities had to be trimmed away by combination of the winglet rudders and the split flaps. For the conceptual sizing of the split flaps, it is defined that the split flaps should provide enough yaw control such that each lateral-directional control requirement of CS-25 is satisfied. The requirements are summarised in section 2.3.

In order to show compliance, a simple asymmetric flight mechanics model is set up for the full-scale Flying V from which it can be extrapolated how much yawing moment is required from the split flaps. It was chosen to limit the model to the asymmetric degrees of freedom, as small symmetrical flight disturbances would not influence the amount of required yaw control, and would thus not influence the required split flap design. It is mainly in place to indicate which flight regulations are the most demanding in terms of directional control, and it will provide an estimation of the amount of yaw power that is required from the split flaps.

Equations of motion

The creation of a high-fidelity simulation model for the Flying V including split flaps was considered out of the scope of the project. Judging on the work of Cappuyns [7], a lot of work has to go into making a highly accurate flight mechanics model which could be enough material for a whole new thesis subject. Cook states in his work on flight dynamics that for investigation of aircraft handling qualities in the conceptual design stage 'it is common practice to conduct handling qualities studies using reduced order dynamic models derived from the full order equations of motion' [22]. The present study therefore makes use of a simplified asymmetric model, to give first-order estimation on how much yaw power is required from the split flaps. For this reason, the equations of motions are linearised by applying a first order Taylor expansion. This decouples the symmetric and asymmetric degrees of freedom, so that the asymmetric considerations of adding split flaps could be investigated individually. The linearisation is performed about a steady, straight and symmetric flight condition, since on average, this flight condition is closest to all prescribed flight conditions for the certification. Due to this simplification, only 1 system has to be used throughout the calculations, but the model will be less accurate at higher values of ϕ and β . At this stage of the design process, the model was deemed sufficient to investigate the critical lateral-directional requirements and to give a first order estimate of the amount of yaw power that is required from the split flaps.

The asymmetric equations of motion in non-dimensional form are presented in matrix form in equation (3.9). Their derivation is adapted from the work of Mulder et al. [36]. It represents the states of sideslip angle β , bank angle ϕ , normalised roll rate $\frac{pb}{2V}$, normalised

yaw rate $\frac{rb}{2V}$ and yaw angle ψ . In the equations, C_{Z_0} is the aircraft weight component in the body z-axis, D_b is a normalised time derivative term, μ_b is a relative density term and K_z/K_{xz} are non-dimensional radius of gyration terms. Furthermore, θ_0 is the initial value of the pitch angle in steady flight.

$$\begin{bmatrix} C_{Y_\beta} + (C_{Y_\dot{\beta}} - 2\mu_b)D_b & C_{Z_0} & C_{Y_p} + 4\mu_b \sin(\theta_0) & C_{Y_r} - 4\mu_b \cos(\theta_0) & 0 \\ 0 & -\frac{1}{2}D_b & 1 & \tan(\theta_0) & 0 \\ C_{l_\beta} & 0 & C_{l_p} - 4\mu_b K_x^2 D_b & C_{l_r} + 4\mu_b K_{xz} D_b & 0 \\ C_{n_\beta} + C_{n_{\dot{\beta}}} D_b & 0 & C_{n_p} + 4\mu_b K_{xz} D_b & C_{n_r} - 4\mu_b K_z^2 D_b & 0 \\ 0 & 0 & 0 & \frac{1}{\cos(\theta_0)} & -\frac{1}{2}D_b \end{bmatrix} \begin{bmatrix} \beta \\ \phi \\ \frac{pb}{2V} \\ \frac{2V}{rb} \\ \psi \end{bmatrix} = \begin{bmatrix} 0 & -(C_Y/C_n)_{sf} & -C_{Y_{\delta_r}} & -C_{Y_{\delta_{CS1}}} & -C_{Y_{\delta_{CS2}}} & -C_{Y_{\delta_{CS3}}} \\ 0 & 0 & 0 & 0 & 0 & 0 \\ 0 & -(C_l/C_n)_{sf} & -C_{l_{\delta_r}} & -C_{l_{\delta_{CS1}}} & -C_{l_{\delta_{CS2}}} & -C_{l_{\delta_{CS3}}} \\ -1 & -1 & -C_{n_{\delta_r}} & -C_{n_{\delta_{CS1}}} & -C_{n_{\delta_{CS2}}} & -C_{n_{\delta_{CS3}}} \\ 0 & 0 & 0 & 0 & 0 & 0 \end{bmatrix} \begin{bmatrix} C_{n_{asym}} \\ C_{n_{sf}} \\ \delta_r \\ \delta_{CS1} \\ \delta_{CS2} \\ \delta_{CS3} \end{bmatrix} \quad (3.9)$$

Aircraft parameters

The mass and moment of inertia were taken from the work of Cappuyns [7], and the stability derivatives of the Flying V were taken from the work of Ruiz Garcia et al. [31]. It is assumed that the value of K_{xz} is negligible based on the values reported by van Overeem [37].

It is chosen to make the split flap influence purely in terms of $C_{n_{sf}}$ instead of δ_{sf} . This allowed direct calculation of the required value of $C_{n_{sf}}$, without knowing the actual split flap geometry. This approach was possible as the behaviour of the ratios for $(C_Y/C_n)_{sf}$ and $(C_l/C_n)_{sf}$ with α were found to be roughly independent of the measured split flap sizes.

The rudder control derivatives were taken from Ruiz Garcia et al. [31], but they were adjusted to fit the decrease with angle of attack as mentioned by Johnson [6]. The derivatives of the other trailing edge control surfaces have not been taken from the report of Ruiz Garcia et al., as they did not evaluate each surface individually. These derivatives with respect to the control surfaces CS1, CS2 and CS3 were therefore calculated using wind tunnel data from Johnson [6], Erdinciler [33] and own captured data. At each time, only one of the two CS3 surfaces is used as aileron, either deflected upward or downward, so that the other wing can possibly deploy split flaps. It is assumed that the control surfaces and rudder have maximum deflections of 30 degrees, which is typical for trailing edge control surfaces according to Obert [38].

The yawing moment due to the inoperative engine ($C_{n_{OEI}}$) is calculated similarly as in section 3.1.3, but a better approximation of ΔT is implemented. The thrust of the working engine is set to maximum continuous power, which would be the worst-case scenario as suggested by the requirements. The additional drag of the inoperative (windmilling) engine is estimated using the work of Litt et al. [23], with the engine dimensions reported by Pascual [39]. ΔT is then the sum of the maximum continuous thrust of the working engine and the added drag of the windmilling inoperative engine.

Trim calculations

To show compliance with several CS-25 regulations, mostly trim calculations had to be performed. These calculations could individually be used to determine equilibrium input settings

to show compliance with the trim, sideslip or coordinated turn regulations. This ultimately means that the accelerations on the aircraft have to be zero. The trim calculations can give rise to how much $C_{n_{sf}}$ is required per each CS-25 regulation.

The trim functions are presented in equation (3.10). The purpose of the trim functions is that the asymmetric accelerations are kept at zero, so that a steady situation is created. The asymmetric accelerations can be simply deducted from the equations of motion, presented in equation (3.9). The trim functions can be solved for the values of β , ϕ , δ_{CS1} , δ_{CS2} , δ_{CS3} , δ_r and $C_{n_{sf}}$. Specific per situation, some of these values are prescribed, either by the requirement or the motion that is to be flown.

$$\begin{aligned}\dot{\beta} &= 0 \\ \dot{p} &= 0 \\ \dot{r} &= 0\end{aligned}\tag{3.10}$$

For the trim in roll, \dot{p} has to be made equal to 0. This can be done in an infinite amount of combinations of CS1, CS2 and CS3. It is therefore specified that first δ_{CS3} is calculated, then δ_{CS2} and lastly δ_{CS1} . Each deflection is calculated according to the amount of rolling moment that is required. If a calculated deflection is greater than the maximum deflection angle of 30° , the deflection angle is set to that maximum value of 30° , after which the next CS deflection can be calculated.

For the trim in yaw, \dot{r} has to be made equal to 0. This is done via the deflection of the rudder. The value for δ_r is calculated according to the amount of yawing moment that is required. Again, if the calculated deflection exceeds the maximum possible deflection angle of the rudder, it is set at that maximum deflection. If more yaw control is needed, the split flaps are deployed on one of the wings, giving rise to a required $C_{n_{sf}}$.

For the trim in steady sideslip, $\dot{\beta}$ has to be made equal to 0. In this case, a small bank angle ϕ is induced to offset the lateral forces. It is checked if this bank angle for steady heading sideslip remains below 5° , as prescribed by CS-25 [20].

For the trim in a level coordinated turn, the yaw rate of the aircraft is not kept at zero, but at a non-zero steady value. This creates a centrifugal force which offsets the lateral force components to keep the sideslip at zero. For coordinated turns, first the value of r is solved for, after which the values of δ_r , $C_{n_{sf}}$ and δ_{CS} are solved to trim for accelerations in yaw and roll.

Linear simulations

By rewriting the equations of motion into a state-space system, short linear simulations can be created for an arbitrary set of inputs of the Flying V. This is used for simulating yaw motions and bank-to-bank manoeuvres, according to the CS-25 regulations. As the equations of motion are quite simplified, these simulations will be mostly qualitative of nature, but can give insight whether these motions are critical for the lateral-directional control of the aircraft. No specific calculations of the amount of required $C_{n_{sf}}$ could be linked to these simulations however.

In order to simulate linear motions for a certain set of aircraft inputs, a state-space system is created in the form:

$$\dot{\mathbf{x}} = \mathbf{Ax} + \mathbf{Bu}\tag{3.11}$$

This is done by using the following relations:

$$\mathbf{P}\dot{\mathbf{x}} = \mathbf{Qx} + \mathbf{Ru}\tag{3.12}$$

$$\dot{\mathbf{x}} = \mathbf{P}^{-1}\mathbf{Q}\mathbf{x} + \mathbf{P}^{-1}\mathbf{R}\mathbf{u} = \mathbf{A}\mathbf{x} + \mathbf{B}\mathbf{u} \quad (3.13)$$

Here, the state vector \mathbf{x} is given in equation (3.14) and the input vector \mathbf{u} is given in equation (3.15). They follow the same logic as the equation of motion, so matrices \mathbf{P} , \mathbf{Q} and \mathbf{R} can simply be adapted from equation (3.9). By using the state vector in equation (3.14), the sideslip angle, bank angle and yaw angle can be outputted from a linear simulation over a short period of time. The inputs and initial states are calculated using the trim calculations. At any time, the inputs are adjusted with the trim relations so that any required trim in roll or yaw is maintained throughout the manoeuvre. From the simulations, the compliance with CS-25 can be monitored for specific aircraft inputs and it can be indicated whether additional yaw power would be required from the split flaps.

$$\mathbf{x} = \left[\beta \quad \phi \quad \frac{pb}{2V} \quad \frac{rb}{2V} \quad \psi \right]^T \quad (3.14)$$

$$\mathbf{u} = \left[C_{n_{asym}} \quad C_{n_{sf}} \quad \delta_r \quad \delta_{CS1} \quad \delta_{CS2} \quad \delta_{CS3} \right]^T \quad (3.15)$$

Trim iteration

As the output of each trim loop will affect its own equilibrium state, an iteration loop is implemented. This is done both for the static trim calculations and the trim during the linear simulations. It is shown in figure 3.9 that sufficient iteration of the trim functions will give rise to a steady system. Here, the input of δ_{CS3} for an OEI level yaw motion is presented, where the input is calculated via the trim relation for roll and is iterated 100 times. It is seen that steady values of the δ_{CS3} input are found after about 10 iterations. All trim calculations are iterated 100 times to ensure a steady system.

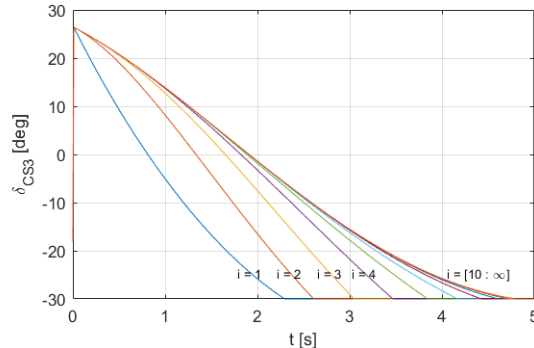


Figure 3.9: Example of the trim input of δ_{CS3} per iteration i .

Model limitations

As discussed, the flight mechanics model consists of a single set of simplified linearised equations of motion. This allows straightforward calculations of purely the asymmetric motions of the aircraft. It however also limits the accuracy of the model. The largest inaccuracies will be found far away from the symmetrical flight situation. In the situations that are specified in the requirements, bank angles up to 30 degrees are required. This will have an influence on the values of $\dot{\beta}$, $\dot{\phi}$ and $\dot{\psi}$. For the trim calculations in a coordinated turn, this will probably result in a slightly conservative yaw estimation, as the yaw rate will be somewhat overestimated. Furthermore, this will result in accumulative inaccuracies in the linear simulations. The simulations are therefore mostly qualitative of nature, in order to assess whether these are critical for the yaw power sizing of the aircraft. It is later shown that the simulations are

in fact not critical for the sizing of the split flaps. The setup of this model is therefore thought to not be too intrusive for calculation of the required $C_{n_{sf}}$. The consequences of the model simplification are highlighted in the validation process.

The effects of weight and balance have not been incorporated in the flight mechanics model. In reality, shifting centre of gravity positions will induce varying control surface effectiveness, due to a variation in their respective lever arm. This will in fact make the calculations slightly less conservative, as calculations for the most adverse centre of gravity location were not performed. Further aft centre of gravity locations would require larger split flaps, as the rudders would become somewhat less effective.

The longitudinal parameters of the aircraft have been neglected. This also includes any required trim elevator deflections or required thrust variations due to split flap deflection. Velocity, thrust or pitching rates changes could also influence the asymmetric states of the aircraft.

3.3.2. Reynolds number scaling

The certification has to be performed with the full size Flying V characteristics. However, due to small Reynolds numbers during the experimental testing of the Flying V sub-scale model, some discrepancies are expected with respect to a full-scale aircraft. Most notably for the final sizing, the maximum lift coefficient and lift curve slope are underestimated during the wind tunnel testing. These parameters are important, as they determine the reference velocities for the calculations.

The absolute maximum lift coefficient of the wind tunnel model, as reported by Viet [26], is equal to 0.95 at $\alpha = 28.5^\circ$. In their report also a 'safe' stall lift coefficient was reported as equal to 0.73 at $\alpha = 20^\circ$, where a pitch break changes the sign of the static stability. This latter condition is used as the maximum usable lift coefficient. It is assumed that the pitch break tendency of the Flying V is not significantly altered by larger Reynolds numbers. The maximum usable lift coefficient is therefore taken at 20 degrees angle of attack.

Using the full scale $C_{L\alpha}$ from the work of Oosterom [40], with the zero-lift angle of attack, the maximum usable lift coefficient is estimated to be equal to 0.915 at $\alpha = 20^\circ$. With this value of $C_{L_{max}}$, the reference stall speed V_{SR_1} can be calculated.

It is reported by Barlow et al. [30] that the larger Reynolds number can also increase the control surface efficiencies. However, applying corrections for the control surface efficiency would be quite ambiguous. Judging on the work of Obert [38] or Jiang et al. [41], the amount of efficiency increase is very case sensitive. No Reynolds number corrections are applied to the control derivatives. This leaves a conservative split flap size estimation, as the control power of the rudder is expected to increase. In order to better consider changing control derivatives, a sensitivity analysis is performed, which is explained in section 3.3.4. It is also assumed that the behaviour of the split flaps is not really affected by Reynolds effects, since the flaps mainly work through creating pressure drag. It is shown by Hoerner that pressure drag does not increase over these ranges of Reynolds number [21]. As the sideforce of the split flaps seems to be linked to its created lift, it is possible that the split flap yaw effectiveness is also slightly increased with Reynolds number. Such an effect is however neglected, which would again leave a slightly conservative split flap design.

3.3.3. Sizing calculations

In summary, table 3.1 states the requirements which are solved for, together with its standard configuration settings. In each calculation, $C_{n_{sf}}$ is taken as a variable for which the minimum needed value is calculated to show compliance with the CS-25 regulations. Of these requirements, only CS 25.147(a) and CS 25.147(d) have to be solved with a linear simulation and

Table 3.1: Summary of each tested requirement, including way of testing and settings.

Requirement	Subject	Velocity	Weight	Thrust
CS 25.143(h)	Manoeuvrability	V_2	MTOW	OEI
CS 25.147(a)	Directional control	$1.3V_{SR_1}$	MLW	OEI
CS 25.147(c)	Lateral control; general	$1.3V_{SR_1}$	MTOW	OEI
CS 25.147(d)	Lateral control; roll response	V_2	MTOW	OEI
CS 25.161(b)	Lateral and directional trim (sideslip)	$1.3V_{SR_1}$	MTOW/MLW	-
CS 25.161(d)	Longitudinal, directional, and lateral trim	$1.3V_{SR_1}$	MTOW/MLW	OEI

can be taken as indicative of whether additional yaw power would be needed during these motions. The other requirements can be solved using only the trim calculations, which can give rise to a specific required $C_{n_{sf}}$.

Several of the requirements have different velocity specification. Most of these are in relation to the reference stall speed (in a certain configuration) V_{SR_1} . This quantity is dependent on the specified weight of the aircraft, which varies per certification requirement. Additionally, V_2 is defined in the present study to be equal to $1.13V_{SR_1}$, which is the minimum value for this speed [20]. It is assumed that the velocity and angle of attack are constant throughout the manoeuvres.

When all regulations are handled, the most critical values of required $C_{n_{sf}}$ will be known. From this, the eventual split flap size can be calculated for a certain chosen δ_{sfmax} . With the experimental data on the split flaps, the behaviour of $C_{n_{sf}}/S_{sf}$ versus α can be set up. This is done for the different sizes of split flaps and different values of δ_{sf} . If this curve is then coupled with the required $C_{n_{sf}}$ (for a certain α), it can be calculated how much surface area is needed from the split flap geometry.

Now knowing the required surface area, the final width of the split flaps can be calculated. The surface area as a function of split flap width has a relation as described in equation (3.16), which is found by fitting the surface area for SF10, SF15 and SF20. Finally, the needed split flap width can be calculated using this relation. Note that the calculated width will be in terms of the 4.6% sub-scale geometry, but with the scaling factor this can directly be extrapolated to the full-scale aircraft, as $C_{n_{sf}}$ is for now assumed to be independent of Reynolds number.

$$S_{sf}[mm^2] = 0.05591 \cdot b_{sf}[mm]^2 + 89.96 \cdot b_{sf}[mm] - 0.726 \quad (3.16)$$

3.3.4. Sensitivity analysis

At this point in the design phase, there are still some performance uncertainties with respect to the full scale aircraft. For instance, it might be possible that due to scaling effects, the rudder is more effective than previously thought. As a result, less yawing moment is required from the split flaps. A sensitivity analysis is performed to check what small changes in input parameters will do to the amount of required split flap yawing moment. The sensitivity analysis is performed only for the most critical CS-25 cases. This gives insight in the most influential input parameters and it gives rise to the certainty of the calculated required $C_{n_{sf}}$.

The investigated input parameters are:

- **Stability derivatives** - the stability derivatives are estimated using sub-scale flight testing, as reported by Ruiz Garcia et al. [31]. Due to Reynolds effects, and the relation of several stability derivatives with lift and drag coefficient, there is some uncertainty in the used stability derivatives with respect to full-scale stability derivatives.
- **Control derivatives** - the control derivatives are estimated using a combination of wind tunnel testing and sub-scale flight testing. Obert suggests an increase in control

derivatives from wind tunnel results to full-scale free flight results due to Reynolds effects [38], sometimes up to a 20% increase.

- **Maximum split deflection angle** - the parameter δ_{sfmax} is an important factor in the amount of yaw power that can be created. While the maximum value of 60 degrees will be used for the recommended geometry, it might be that the aircraft manufacturer will put a constraint on δ_{sfmax} , due to complexity or structural issues. Changing δ_{sfmax} will ultimately require a larger S_{sf} and thus larger b_{sf} .

It is difficult to quantify the amount of uncertainty for each of these parameters. An arbitrary maximum uncertainty of 20% is set for the sensitivity of the stability and control derivatives. Each parameter is evaluated for changes between -20% and +20%. The value of δ_{sfmax} is evaluated between 10 and 60 degrees.

4

Verification and Validation

In order to establish the confidence of the results, several validation and verification steps have been taken. This section will elaborate on these steps, and what their influence will be on the thesis results.

4.1. Short term repeatability

The short term repeatability of the experiments is evaluated by calculating the uncertainty levels for the datapoints. The uncertainty levels for all 6 aerodynamic coefficients are plotted in figure 4.1. This figure shows the uncertainty levels for a 95% confidence interval, for both a clean wing and a wing including split flaps. The uncertainty levels are considered low, as the errorbars are generally much smaller than the absolute difference between the measurements of the clean wing coefficient and the split flap coefficients. This means that the confidence in the resulting deltas can be guaranteed.

The observed maximum uncertainty levels are presented in table 4.1. Here, it is seen that for all parameters, except the drag coefficient, the calculated measurement uncertainty is increased with the addition of split flaps. A simple explanation for this is that the split flaps cause large unsteady patterns, which increase the vibrations (and thus the uncertainty) of the model. The increase in vibrations was also visually noted during the wind tunnel tests.

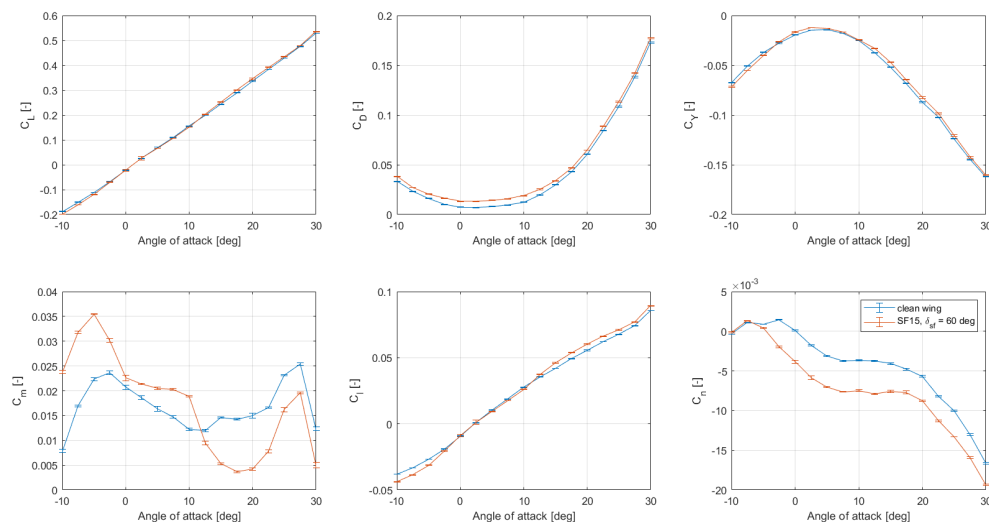


Figure 4.1: Errorbar plot of the measurement uncertainty for a clean wing and a wing including split flap. Uncertainty is calculated using a 95% confidence interval.

Table 4.1: Maximum uncertainty values found from figure 4.1.

Coefficient	Clean wing	SF15, $\delta_{sf} = 60$ deg
C_L	2.15e-3	7.49e-3
C_D	9.57e-4	7.22e-4
C_Y	5.65e-4	8.48e-4
C_m	5.19e-4	5.86e-4
C_l	4.50e-4	1.52e-3
C_n	1.43e-4	2.33e-4

4.2. Long term repeatability

In order to investigate the long term repeatability of the wind tunnel campaigns, a look is taken at the studies performed by Johnson [6] and Erdinciler [33]. Several other studies have also investigated the aerodynamic properties of the Flying V wind tunnel model, but they did not include the winglet, which was featured in the current research. The long term repeatability is investigated in terms of lift, drag and yawing moment of the clean wing.

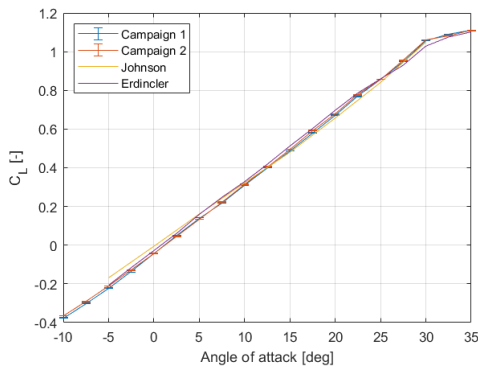


Figure 4.2: Lift coefficient repeatability. Errorbars are included with a 95% confidence interval.

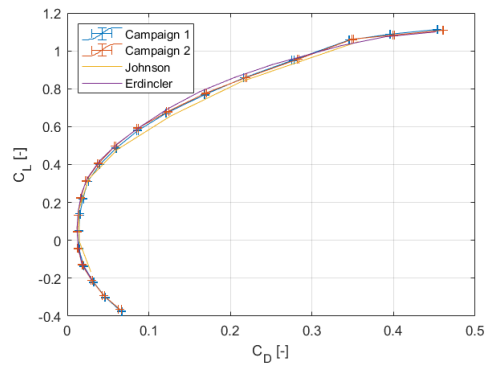


Figure 4.3: Drag polar repeatability. Errorbars are included with a 95% confidence interval.

The lift curve is presented in figure 4.2. It can instantly be seen that the results from the two wind tunnel campaigns match quite well in terms of slope and stall behaviour, which makes the confidence in the repeatability between the campaigns larger. Several small differences can however be seen when comparing the current research with the results of Johnson and Erdinciler. Starting with the lift curve of Johnson, it is seen that the lift curve slope of the current research is slightly higher. It is thought that this is due to small differences in the setup of the wind tunnel model. Each wind tunnel campaign, the wind tunnel setup is created with the same individual components. However, as the setup is quite large, and many components have to be bolted/screwed together to create the whole setup, some small differences in mounting angle of the wing can easily be introduced. It is therefore thought that the smaller $C_{L\alpha}$ from the work of Johnson is because of a slightly higher mounting angle, as exaggeratedly illustrated in figure 4.4. This would have increased the effective sweep of the wing, and thus decreased the lift curve slope.

It is seen that the current research matches quite well with the clean lift curve of Erdinciler in terms of lift curve slope and stall onset. It is observed however that they have a slightly higher absolute C_L . This difference possible stems from the fact that angle of attack calibration is performed by eye, by adjusting the zero angle of attack point so that the wing root section is matched with a guidance laser line. This can again create some small differences between researches. It is suggested that the work by Erdinciler has a somewhat larger incidence angle

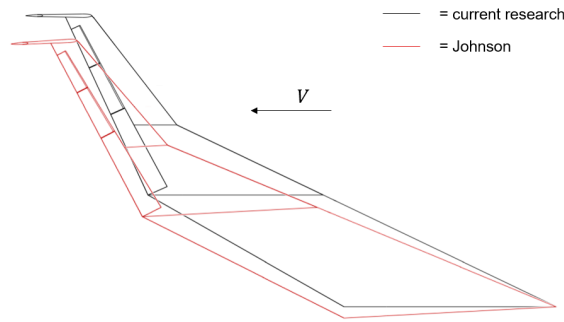
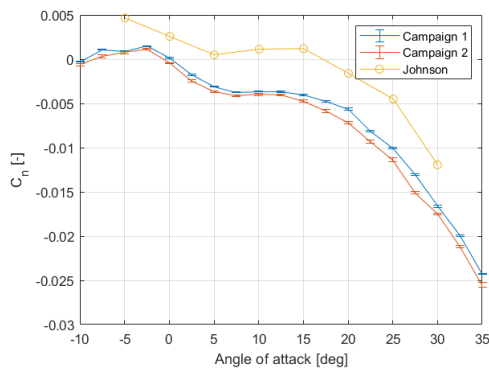
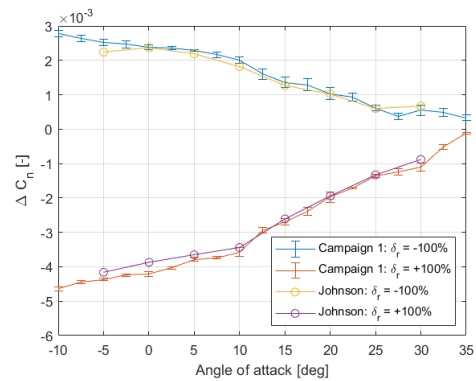


Figure 4.4: Illustration of difference in setup mounting angle

Figure 4.5: Repeatability of the calculated absolute C_n between the current research and the research by Johnson. Errorbars are included with a 95% confidence interval.Figure 4.6: Repeatability of the calculated ΔC_n between the current research and the research by Johnson. Errorbars are included with a 95% confidence interval.

as zero-point.

When looking at the drag polars in figure 4.3, it is again seen that there is a large overlap between the campaigns, further ensuring similarity between the two wind tunnel campaigns. It is seen that for low values of lift, the drag polars of the studies are very similar. The difference in curves are mostly present away from the zero-lift point. It is suggested that the differences in drag polar of Johnson are mostly due to the lift induced drag. It thus follows similar reasoning as the differences in lift polar, which are already discussed.

As the research mainly focuses on creating additional yawing power for the Flying V, also a look is taken at the repeatability of the yawing moment results. Only 1 previous paper was found in which the yawing moment of the Flying V was presented, which is the work by Johnson [6], in which the effect of rudder deflection was evaluated. The absolute yawing moment of both wind tunnel campaigns and the results of Johnson are presented in figure 4.5. Here it can be clearly seen that there is a large offset between the previous work and the current results, while the behaviour with increasing angle of attack seems to be similar. It is illogical that the majority of the yawing moment curve of Johnson is positive. The yawing moment coefficient should largely be negative, due to the positive drag and negative sideforce that the clean wing creates. The similar behaviour with α points to similarities in flow field, while the absolute value is shifted due to the difference in setup. The difference in mounting angle from figure 4.4 will cause the winglet rudder to have a higher incidence angle, causing an outboard sideforce and a positive yawing moment. Due to the large absolute differences, the question is raised whether the results of yaw can be presented with confidence.

The absolute value of C_n might be different, but the report mainly focuses on the deltas

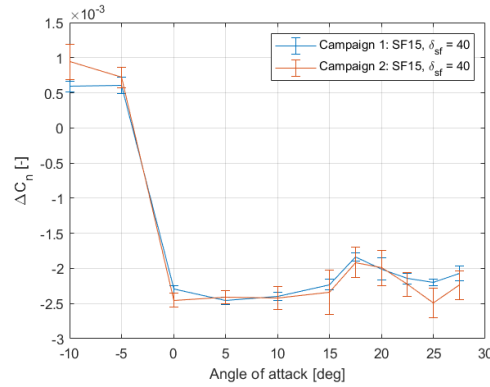


Figure 4.7: Repeatability of ΔC_n between wind tunnel campaigns. Errorbars are included with a 95% confidence interval.

that are found between configurations. The difference in yawing moment for rudder deflection of -100% and +100% is shown in figure 4.6. Here the results of Johnson are plotted together with the results of the first wind tunnel campaign, with similar model configuration settings as Johnson. It is observed that there is a high likeness between the data of Johnson and the current results, with exception of very low incidence angles, where the current research shows slightly higher rudder effectiveness. Overall, this shows that while the absolute term of C_n might differ, the parameter of interest ΔC_n can be accurately estimated. This makes that in terms of yawing moment coefficient, repeatability of the results is deemed sufficient.

Additionally, the repeatability between the two wind tunnel campaigns is evaluated by looking at the ΔC_n of a split flap configuration. This is shown in figure 4.7. It is here seen that there is a high resemblance between the campaigns, meaning that the presented deltas in this paper will be accurate.

4.3. Tuft photographs

Tuft photographs were taken to have an additional medium for explaining the behaviour of the measurements. The addition of yarn tufts is one of the easiest methods to visualise the flow field over the wing. In order to make sure that these tufts represent the flow field over the outboard wing accurately, a look is taken at the measurements with and without tufts attached to the wing, presented in figure 4.8. Here only very slight differences are found between the curves, as only very small portions of the wing are covered with tufts. The tufts cause a small decrease in lift behind the centre of gravity, causing the shift in pitching moment curve. Also an increase in drag is noticed. Both these differences are expected with the implementation of tufts [30]. The behaviour with angle of attack of the curves including tufts are similar to the behaviour of the clean wing. It is thus concluded that the tuft photographs accurately represent the flow field over the wing.

4.4. Verification of the preliminary design calculations

Figure 4.9 shows a comparison between the calculations from section 3.1.2 and the resulting test measurements. All results are shown for $\alpha = 0^\circ$, as the calculations are performed for this incidence angle. It can be seen that for small angles of deflection, the calculations for all the split flap sizes deviate a lot from the measurements. It is however observed that the calculations are close to the measurements for higher angles of deflection ($\delta_{sf} > 40^\circ$). This makes that the calculated preliminary design point, which is calculated for a 60° deflection angle, represents reality closely. If more split flap testing is to be performed in the future,

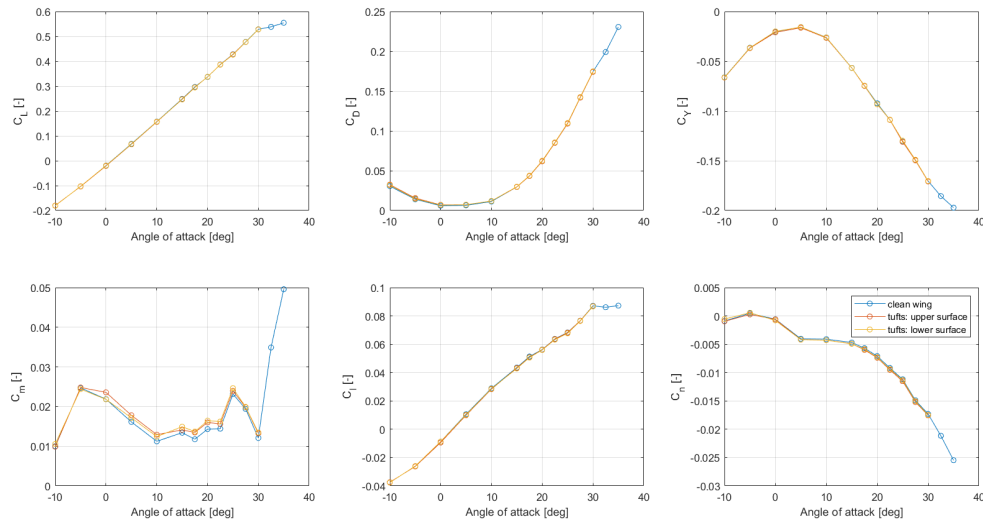


Figure 4.8: Comparison of the half-wing aerodynamic coefficients, with and without the implementation of yarn tufts.

a similar preliminary sizing method as presented in this paper can be used to estimate the performance around $\alpha = 0^\circ$.

It is observed that over the entire range of tested δ_{sf} , the calculated value of ΔC_n is slightly overestimated. A reason for this is that the resulting yaw is based on the increase in normal area due to the split flaps, and that the frontal area of the plain wing is not taken into consideration.

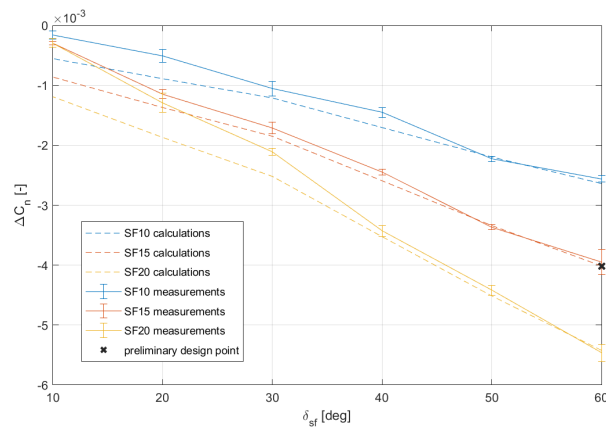


Figure 4.9: Comparison of ΔC_n calculations (according to section 3.1.2) versus test measurements. All results are shown for $\alpha = 0^\circ$. Errorbars are included with a 95% confidence interval.

4.5. Validity of split flap model placement

In order to mimic the split motion on the outboard wing of the Flying V, several 3D-printed flaps were placed on the most outboard CS3 control surface, as explained in section 3.1.1. It was assumed that the remaining CS3 volume in between the upper and lower split flap does not have a significant effect on the test results, as it is stationed in the wake of the split flaps. This hypothesis is outlined in the current section.

In order to do so, several additional configurations are tested in the wind tunnel with the

SF22 flaps. The regular cross section for which tests are performed is shown in figure 4.10, which represents test conditions throughout the report. A second cross section is shown in figure 4.11, which mimics the conditions for an actual working split flap, without volume in the centre. This split is created by deflecting CS3 upwards by either 10 or 20 degrees, and placing a lower split flap on the bottom so that the total deflection of the split is similar to its regular counterpart. Note that the brackets which hold the split flaps in place are still included in both cross sections.

Two separate notions on the setup of figure 4.11 have to be made here. First of all, the rotational axis of CS3 is not entirely the same as the rotational axis of the split flaps. This is however not to be too intrusive as the axes are very close to each other. Secondly, the upward rotations of CS3 to 10°/20° were performed by hand, as the control surface actuator was broken in a previous study. This means that there might be a very slight difference in split flap global rotational angle between the normal and verification setup.

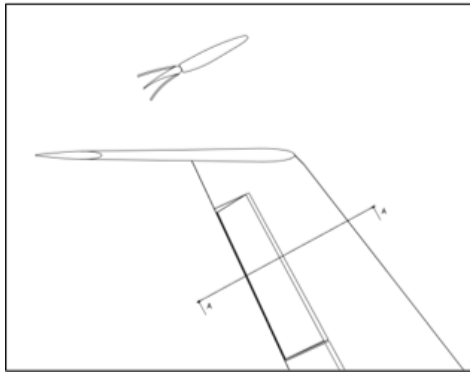


Figure 4.10: Top-side visualisation of split flap cross section in normal condition

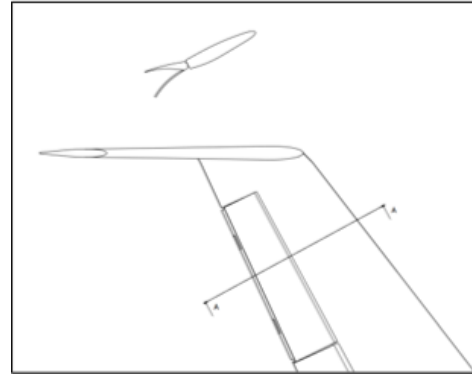


Figure 4.11: Top-side visualisation of split flap cross section for verification

Measurements are performed for $\delta_{sf} = 10^\circ$ and $\delta_{sf} = 20^\circ$, and both setups are compared to evaluate the influence of CS3. The outcome of the measurements is shown in figure 4.12. Here, the lines with the legend index including 'veri.' represent the situation depicted in figure 4.11. It can be seen that overall, both setups behave in a very similar fashion. Some small differences can however be noted in for instance the ΔC_n plot, where it is seen that the configuration without CS3 volume slightly outperforms the normal configuration. It is thus possible that the volume behind the flaps (CS3 volume + brackets) still have some effect on the outcome. Considering the differences, the split flap yaw behaviour presented throughout the report might be somewhat conservative. For now it is assumed that the differences are not very significant, as the uncertainties in most measurements have an overlap between the normal and verification run.

4.6. Validation of the flight mechanics model

The behaviour of the asymmetric flight mechanics model is benchmarked with data found in the report of Xie et al. [42]. In their report, a testing module was created using data of the single aisle Boeing 737-800 aircraft. Several asymmetric certification motions were evaluated in this report, for which an attempt is performed to mimic their dynamic behaviour.

In the current analysis, the moments of inertia of the Boeing 737-800 are taken from the report by Tian et al. [43]. This paper also provided the centre of gravity position of the aircraft. The stability and control derivatives for this aircraft are approximated by the use of AVL [44].

In order to assess the trim calculations, the CS 25.147(c) regulation for the trim in a 20°

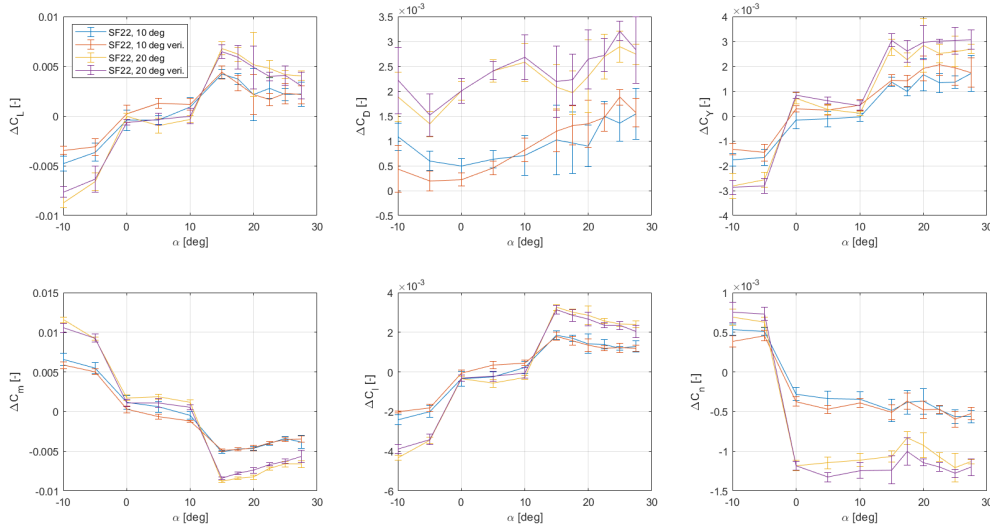


Figure 4.12: Errorbar plot of the measurement uncertainty for the regular and verification runs. Uncertainty is calculated using a 95% confidence interval.

Table 4.2: Verification of trim calculations for regulation CS 25.147(c)

Configuration	Velocity	ϕ	α	δ_r	δ_a
Take-off (OEI)	1.3 V_{SR1}	20	11.88	-15.45	-7.24
Take-off (OEI) [42]	1.3 V_{SR1}	20	11.59	-13.58	-7.38

banked turn (into the operative engine) has been compared between the studies. The results are shown in table 4.2. It is seen that the acquired values for the rudder and aileron deflection have the correct sign and have similar orders of magnitude. It is however observed that the trim rudder deflection δ_r has a slight conservative values. It is possible that the stability & control derivatives slightly differ between the studies, as this is something that could not be checked. For the remainder of the research it is taken into account that the trim calculations in the current research are possibly slightly conservative. The trim calculations are deemed sufficient to aid in the sizing of the split flaps at this stage of the design process.

Additionally, a bank to bank simulation is compared between the researches. CS 25.147(d) specifies that the aircraft, including adverse asymmetric thrust, has to be able to roll from 30° bank angle to -30° bank angle within 11 seconds [20]. Xie et al. have reported their simulation for such a motion, including the inputs of the aileron and rudder deflections [42]. Using the same inputs and initial conditions, a linear simulation is performed. A comparison between the results is plotted in figure 4.13. Here, it can be clearly seen that differences occur in the established roll angle ϕ . It is seen that in general, the behaviour of both attitudes over the course of the motion are similar. However, it is seen that errors are accumulated as time goes by, especially apparent for the roll angle. In terms of the regulation, the -30° bank angle is established after about 3 seconds, whereas the report by Xie et al. show a required period of about 3.5 seconds. It is thought that this large difference is mainly established due to the omitted influence of I_{xz} . For this reason, the linear simulations performed in this study should probably be taken as indicative. For short time periods, the simulations can give an indication whether the required bank to bank and yaw motions are critical for the lateral-directional control of the Flying V. This will give insight into whether sizing based on the trim calculations is sufficient, or additional sizing efforts should be implemented in the future. The simulations

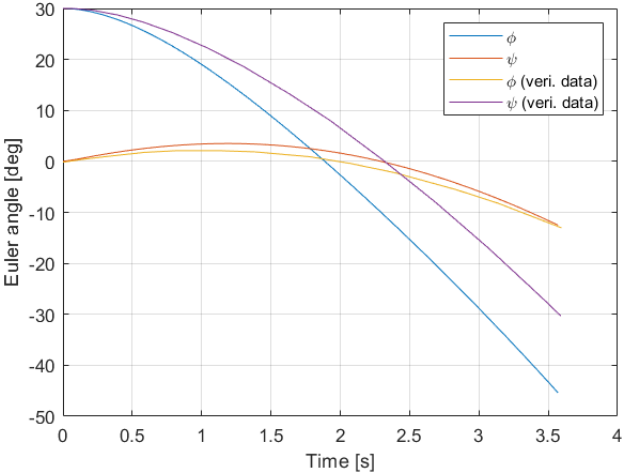


Figure 4.13: Comparison of the roll simulation for regulation CS 25.147(d)

should not be used to accurately predict the aircraft states for longer time periods.

5

Results and Discussion

This chapter will present and discuss the findings of the wind tunnel campaigns. It will begin with discussing the general influence of the addition of split flaps on the aerodynamic coefficients of the aircraft. This will mostly consist of the qualitative behaviour of split flaps with angle of attack. After this, it will further elaborate on split flap effects in terms of directional control. The effects of varying size and deflection angle will be evaluated, after which some control derivatives are set up. Next, any interference effects between the split flaps and the other control surfaces is discussed. Lastly, a look is taken at different possible split flap configurations which can mitigate its adverse effects on pitch and roll.

5.1. General effect of split flaps on aerodynamics

As split flaps are unconventional, it is hard to imagine the effect these devices have on the Flying V aerodynamic behaviour. This section will show the general effects of applying split flap deflection on the outboard wing. First, the effect of split flaps under varying angle of attack is discussed. Next, the effect of increasing the split flap deflection angle is highlighted. This section will lay the grounds for the fundamental understanding of split flaps on the Flying V, where the next sections will build on this knowledge to give more detailed conclusions.

5.1.1. Effect on aerodynamic forces

The behaviour of the force coefficients for the baseline SF15 configuration with several deflection angles is presented in this section. It will mainly show the general trends that are perceived by the aircraft with SF15 for a low, medium and high deflection angle of 10°, 30° and 50°. Similar trends have been seen in the other investigated deflection angles, but to keep the figures clear it was decided to only show 3 values. The split flaps have been found to influence the lift, drag and sideforce of the Flying V. Therefore, the lift coefficient C_L , the drag coefficient C_D and the sideforce coefficient C_Y are discussed. For each of the coefficients, both absolute values and incremental values are presented. The absolute values are presented as left-wing only results. The difference due to split flap deflection are calculated by subtracting the clean wing results. All coefficients are presented to cohere to the aircraft reference system as discussed in section 3.2.2.

Effect on lift coefficient C_L

The effect of split flaps on the lift coefficient is shown in figure 5.1, where both the absolute and the change in C_L is plotted.

Due to the higher inclination of the upper and lower split flap, with respect to the incoming flow, the pressure in these regions will increase compared to the clean wing. It is therefore expected that the lift coefficient is changed at several angles of attack. Prior to the experiments it was expected that at angles of attack around 0, the deflection of split flaps would not create

a large difference in lift force, as the downward deflected flap would create approximately as much lift as the upward deflected flap would create downforce. It is however observed from the graph of ΔC_L that around these small incidence angles, a small increase in lift is created. This is thought to be due to the difference in curvature between the upper and lower flap, where the concave structure of the lower flap would have more influence than the convex upper flap. The work of Johnson shows similar results, as he shows that per angle of deflection, the lift increase due to trailing-edge down deflection of CS3 is higher than the lift decrease of trailing-edge up deflection [6].

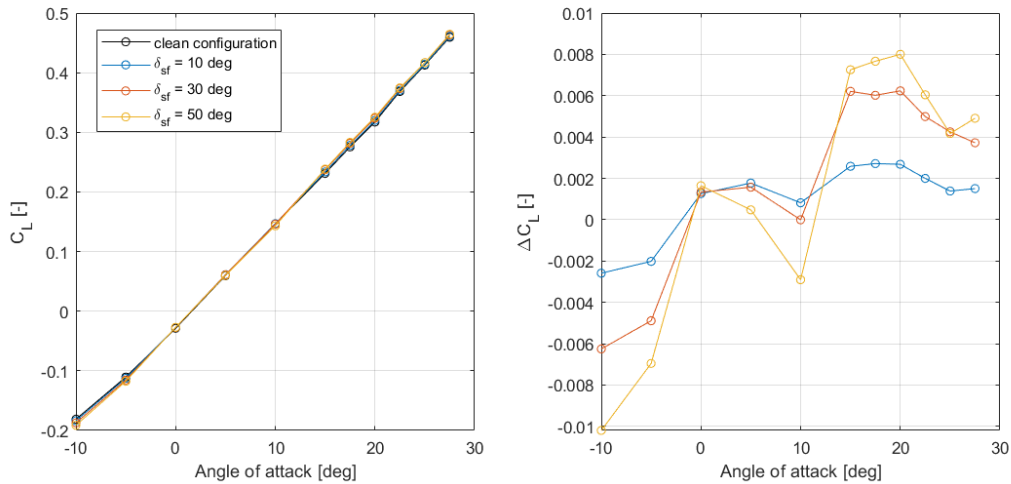


Figure 5.1: Lift coefficient behaviour of SF15

It can be seen in the graphs that the split flaps mainly have a larger influence on the C_L in the extremities of the investigated angles of attack. At negative angles of attack, a large decrease in lift coefficient is measured. It is suspected that this is due to the lower flap becoming less effective than the upper flap. With decreasing incidence angle, the lower side of the wing will start to show forms of tip stall. The leading edge around the wing tip will start to separate, especially since the outboard wing already has a -4.4° twist angle. This makes that a part of the lower split flap will become submerged in the wake of the main wing, decreasing the pressure on this side, while the upper flap is fully in the freestream. Subsequently, a net force is created in the negative lift direction. The tuft photographs in figures 5.2 and 5.3 cement this claim, where it can be clearly seen that the tufts on the lower surface show areas of separated flow in front of the location of the split flaps.

At medium angles of attack ($5^\circ < \alpha < 10^\circ$), it is observed that a decreasing lift force is created with angle of attack, especially for high deflections. It is thought that this is due to the orientation of the lower flap, which will become more orthogonal to the flow when α is increased. This will create more drag and less lift. For the upper flap, the opposite will happen.

It is clearly observed that some aerodynamic phenomena appears between $\alpha = 10^\circ$ and $\alpha = 15^\circ$. It is suggested that this all has to do with the formation of a vortex on the suction side of the wing, from the kink to the more outboard sections of the wing. The research by Viet [26] confirms the presence of such a vortex, as shown in figure 5.4. In his work, he discusses that this phenomena largely influences the flow structure of the outboard wing sections, around where the split flaps are located. The tuft pictures in figures 5.5 and 5.6 support this claim. By looking at the orientation of the tufts, it can be seen that a leading edge vortex over the upper surface of the wing is created around $\alpha = 15^\circ$, where the flow

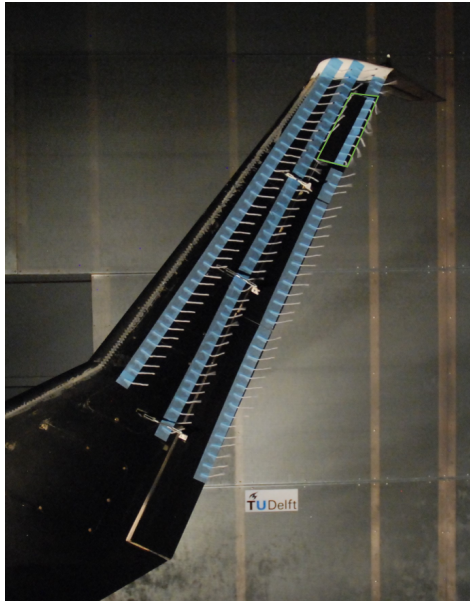


Figure 5.2: Tuft image of the outboard wing lower surface at $\alpha = 0^\circ$, including SF15 with $\delta_{sf} = 40^\circ$ outlined in green.

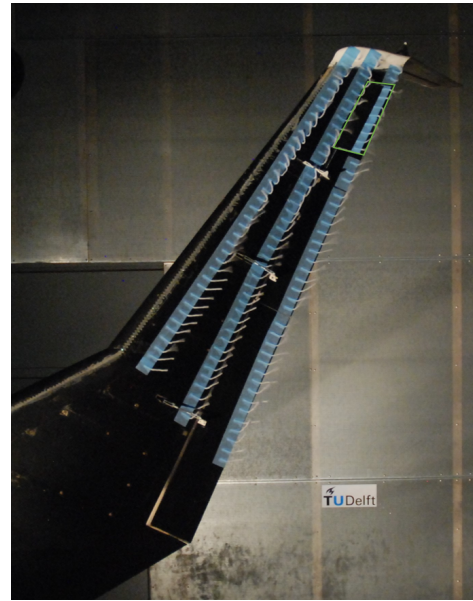


Figure 5.3: Tuft image of the outboard wing lower surface at $\alpha = -5^\circ$, including SF15 with $\delta_{sf} = 40^\circ$ outlined in green.

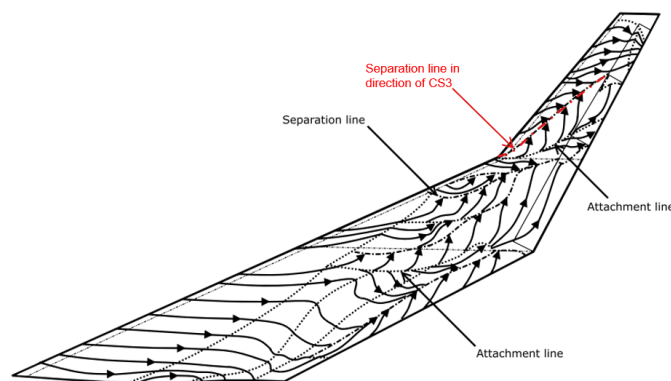


Figure 5.4: Depiction of vortex separation line at $\alpha = 15^\circ$. Adapted from Viet [26].

structure over the outboard wing is heavily altered. Judging by the orientation of the tufts, vortices and local separated flow field occur in the vicinity of the split flap on the suction side of the wing. This directly affects the performance of the upper split flap.

Lochert et al. show in their work that the upper surface of split flaps can have significant interaction effects with leading edge vortex structures [17]. In their work, it is shown that the high pressure on the top surface of the split flap is heavily decreased due to the low dynamic pressure near the core of the vortex. This makes the pressure difference over the upper split flap smaller, hence decreasing the forces and moment created by the upper flap. The large vortex interaction effect of the split flaps on the Flying V at $\alpha \leq 15$ is an important property of the split flaps in the current report and will be handled in various findings throughout this report. In terms of the lift, it can be concluded that the increase in ΔC_L is due to the decrease in effectiveness of the upper flap, caused by the creation of a leading edge vortex over the outboard wing.

After 20 degrees angle of attack the ΔC_L starts to drop again. This is thought to be due

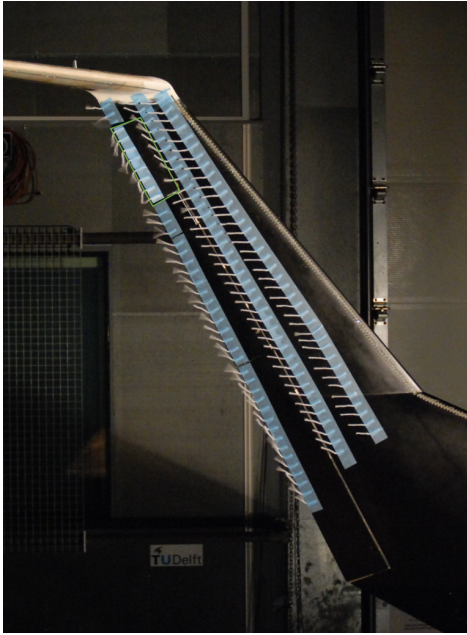


Figure 5.5: Tuft image of the outboard wing upper surface at $\alpha = 10^\circ$, including SF15 with $\delta_{sf} = 40^\circ$ outlined in green.

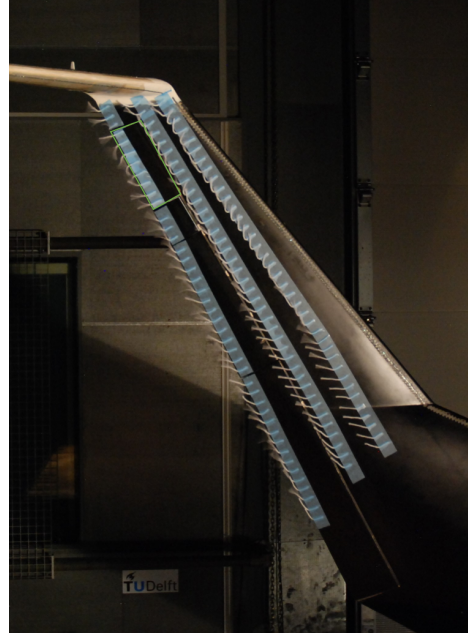


Figure 5.6: Tuft image of the outboard wing upper surface at $\alpha = 15^\circ$, including SF15 with $\delta_{sf} = 40^\circ$ outlined in green.

to a change in direction of the leading edge vortex, to a more inboard location. A tuft picture at $\alpha = 25^\circ$ is shown in figure 5.7. Here it is seen that the more inboard tufts are now heavily deflected, whereas the outboard tufts in front of the split flaps slightly retrieved their orientation, compared to the picture in figure 5.6. It is thought that the intensity of the vortex interaction of the upper split flap is therefore slightly decreased. The upper split flap starts to regain some downforce, creating less net lift over higher angles attack. Another reason for decrease in ΔC_L might again lie in the orientation of the lower flap, which will become even more orthogonal to the incoming flow.

Effect on drag coefficient C_D

The increase in drag is an important factor of the split flaps, as it is the main working mechanism to create yaw. Figure 5.8 shows the behaviour of the drag coefficient with angle of attack, of the Flying V including split flaps. It is seen that over the whole range of α , the drag is increased significantly by the split flaps, as expected from the increase of frontal area and separated flow.

Some clear features can be spotted in the ΔC_D behaviour, presented in figure 5.8. It seems like the increment in drag is characterised by a region of maximum added drag between $\alpha = 0^\circ$ and $\alpha = 10^\circ$. Here the increase in drag reaches a maximum value. It is suggested that this behaviour is due to the fact that neither the lower or upper surface of the main outboard wing show areas of disturbed flow. The relative increase of the wake area due to the split flaps is therefore large, which explains the large value of ΔC_D .

Next, both around $\alpha = -5^\circ$ and $\alpha = 15^\circ$ there seems to be a dip in created drag. The dip at $\alpha = -5^\circ$ has to do with the separation of the lower surface, where the clean wing would also see an increase in drag due to an area of separated flow. The addition of the split flap will become relatively less effective in adding to the total drag. At $\alpha = -10^\circ$, ΔC_D interestingly goes up again. Looking at figure 5.9, it is seen that the tufts on the outboard section of the split flaps are again slightly more aligned to the flow direction. This possibly points to some reattachment at this outboard location which would restore some of the pressure on the lower



Figure 5.7: Tuft image of the outboard wing upper surface at $\alpha = 25^\circ$, including SF15 with $\delta_{sf} = 40^\circ$ outlined in green.

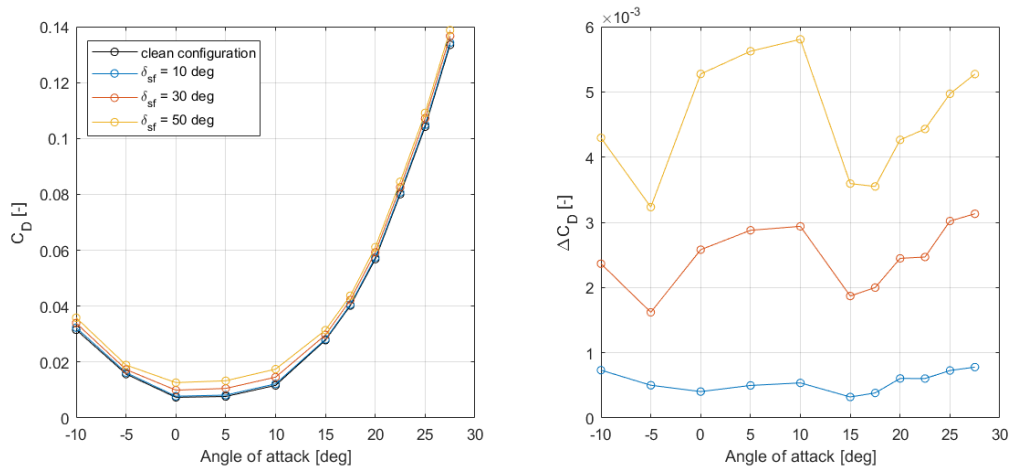


Figure 5.8: Drag coefficient behaviour of SF15

flap, explaining the renewed increase in ΔC_D .

At $\alpha = 15^\circ$, it is thought that interaction with the leading edge vortex will decrease the high pressure in front of the upper split flap, effectively decreasing the drag that is created by this flap. After the second dip at $\alpha = 15^\circ$, it is seen that the ΔC_D tends to increase again when further increasing the angle of attack. This is explained similarly as the decrease in ΔC_L from figure 5.1. The leading edge vortex from the wing kink moves more inboards, decreasing the interaction between the vortex and the upper split flap and restoring some of the pressure over the upper split flap.

As drag is an important factor in the aerodynamic performance of any aircraft, the percentile total drag increase due to split flaps is presented in figure 5.10. Here, the $\Delta C_{D_{sf}}$ of the left-wing deflected split flap is normalised with the total (full-wing) drag coefficient. This figure shows the significance of the drag increase due to the deflection of the split flaps. The percentile increase in drag is high between $\alpha = 0$ and $\alpha = 5$, where values nearing +40% are found for $\delta_{sf} = 50$. This is logical, as the clean drag coefficient is lowest around this incidence

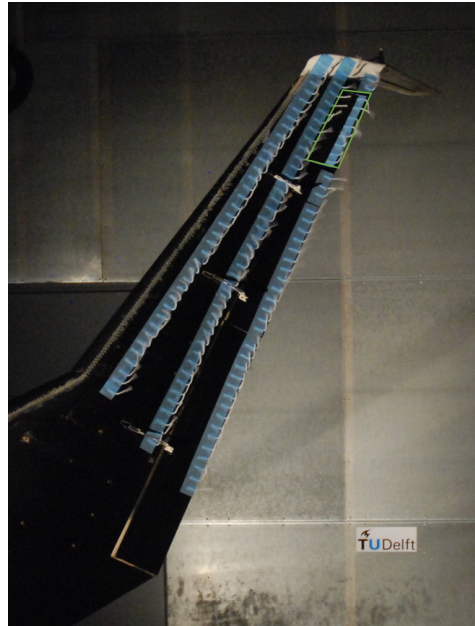


Figure 5.9: Tuft image of the outboard wing lower surface at $\alpha = -10^\circ$, including SF15 with $\delta_{sf} = 40^\circ$ outlined in green.

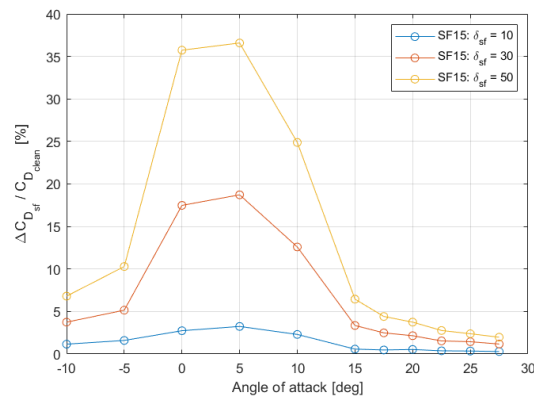


Figure 5.10: Total drag coefficient increase for several SF15 deflections

angle. At higher or lower angles of attack, the percentile increment in drag decreases to values below +10%. This is due to the high values of lift-induced drag in these ranges. Figure 5.10 can give an impression of the required change in thrust mapping when applying split flaps at each angle of attack. On the full-scale aircraft, the percentile drag increase is envisioned to be smaller than the values reported in figure 5.10, as the clean friction drag will increase due to Reynolds effects. Overall, the total drag of the aircraft is significantly increased when deflecting the split flaps. In a potential future split flap integration study, it should therefore be investigated whether enough excess thrust is available when split flaps are deployed during directionally demanding flight situations.

Effect on sideforce coefficient C_Y

The created sideforce is an important factor of the split flaps, as this parameter also determines the amount of yaw that is created. The variation of the sideforce due to split flaps is presented in figure 5.11. The ΔC_Y is negative over negative angle of attack, but becomes positive over when $\alpha > 0$. This is beneficial, as positive sideforce would aid to the created yawing moment.

Overall, the ΔC_Y that is created is thought to be related to the drag and lift values, via the positive sweep and positive dihedral of the outboard wing. The behaviour of ΔC_Y overall looks quite similar to the behaviour of ΔC_L from figure 5.1. It is suggested that due to the positive dihedral angle of the outboard wing, an increase in lift would create a positive (inboard) sideforce, while an increase in downforce would create a negative (outboard) sideforce. This is confirmed in the plots, where the sideforce has a negative value over the negative angles of attack and has a positive value over the positive angles of attack. Overall, the sideforce is offset by positive drag that is created, as positive drag force would create positive (inboard) sideforce due to the positive sweep of the split flap hingeline. This is most visible at $\alpha = 0$.

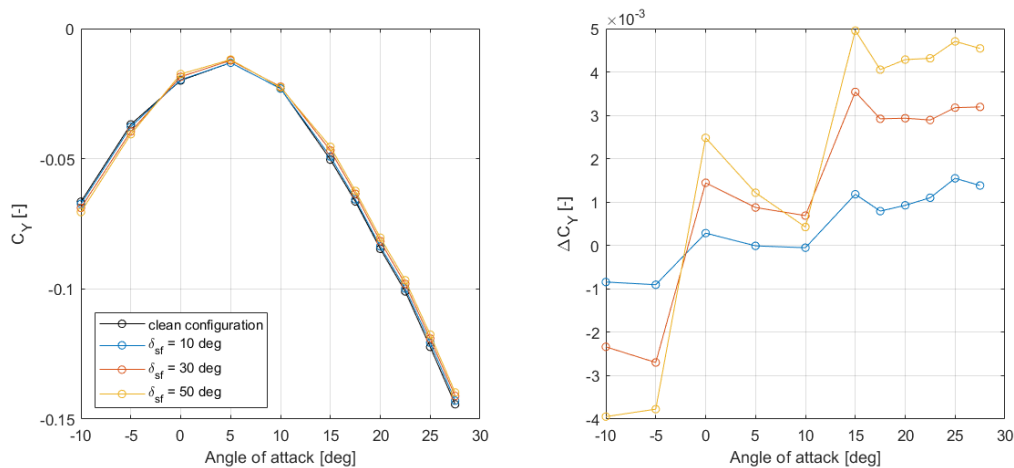


Figure 5.11: Sideforce coefficient behaviour of SF15

5.1.2. Effect on aerodynamic moments

Following the discussion on the behaviour aerodynamic forces with angle of attack, the aerodynamic moment coefficients for pitch (C_m), roll (C_l) and yaw (C_n) are discussed in this subsection. The effects largely follow from the differences in forces on the outboard wing, which makes the discussion of the aerodynamic moments less extensive. The yawing moment coefficient is however especially highlighted as it is the main driving parameter for the current research.

Effect on pitching moment coefficient C_m

The behaviour of the pitching moment is presented in figure 5.12. The differences due to the split flaps is a direct consequence of the variations that the flaps cause on the lift coefficient. The split flaps are located behind the centre of gravity. This means that a local increase in lift at this location will cause a negative (nose-down) pitching moment on the aircraft. Vice versa, a local downforce will cause a positive (nose-up) pitching moment. This is confirmed in figure 5.12, where the effect of split flaps on the pitching moment is plotted. When comparing the graphs of ΔC_m with the graph of ΔC_L from figure 5.1, it is clearly seen that the behaviour is very similar, but mirrored in the x-axis. In theory, the increase in drag would also create a nose-up pitching moment, as the flaps are above the centre of gravity. But this effect is not very noticeable, as the lever-arm is small.

Effect on rolling moment coefficient C_l

The effect of deflecting split flaps on the rolling moment coefficient is shown in figure 5.13. The curve of ΔC_l with angle of attack is again very similar to the lift curve of figure 5.1. It

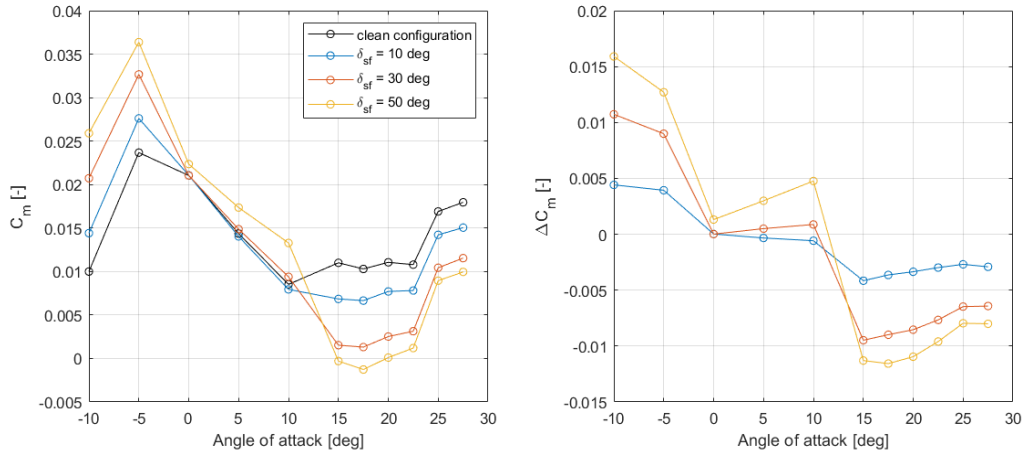


Figure 5.12: Pitching moment coefficient behaviour of SF15

follows a similar explanation as the pitching moment curve. The split flaps are located on the outboard wing, away from the centre of gravity. A local increase in lift (of the left-wing) will therefore cause an increase in rolling moment. If a right wing model would be investigated, a negative rolling moment would be observed.

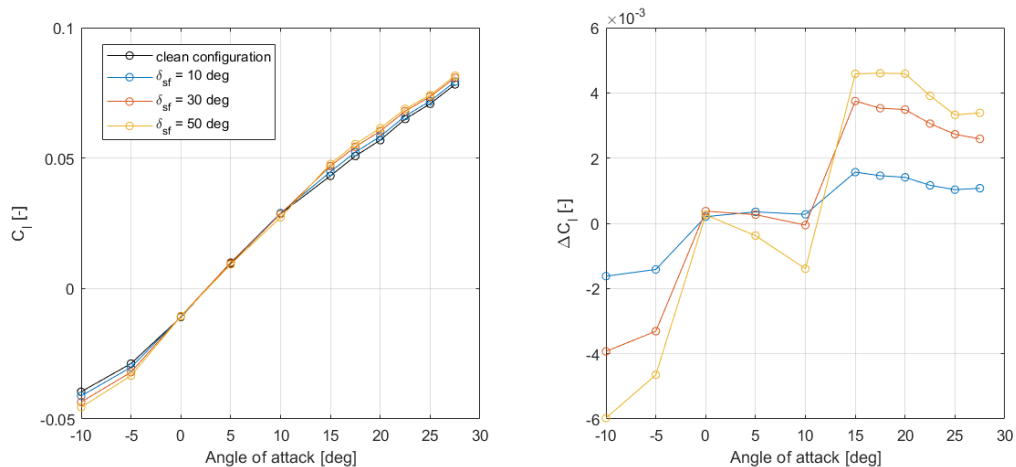


Figure 5.13: Rolling moment coefficient behaviour of SF15

Effect on yawing moment coefficient C_n

Creating additional yawing moment is the main purpose of this study. Before the yawing moment due to split flaps is thoroughly investigated in section 5.2, this subsection will give the basic properties of the created yawing moment.

The yawing moment coefficient behaviour of the wind tunnel model is shown in figure 5.14. The absolute values are presented as left-wing only results. The difference due to split flap deflection are calculated by subtracting the clean wing results. Note that as a left-wing model is used, negative yawing moment coefficients represent the desired nose-left moment. The yawing moment curve is expected to be a direct result of the increments in drag and sideforce due to the split flaps. Positive drag and positive sideforce should create negative yawing moment for the left-wing split flap.

Several clear features can be seen from the plots. First of all, it can be seen from the plot

of ΔC_n that at $\alpha < 0$, the split flaps lose virtually all their effectiveness as yawing devices. In fact, it seems that a small adverse yawing moment is caused at these incidence angles. This has to do with the stall of the lower surface, and the negative sideforce coefficient that is produced, as previously discussed. The negative sideforce counteracts the drag force, making the yawing close to zero over these negative angles of attack. The split flaps should thus not be used over negative angles of attack. Considering that the winglet rudders are still very effective in this range [6], the ineffectiveness of the split flaps at negative angle of attack is not an issue.

Next, it is seen that the desired negative yawing moment is gained when $\alpha \leq 0$. When compared to the winglet rudders, where the effectiveness is progressively decreased with increasing angle of attack, it is observed that the split flaps have a maximum effectiveness falloff around $\alpha = 17.5^\circ$. The split flaps only partially lose effectiveness, which is a promising feature compared to the winglet rudders. The dip in yawing moment coefficient is probably due to the interaction with the created kink leading vortex. As explained earlier, the upper flap loses pressure which results in a lower drag increase. This therefore results in a lower created yawing moment. Lochert et al. also show such a dip of yaw control power caused by the submersion of the upper split flap [17]. For $\alpha > 17.5$, the effectiveness of the split flaps is again slightly increased, which can be explained by the increase in drag over these angles of attack.

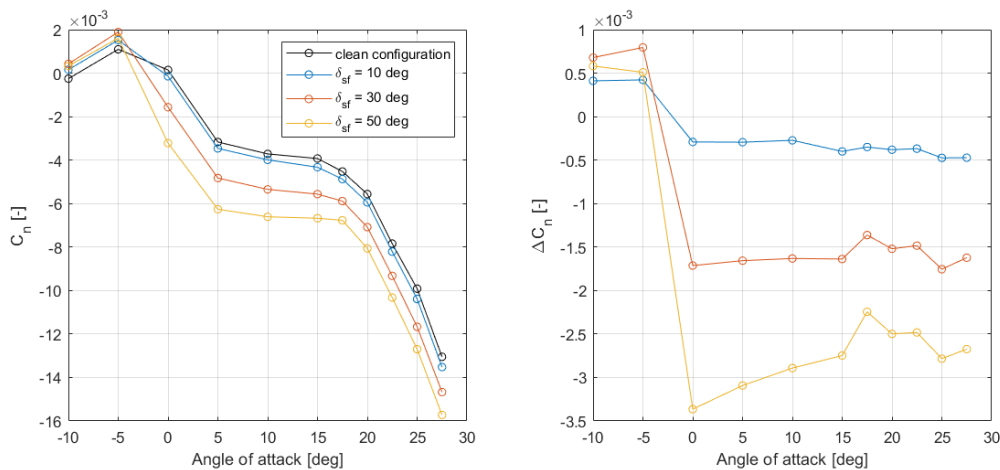


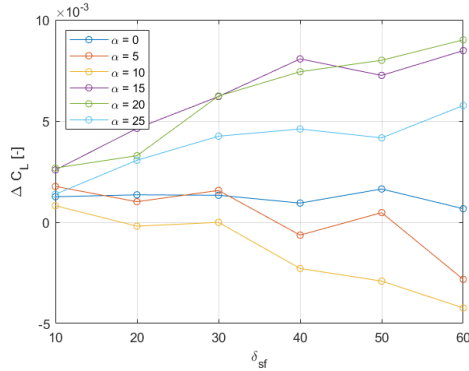
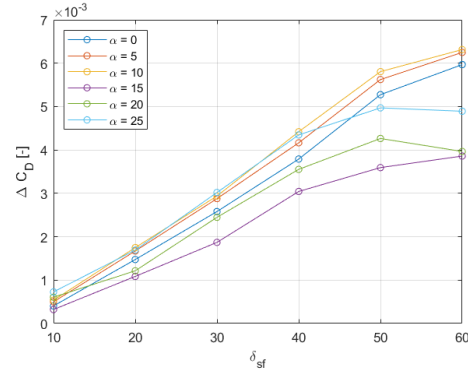
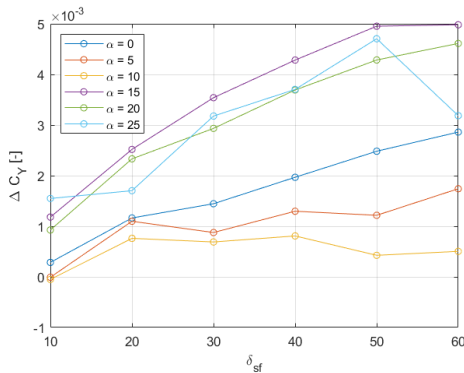
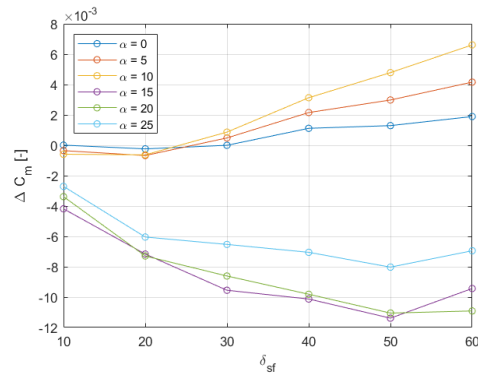
Figure 5.14: Yawing moment coefficient behaviour of SF15

5.1.3. Coupling effects and linearity of split flap deflection

Ideally, the split flaps would only create a yaw power without changing the pitch and roll parameters. Such coupling effects are however inevitable. A look is taken at the behaviour of aircraft parameters in comparison to the created yawing moment, in order to further assess the coupling effects of the split flaps and the linearity of the parameters with deflection angle. While the previous sections already discuss the general behaviour of split flaps with angle of attack, the current section further shows the effect of varying the split deflection angle δ_{sf} . It tries to elaborate on the challenges which come with the application of split flaps. The results presented in this section are for the SF15 configuration on the left wing, for δ_{sf} from 10 to 60 degrees.

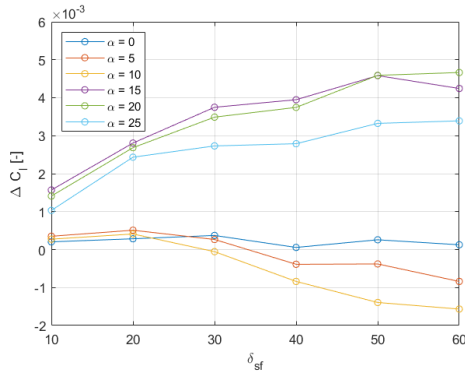
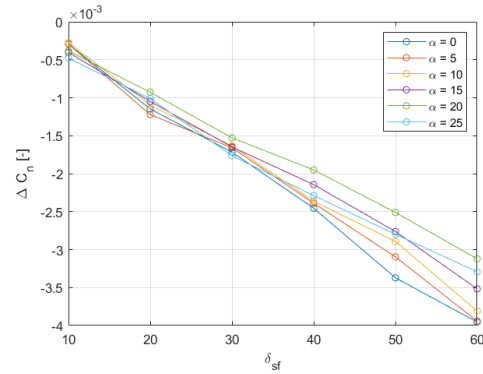
The behaviour of the deltas in each aerodynamic parameter with increasing δ_{sf} is presented in figures 5.15 to 5.20. These figures are presented together in order to more clearly discuss the coupling effects of split flaps, as well as the level of linearity of each parameter. In

these graphs it is highlighted how increasing the deflection angle will affect each aerodynamic parameter for several positive angles of attack. Negative angles of attack have not been looked at, since the split flaps are not effective yaw effectors in this range. Each delta can be compared to the behaviour of ΔC_{n_r} as they are the coupled consequence of deflecting the split flaps to create a certain target yawing moment.

Figure 5.15: δ_{sf} vs ΔC_L Figure 5.16: δ_{sf} vs ΔC_D Figure 5.17: δ_{sf} vs ΔC_Y Figure 5.18: δ_{sf} vs ΔC_m

Let us first focus on the level of linearity of each parameter. It is observed in figure 5.20 that ΔC_n is rather linear with δ_{sf} for each presented α . The same can be said of ΔC_D , up till very high δ_{sf} . The fact that the device is linear with respect to yaw is a useful property of the split flap behaviour, as it makes the needed δ_{sf} for a target yawing coefficient easy to extrapolate. Looking at the graphs for the lift, sideforce, pitch and roll, in figures 5.15 and 5.17 to 5.19, it is however seen that these properties show less linear behaviour with increasing δ_{sf} . Also, a larger spread is observed when increasing α , due to the creation of the leading edge vortex around $\alpha = 15$. The linearity of split flaps in yaw, but non-linearity in other aerodynamic parameters is confirmed in the report by Dorsett and Mehl [11].

For low angles of attack, the coupling effects can be kept small, but at $\alpha > 15$, the coupling effects go towards their maximum influence. The findings are similar to the reported results of Lochert et al. [17], where at low α the coupling effects were kept small. When increasing α , the coupling effects grew significantly due to the upper flap ineffectiveness. The maximum order of magnitude of the values of ΔC_L , ΔC_m and ΔC_l are similar to the values found for CS3 deflections, as presented by Johnson [6]. The coupling of the split flaps are therefore deemed significant and can not be neglected in the creation of an aerodynamic model. Due to the slight non-linearity and large spread with angle of attack, ΔC_L , ΔC_Y , ΔC_m and ΔC_l can however

Figure 5.19: δ_{sf} vs ΔC_l Figure 5.20: δ_{sf} vs ΔC_n

be difficult to adopt in such a model.

The differences in lift, pitch and roll for a certain target ΔC_n are considered as adverse coupling effects as additional control surface or attitude inputs have to be given to trim these forces and moments away. These deflections will cause further drag increases, and sometimes even counteracting yawing moments. Efforts to minimise the adverse differences in pitch and roll are therefore later discussed in section 5.4.

5.2. Effect of split flaps on directional control in detail

As mentioned, the current research investigates the application of split flaps in order to increase the directional control power of the Flying V. Thus far it is shown how the increase in yawing moment generally acts for varying α and δ_{sf} . This section will dive deeper into the measured yawing moment of the wind tunnel model in different configurations and will discuss further how the split flaps can be used for the Flying V.

5.2.1. Comparison with winglet rudders

In order to provide the significance of the yaw values presented in previous sections, a comparison is made with the current winglet rudders. These are the only devices to which a direct comparison can be made. This section will show in which regions the application of split flaps can become especially beneficial. The comparison in terms of ΔC_n is presented in figure 5.21. Here, the accumulated winglet rudder yawing moment of the two rudders is presented for several model deflection settings, against one SF15 split flap for several deflection angles. The values of the winglet rudders is taken from Johnson. The maximum rudder setting of 100% corresponds to an average rudder deflection of 22.98° [6].

It is seen from this figure that the split flaps have a much steadier decrease of ΔC_n with increasing angle of attack. The split flaps can therefore especially be a major contributor to the total yawing power at higher angles of attack. Where the SF15 flaps at 50° increase maximum model directional control at $\alpha = 0^\circ$ by about 55%, the model directional control power can be increased by about 150% at $\alpha = 27.5^\circ$. Note that this graph does not specifically represent how much the yawing power the Flying V will gain from split flaps, as the geometry size and maximum deflection angle is not yet fixed. This is later investigated in section 3.3.

5.2.2. Effect of split flap size

In the previous section, only results for the SF15 configuration were presented. However, for the final split flap sizing, it is very well possible that a smaller or larger size is eventually needed. Therefore, the effects of size is investigated in the current section. The placement is

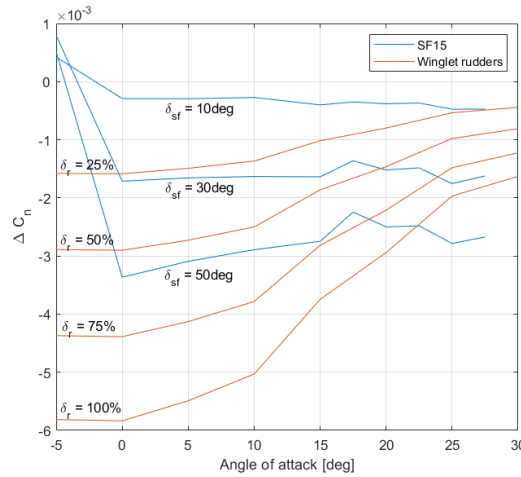


Figure 5.21: Yawing moment comparison of SF15 and winglet rudders

consequently also taken into account, as this is restricted by the size of the flap.

In addition to the presented trends of the SF15 split flap, the trends of different split flap deflections for SF10 and SF20 with α are shown in figures 5.22 and 5.23. Obviously, a larger magnitude is created by SF20 and a smaller magnitude for SF10, due to difference in split flap area. Aside from the magnitude however, the trends of ΔC_n with α are very similar. No significant differences can be noted at this point.

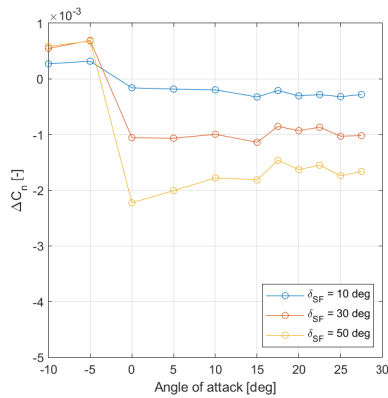


Figure 5.22: ΔC_n behaviour of SF10

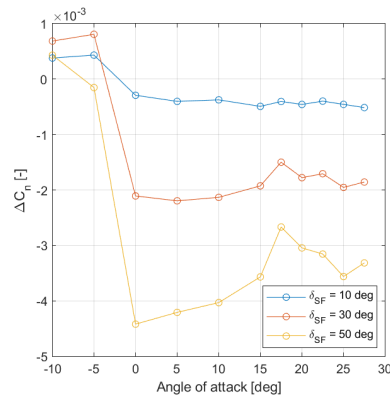


Figure 5.23: ΔC_n behaviour of SF20

In order to investigate whether size has a significant contribution to the split flap effectiveness, the aerodynamic parameters for each configuration are here normalised with their respective split flap area (S_{sf}). The total areas of the split flaps are documented in table 5.1. Figure 5.24 shows the ΔC_n , normalised by the respective split flap total surface area, over the positive range of angle of attack.

Table 5.1: Total surface areas of the split flaps (summation of upper and lower surface area) in mm².

SF10	SF15	SF20
9554.72	14751.77	20228.39

It should be directly noted here that the differences in $\Delta C_n/S_{sf}$ between the three split flap configurations is not considered very significant, as a large portion of the error bars overlap between the sizes. The consistency with differing b_{sf} makes this parameter very useful in the

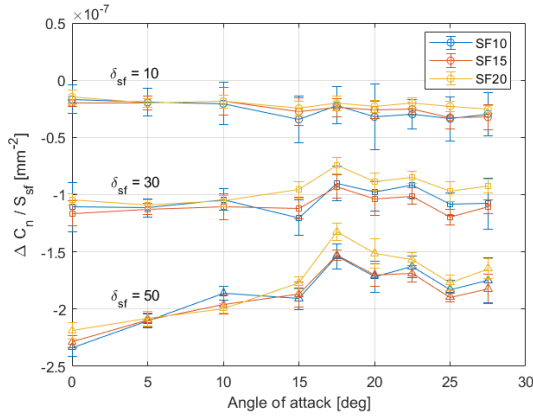


Figure 5.24: Normalised yawing moment $\Delta C_n/S_{sf}$, including 99% confidence error bars.

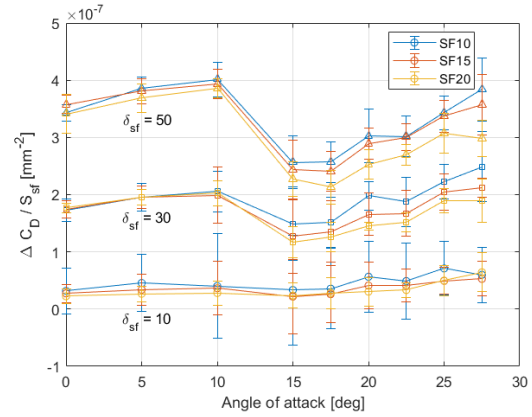


Figure 5.25: Normalised drag force $\Delta C_D/S_{sf}$, including 99% confidence error bars.

later sizing procedure in chapter 6. Neglecting the overlap in error bars, it can still be seen that the larger SF20 split flap is generally slightly outperformed by the smaller flaps over a large portion of the angles of attack. The smaller yawing moment per unit surface area of larger split flap can be explained by the average moment arm of each flap. All three sizes are located as far outboard as possible and flap width is increased towards the root of the wing. This means that the average lever arm becomes smaller when the split flap width is increased. Additionally, it is shown in figure 5.25, that less drag is created per unit surface area for the larger split flaps, especially at higher angle of attack. This further explains the difference which is seen in figure 5.24.

5.2.3. Split flap yaw control derivatives

It was noticed in section 5.1.3 that the yaw increase with δ_{sf} is roughly linear. Here, also a varying effectiveness with α was observed. It is therefore proposed in this section to set up a control derivative for the split flaps in terms of ΔC_n . It is chosen not to investigate control derivatives for the remaining aerodynamic parameters, as less linear behaviour was found for these parameters.

An example of the ΔC_n versus deflection angle for the SF20 configuration is presented for two different angles of attack in figure 5.26, which shows how the control derivative is set up. Here, also a linear regression in the form of $f(x) = a + bx$ is included. The reason for the non-zero intercept term a in this regression is probably because of the split flap being submerged in the main wing boundary layer for very small deflection angles. These very small deflection angles would therefore not result in any significant ΔC_n .

The control derivative $C_{n\delta_{sf}}$ is set up by linear regression, for each SF10, SF15 and SF20. Figure 5.27 shows the calculated control derivative for the three different split flap sizes, over the positive range of angles of attack. It can be seen in this figure that the behaviour of the control derivative is similar to the behaviour of the increase in the incremental C_n , shown in figure 5.14. The effectiveness goes down with angle of attack, up until a maximum decrease at $\alpha = 17.5^\circ$, after which the effectiveness slightly increases again.

An asterisk has to be made with figure 5.27, as the linearity of the control derivative can not be guaranteed with confidence over all angles of attack. Therefore, the coefficient of determination (R^2) of the linear regression is calculated. This term expresses the degree of linearity in the regression [35]. The R^2 value is presented in figure 5.28. Here it can be noted that only the calculated $C_{n\delta_{sf}}$ over the positive angles of attack have higher values of R^2 . It

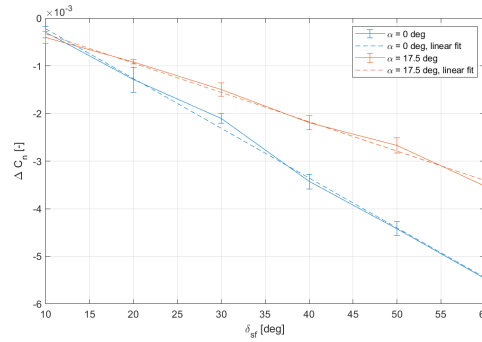


Figure 5.26: Example of yaw effectiveness of SF20 including linear fit. Error bars are included with a 99% confidence interval.

is seen that for these positive values of α , the calculated R^2 value is largely over 0.9. There are generally no target values for R^2 , as its meaning depends on the used regression and its interpretation for the problem, but 0.9 is considered a appropriate degree of linearity for the current research. The linear control derivatives are therefore only considered valid over the positive range of angles of attack. This is not of influence, as it was previously shown that the split flaps are ineffective when $\alpha < 0^\circ$ and should not be deployed here.

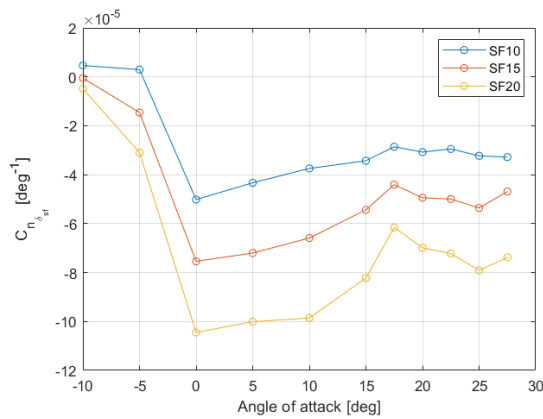


Figure 5.27: Linear split flap yaw control derivatives

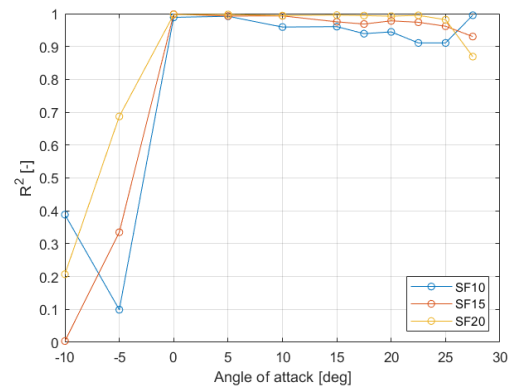


Figure 5.28: R^2 values of the linear split flap yaw control derivatives from figure 5.27.

The maximum decrease in split flap effectiveness is reported in table 5.2, compared to its default value at $\alpha = 0$. Here it is observed that the $C_{n\delta_{sf}}$ maximally goes down about 40% at $\alpha = 17.5^\circ$. Comparing this with the winglet rudders, Johnson shows such a decrease already around $\alpha = 15^\circ$, after which the decrease only grows further, to about 70% at $\alpha = 30^\circ$ [6]. This again shows that the relatively steady value of $C_{n\delta_{sf}}$ can become a very beneficial property at the higher ranges of angle of attack.

Table 5.2: $C_{n\delta_{sf}}$ per configuration and its maximum decrease

Configuration	$\alpha = 0^\circ$	$\alpha = 17.5^\circ$	$\Delta C_{n\delta_{sf}}$ [%]
SF10	-5.026e-5	-2.904e-5	-42.22
SF15	-7.540e-5	-4.406e-5	-41.57
SF20	-10.501e-5	-6.205e-5	-40.91

The results above are for the case where the centre of gravity lies 1.36 meters aft of the

nose of the model, as this is the average proposed location in the work of Palermo [10]. This corresponds to a location of 29.56 meters behind the nose of the full-scale aircraft. In reality, the centre of gravity is obviously not fixed and can change with different combinations of weight and balance. More aft centre of gravity locations will result in lower split flap efficiencies, due to a lower sideforce lever arm. The lever arm of the created drag will however not change. The sensitivity with changing centre of gravity is briefly discussed here. The control derivatives for $\alpha > 0^\circ$ are again calculated for a centre of gravity location at 1.46m behind the nose, which is considered the aft limit of the centre of gravity. It was found that on average, the values of $C_{n_{\delta_{sf}}}$ decreased by -3.48%. A similar shift was calculated for the control derivatives of the winglet rudder, which resulted in an average decrease of -9.76%, since the rudder control power mostly comes from its created sideforce. The small change of $C_{n_{\delta_{sf}}}$ with shifting centre of gravity therefore shows that the split flaps can also remain useful throughout different weight excursions.

5.3. Effect of split flaps on surrounding control surfaces

The deflection of the upper and lower split flap create large areas of low pressure behind the flaps, while increasing the pressure in front of the flaps due to higher inclination of the surfaces. These changes in pressure might affect the flow structures in the near vicinity around the split flaps. The question arises whether the effectiveness of nearby control surfaces is changed due to the deflection of split flaps. The effect of split flaps on the winglet rudder and nearby CS2 control surface is therefore investigated in this section.

5.3.1. Effect of split flaps on rudder effectiveness

The winglet rudder is the current main source of directional control for the Flying V. As the split flaps are located as far outboard as possible, the flaps are in the vicinity of the rudder surfaces. The large wake structures might therefore interact with the inboard winglet surface and might change the rudder effectiveness, which is evaluated in this section.

Johnson evaluated the change of yawing moment with rudder deflection for the Flying V wind tunnel model [6]. They reported that for each angle of attack, the rudder control derivative $C_{n_{\delta_r}}$ can be taken as linear when the rudders on both the left and right wing are combined. The current research therefore only evaluates the extremities of rudder deflection. Split flap deflection angles of 20, 40 and 60 degrees are tested with the SF15 flap. For these several angles of split flap deflection, the rudder is set to its maximum starboard or port deflection (-100% or +100%). This way, the effect of split flaps on the rudder could be evaluated. These percentile deflections can be linked to absolute deflection angles of -22.4525° and 22.9695° , respectively.

The yawing moment due to left wing rudder deflection is presented in figure 5.29 for several positive angles of attack. Here, the effect of deflecting the rudder is evaluated for the clean wing and for a wing with the three settings of δ_{sf} . The values of ΔC_n are isolated for δ_r and thus only represent the influence of deflecting the rudder. It is observed that the influence of the split flaps on the rudder effectiveness is not significant at small α .

Once the angle of attack is increased to $\alpha \geq 15$, the leading edge vortex starts interacting with the split flap. It is observed that at the same time some interaction between the split flap and the rudder is formed. This is seen in the subplots of $\alpha \geq 15$, where several of the measured SF15 data points lie outside the clean wing error bar. At these higher angles of attack, the effectiveness of the left side rudder seems to increase with the application of split flaps. This is observed from figure 5.29, where ΔC_n for negative δ_r is increased when split flaps are deflected. At the same time, at $\delta_r = +100\%$ the values of ΔC_n are not significantly

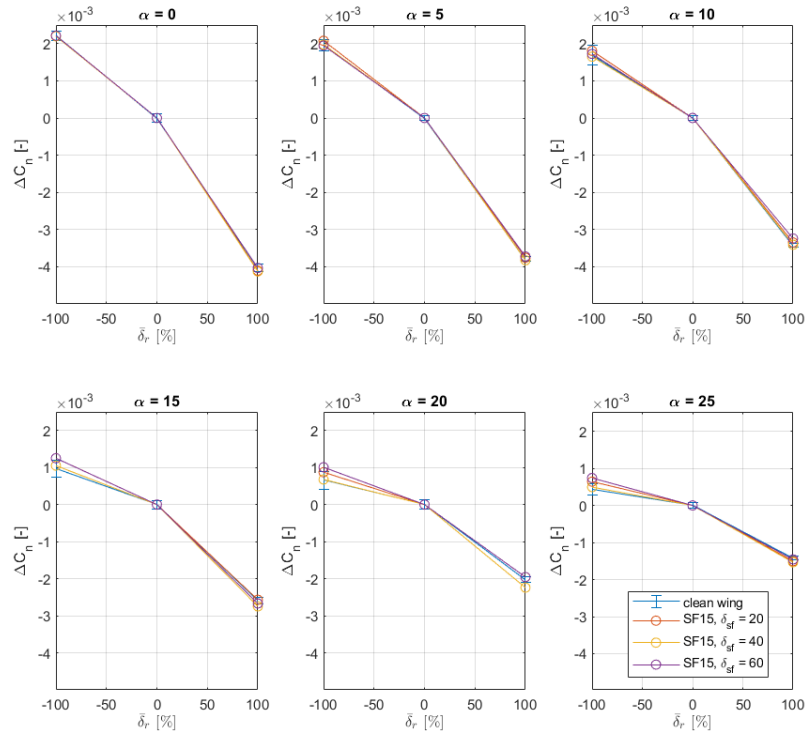


Figure 5.29: Isolated ΔC_n due to varying rudder deflection for several configurations at $\alpha = 0, 5, 10, 15, 20$ and 25 degrees.

changed as the data is more distributed around the clean wing data point. The influence of split flaps are thus only really present for negative δ_r . The maximum increase of ΔC_n is found to be $3.48e-4$, at $\alpha = 20^\circ$ and $\delta_{sf} = 60^\circ$. Due to the low effectiveness of the rudder at high α , this would be a 52% increase in rudder power, showing the significance of the interaction. However, it should be noted that the combination of an inboard deflected rudder with a deflected split flap will not be used to yaw the aircraft, as these two control modes will counteract each other. It is therefore concluded that during normal flight, the split flaps will not have a significant effect on the rudder control effectiveness.

5.3.2. Effect of split flaps on CS2 effectiveness

Next to the split flap influence on the rudders, their effect on near control surfaces along the wing trailing edge are investigated. In order to do so, the SF22 flap is tested in combination with some CS2 deflection angles. Split flap deflection angles of 20, 40 and 60 degrees are tested. The CS2 control surfaces are used on the Flying V for the creation of either a pitch or a roll moment, so both these properties are investigated for maximum and minimum CS2 deflection. These percentile deflections of -100% and +100% can be linked to absolute deflection angles of -16.534° and 12.057° , respectively.

The effect of split flap deflection on the pitching moment caused by CS2 deflection is presented in figure 5.30, where the isolated ΔC_m due to only the CS2 deflection is shown. The influence of split flaps is most significant on positive (trailing edge down) deflection of CS2. It is observed that deflecting the split flaps will lead to more positive ΔC_m values. For the positive (trailing edge down) δ_{CS2} this consequently means that a less effective control surface is created. A maximum decrease of ΔC_m of 39.5% is found. A similar influence can

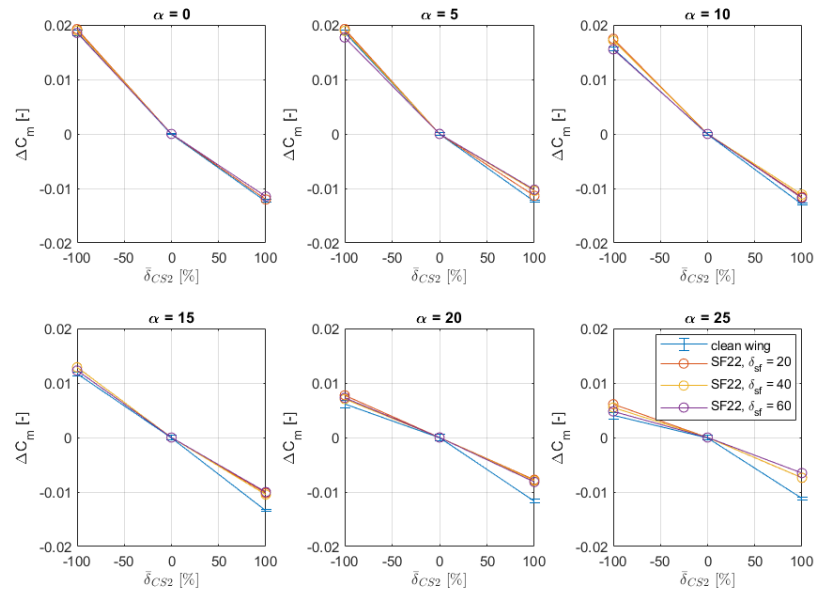


Figure 5.30: Isolated ΔC_m due to varying CS2 deflection for several configurations at $\alpha = 0, 5, 10, 15, 20$ and 25 degrees.

be found in the isolated value of ΔC_l , presented in figure 5.31. Here, more negative values of ΔC_l are found when deflecting the split flaps. This is again mostly the case for the positive (trailing edge down) δ_{CS2} , where a less effective roll control surface is found with a maximum decrease of 49.6%. The simultaneous application of split flap deflection and adjacent CS2 trailing edge down deflection can thus cause quite a substantial decrease in effective pitch or roll creation, especially at higher angles of attack.

It is hypothesised that the variation in created pitch and roll is due to some interaction between the pressure peak at the CS2 surface (due to its deflection) and the low pressure area in the region behind the split flap. As the interaction effect is most significant for trailing edge down deflection, it seems like the high pressure on the lower surface interacts most with the low pressure behind the split flap. It is however really difficult to precisely identify how this leads to the exact interaction that is seen in the plots. Accurate pressure distributions and flow topology in the area between CS2 and the split flap would be needed for definite conclusions.

Another explanation might lie in the rigidity of the model. At higher angle of attack, both control devices have a high rear aerodynamic loading, which can possibly slightly deform the model. This would in turn decrease the effectiveness of the CS2 surface. This hypothesis would again need further investigation for definitive conclusions.

5.4. Mitigating adverse split flap effects

It is shown in section 5.1.3 that normal deflection of the split flaps can cause some substantial pitching and rolling moments. Especially at higher angles of attack, these moments can result in large trim requirements for the other trailing edge control surfaces. As these additional trimming deflections will cause even more drag, the creation of pitching and rolling moments are defined as adverse effects of split flaps. This section will look into possibilities of minimising the adverse pitch and roll moments caused by split flaps, while trying to maintain its directional control power.

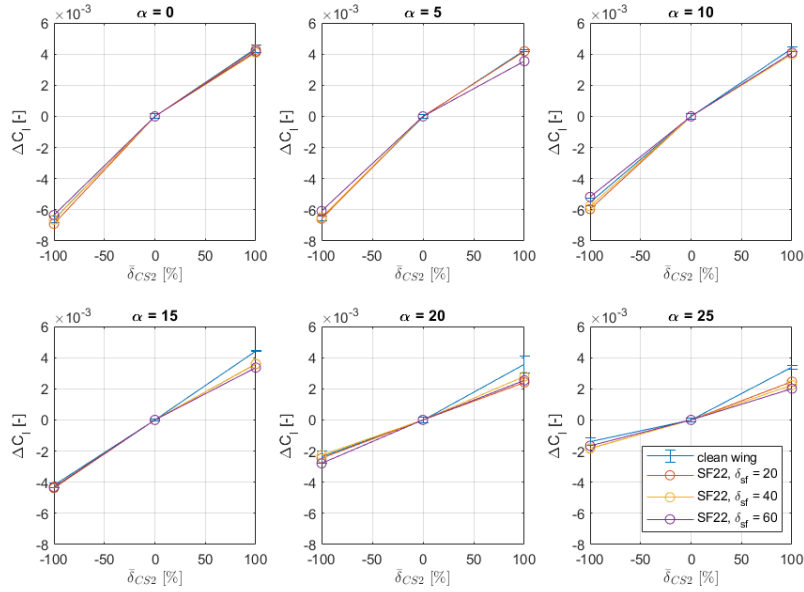


Figure 5.31: Isolated ΔC_l due to varying CS2 deflection for several configurations at $\alpha = 0, 5, 10, 15, 20$ and 25 degrees.

5.4.1. Differential deflection between upper and lower flap

It is hinted by Lochert et al. [17] that a different deflection angle of the upper and lower split flap might reduce adverse pitching and rolling moments caused by split flaps. The application of differential deflection is examined in this section. Differential deflection is here defined as a case where the upper split flap deflection $\delta_{sf,u}$ has a different value than the lower split flap deflection $\delta_{sf,l}$.

The effect of different combinations of upper and lower flap deflection on the aircraft aerodynamic moment coefficients is presented in figure 5.32. These combinations are performed with the SF15 configuration. Next to the differential deflections, also the mutual deflection setting of $\delta_{sf,u} = \delta_{sf,l} = 40^\circ$ is presented as default setting.

The values of ΔC_n for various combinations of upper and lower deflection angle is presented in figure 5.32. Here, some surprising behaviour is found concerning the yaw creation of the upper split flap. It is observed that the deflection of the upper split flap has very limited influence on the created yawing moment of the split flaps. When looking at the line for $\delta_{sf,u} = 40, \delta_{sf,l} = 0$, it is seen that the created yawing coefficient is very low; it does not exceed $0.3e-3$. Additionally, it can also be observed that all cases where $\delta_{sf,l} = 40$ lie very close to each other, regardless of the value of $\delta_{sf,u}$.

The reason for this small yawing influence of the upper flap at low angles of attack is found in the created drag and sideforce. It is found that for $\alpha < 15$ the upper flap produces a substantial negative sideforce. This is possibly due to the created downforce, which is translated to sideforce through the dihedral of the wing. It is also possible that the high pressure in front of the split flap slightly pushes the winglet outboard, as this pressure area would be close to the inboard of the winglet near the winglet, creating a negative sideforce. A final culprit might lie in flow against the brackets behind the split flaps, but this is considered unlikely. The sideforce behind the centre of gravity is thought to counteract the drag in creating a yawing moment, thus explaining why the upper flap is ineffective in terms of ΔC_n . The question arises whether the upper split flap is even needed in operation.

Next, the created pitching and rolling moments for differential deflection combinations are

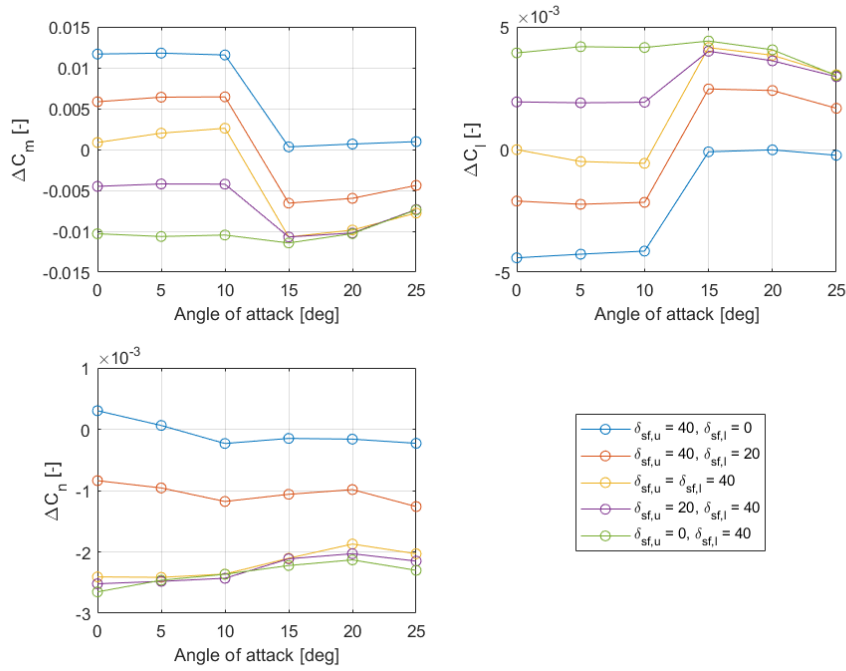


Figure 5.32: Aerodynamic moment coefficients behaviour for SF15 with several differential deflection angles between the upper and lower split flap.

investigated. The values of ΔC_m and ΔC_l are also presented in figure 5.32. In these plots it is seen that only deflecting the lower split flap to purely create ΔC_n will result in very large pitching and rolling moments over the whole range of α . It therefore becomes apparent that the upper split flap is mostly necessary for trimming out these adverse moments. As the upper flap does not contribute much to the yaw however, it is proposed that a more optimal combination of $\delta_{sf,u}$ and $\delta_{sf,l}$ can be found to minimise the coupling in pitch and roll.

In order to make a proper comparison between configurations with different preset deflections, a look is taken at the ratio of created pitching moment to yawing moment ($\Delta C_m / \Delta C_n$) and the ratio of created rolling moment to yawing moment ($\Delta C_l / \Delta C_n$). This will give further understanding of how the adverse moments can be reduced, while maintaining a certain level of created yawing moment. Both ratios would ideally be as close to zero as possible. As it was established that the amount of ΔC_n is mostly dictated by the deflection angle of the lower flap, the upper flap deflection angle is varied while keeping the lower flap at $\delta_{sf,l} = 40^\circ$. The ratios of pitch-to-yaw and roll-to-yaw are plotted in figure 5.33. It is observed in this figure that for the configuration without differential deflection at $\alpha \leq 10$, both ratios are already quite close to zero. Decreasing $\delta_{sf,u}$ slightly can further decrease the coupling in pitch and roll. For $\alpha \geq 15$, the ratios move away from zero. In order to slightly trim away the pitch and roll created by the split flaps, $\delta_{sf,u}$ should be increased. This can however only marginally decrease the coupling. The coupling at $\alpha \geq 15$ should therefore be further trimmed away by the other trailing edge control surfaces.

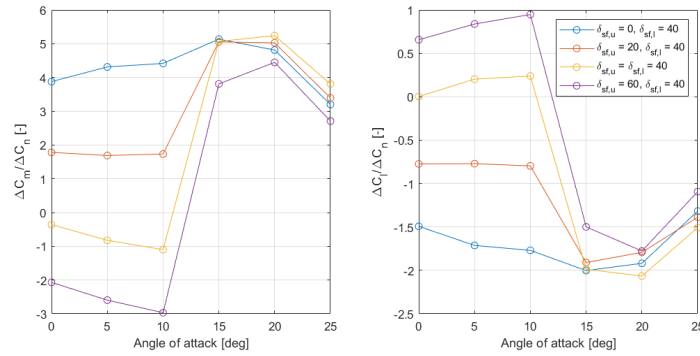


Figure 5.33: Pitch-to-yaw and roll-to-yaw behaviour for SF15 with several differential deflection angles between the upper and lower split flap.

It can be argued that additional drag created by these differential split flaps is also an adverse effect which should be taken into account. The value of ΔC_D was also monitored for the combinations of differential deflection. Decreasing $\delta_{sf,u}$ at angles $\alpha \leq 10$ showed a beneficially decrease the amount of drag, while maintaining the yawing moment. However, the advised increase of $\delta_{sf,u}$ for $\alpha \geq 15$ would further increase the drag. This has to be taken into account when designing the controller for the split flaps, to make sure that further increasing the drag will not detrimentally affect the Flying V performance.

5.4.2. Global rotation of mutual deflected split flaps

As stated in the split flap terminology, the split flaps to be implemented on the Flying V are considered to be able to operate as split ailerons. This means that upper and lower flaps have a hingeline for split deflection and that there is a separate hingeline to provide rotation for ordinary elevon modes (see figure 2.4). It is now imagined that the split flaps can be deflected to some δ_{sf} , while simultaneously being rotated over some elevon deflection angle, or in this case some δ_{CS} . This section will investigate whether this can serve as a solution for decreasing the adverse coupling in pitch and roll. The SF22 flaps are used for this case, as these cover the entirety of the CS3 surface. With these split flaps extended, the CS3 control surface is deflected to settings between -100% and 100% (with increments of 50%) in order to investigate the effects of global split flap rotation.

The behaviour of the aerodynamic moments of SF22 at $\delta_{sf} = 40$ with global CS3 rotation is presented in figure 5.34. It can be seen that all aerodynamic moments are quite sensitive to the variations in δ_{CS3} . This was to be expected, as the investigation into differential deflection of section 5.4.1 showed the sensitivity of these moments with varying absolute upper and lower flap deflection. The value for ΔC_n is thus also quite influenced over the whole range of angle of attack. It is seen that positive (trailing edge down) deflection will increase the created yawing moment. At the same time, positive deflection decreases ΔC_m and increases ΔC_l . These moment influences were expected as they follow partly the CS3 effects as reported by Johnson [6]. It can be concluded that some positive δ_{CS3} can be applied for $\alpha \leq 10$. Here, the created ΔC_n can be increased while decreasing the adverse pitch or roll moments can be put closer to 0. Contrarily, for $\alpha \geq 15$ application of global deflection is not beneficial. In order to get the created pitching or rolling moments closer to 0, negative δ_{CS3} should be applied. This would however largely decrease the created ΔC_n , making global rotation a counteractive measure. Also cases for $\delta_{sf} = 20^\circ$ and $\delta_{sf} = 60^\circ$ were investigated, which resulted in similar conclusions.

Also a look is taken at the changing drag for positive δ_{CS3} at $\alpha \leq 10$, as further increase in drag can be considered an additional adverse effect. It was observed that in this range of

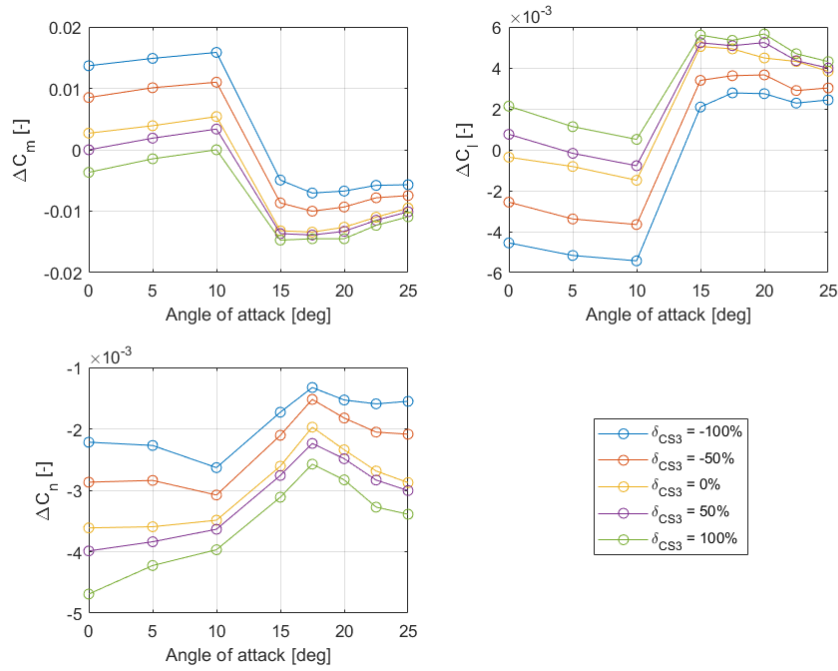


Figure 5.34: Aerodynamic moment coefficients behaviour for SF22 at $\delta_{sf} = 40$ for several global CS3 deflection angles.

angles of attack, the ΔC_D is not significantly affected. Applying δ_{CS3} to trim out pitch or roll at $\alpha \leq 10$ will thus not further adversely create drag.

Simultaneous roll and yaw creation

An interesting notion has to be made in this section. As stated in the methodology, the split flaps will replace some of the outboard CS3 control surfaces. It was initially presumed that this would cause a loss in total roll/pitch control in exchange for yaw control, when the split flaps are used in rudder functionality. From the plots of ΔC_l and ΔC_m in figure 5.34 it was previously noticed that still a substantial amount of roll/pitch control can be exerted by rotation of CS3, even when the surface is used as split flap. It is therefore investigated if the split flaps can be used in a dual functionality, simultaneously controlling both yaw and pitch/roll. Only the roll control will be highlighted below, but similar results were found in terms of pitch control.

The isolated influence of δ_{CS3} on rolling moment coefficient of a split flap is investigated, with respect to a SF22 split flap at $\delta_{CS3} = 0\%$. The isolated ΔC_l of varying δ_{CS3} for three values of δ_{sf} is presented in figures 5.35 to 5.37. Here, also the ΔC_l for CS3 deflection of a clean wing is shown as baseline value. The clean wing CS3 values are taken from the work of Johnson [6].

It is observed in figure 5.35 that the influence of δ_{CS3} on ΔC_l of the clean wing closely matches that of the SF22 at $\delta_{sf} = 20$. Comparing this behaviour with the results presented in figure 5.36 and figure 5.37, it is observed that increasing δ_{sf} to higher values decreases the effectiveness of CS3 rotation in roll. While it is still possible to gain some roll control from CS3 rotation with high split flap deflections, its effectiveness is decreased significantly. For a dual functionality of the split flap, low to intermediate levels of δ_{sf} maintain roll/pitch control.

It was shown in figure 5.34 that positive δ_{CS3} increases the effective ΔC_n of the split flaps, while negative δ_{CS3} decreases ΔC_n . For dual functionality of the split flaps it is thus most effective to combine low to intermediate values of δ_{sf} with positive (trailing edge down)

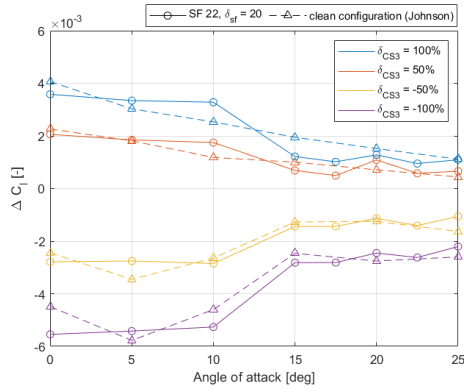


Figure 5.35: Isolated CS3 influence on C_l for SF22 configuration at $\delta_{sf} = 20^\circ$, compared to the clean wing configuration.

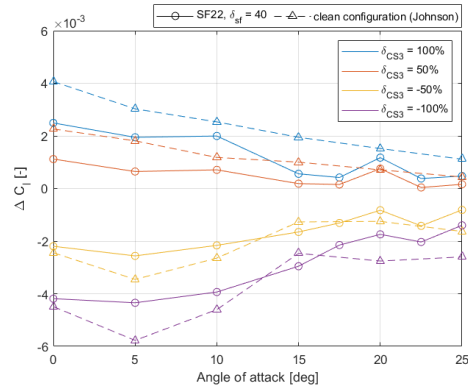


Figure 5.36: Isolated CS3 influence on C_l for SF22 configuration at $\delta_{sf} = 40^\circ$, compared to the clean wing configuration.

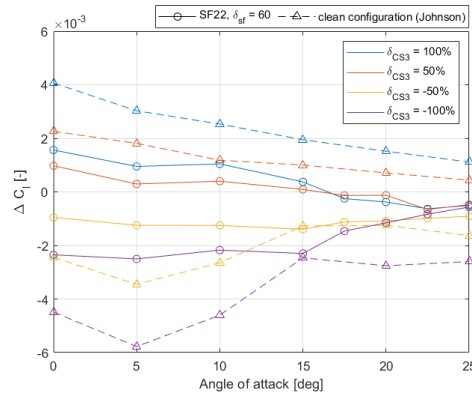


Figure 5.37: Isolated CS3 influence on C_l for SF22 configuration at $\delta_{sf} = 60^\circ$, compared to the clean wing configuration.

rotation of δ_{CS3} . This would allow effectiveness in both roll control and yaw control from the same split flap surface. This shows that the (partial) replacement of the current control surfaces with split flaps will not necessarily indicate a total loss in roll/pitch control. The limitation here obviously lies in the fact that negative (trailing edge up) rotation of the split flaps will decrease the yaw effectiveness. A higher value of δ_{sf} would thus be needed, which would in turn lower the effective ΔC_l from global rotation, which would thus require a higher value of δ_{CS3} , and so forth. To make proper use of such a dual functionality, very intricate flight control rules should be created.

6

Split flap conceptual sizing

Now that the split flap performance is known from the experimental wind tunnel tests, an effort is made to estimate a proper size for the split flaps of the full-scale Flying V. This chapter will present the steps taken to get to a conceptual split flap size estimation and will discuss its performance for the aircraft.

6.1. Required split flap yawing moment

As explained in section 3.3, the required directional control power comes from the compliance with several lateral-directional aircraft capabilities. It has been estimated for each CS-25 requirements how much yawing moment the split flaps should deliver. This section will elaborate on the required split flap control power and the consequent directional capabilities of the aircraft. It will show which of the CS-25 specifications are critical, thus for which requirements the conceptual sizing should take place. In this section reported values for δ_{CS1} , δ_{CS2} or δ_{CS3} represent aileron deflections, where positive values represent right wing trailing edge down and left wing trailing edge up deflections.

6.1.1. Trim calculations

Let us first consider the performed trim calculations. Three different certification requirements have been analysed by their capability to trim the aircraft in certain flight situations.

CS 25.143(h): Manoeuvrability

The coordinated turn capability is calculated for a 30 degree banked turn at take-off. This is done for either a starboard or port engine failure, with the remaining operating engine at maximum continuous thrust. It is chosen to interpret the prescribed asymmetric thrust setting in this way, as it would be the most adverse situation possible. It is considered that the turn is perfectly coordinated, meaning that a certain yaw rate is attained which is perfectly in balance with the other sideforce contributions. As a result, the sideslip angle is equal to zero. The turns have been investigated for MTOW at V_2 . The results are shown in table 6.1.

Table 6.1: CS 25.143(h): 30° coordinated turn

Configuration	OEI	Velocity	ϕ	α	δ_r	δ_{CS1}	δ_{CS2}	δ_{CS3}	$C_{n_{sf}}$
Take-off	Starboard	81.40	30	15.17	25.94	0	6.39	30	0
Take-off	Port	81.40	30	15.17	-30	0	0	-21.78	2.2178e-3

It can be seen that in a turn to the right, the failure of the starboard engine does not pose directional difficulties. This was to be expected, as the OEI yawing moment would be directed in the direction of the turn. However, for a port engine failure, the adverse OEI yawing moment

makes that the ordinary directional control allocation can not hold a steady coordinated turn. It is seen that a yawing moment coefficient magnitude of $2.2178e-3$ is needed from the split flaps.

CS 25.147(c): Lateral control

The next trim check calculation was for the requirement specified by CS 25.147(c) on the lateral control of the aircraft. It is similar to the requirement on the coordinated turn manoeuvrability, but with other configuration specifications. The results are shown in table 6.2. The current control power is well able to perform the banked turn manoeuvre, with and against the operating engine. Since the worst case scenario of asymmetric thrust is assumed for CS 25.143(h), the current requirement is much less critical. On top of that, the current requirement has a lower bank angle and a higher velocity, also resulting in less demanding values.

Table 6.2: CS 25.147(c): 20° banked turn

Configuration	OEI	Velocity	ϕ	α	δ_r	δ_{CS1}	δ_{CS2}	δ_{CS3}	$C_{n_{sf}}$
Take-off	Starboard	93.31	20	12.28	17.30	0	0	23.39	0
Take-off	Port	93.31	20	12.28	-23.14	0	0	-7.47	0

CS 25.161(b): Lateral and directional trim in steady heading sideslip

Next, the aircraft capabilities in steady heading sideslips are investigated. The aircraft has to be able to counteract a 30-knot crosswind, while maintaining steady heading flight. Subparagraph CS 25.161(b) states that all relevant operating limitations during normally expected flight have to be investigated. The displacement of the centre of gravity is not accounted for in the calculation approach. In order to still look into weight factors, the aircraft mass has been investigated for MTOW, MLW and a zero-fuel-weight (ZFW) condition, where the latter is considered around the worst-case scenario of low weight cross wind landing in 'normal flight operations'. The value of ZFW is estimated by subtracting total fuel weight from the maximum take off weight. The tests have been performed at $1.3V_{SR1}$. The trim results are presented in table 6.3.

Table 6.3: CS 25.161(b): lateral and directional trim in steady heading sideslip

Configuration	Velocity	β	α	ϕ	δ_r	δ_{CS1}	δ_{CS2}	δ_{CS3}	$C_{n_{sf}}$
MTOW	93.31	9.52	11.54	2.76	30	0	-10.21	-30	-1.297e-4
MLW	83.46	10.66	11.54	3.55	30	0	-12.76	-30	-1.1514e-3
ZFW	73.88	12.06	11.54	4.53	30	0	-15.91	-30	-2.4113e-3

It is observed that it is not possible to maintain the 30-knot crosswind with the ordinary control allocation. The split flaps have to create a negative yawing moment for positive values of sideslip angle, in order to maintain sideslipping flight. This is mostly due to the positive weathercock stability ($C_{n_{\beta}}$) of the aircraft. It can be seen that with lower aircraft weight, more yaw control is needed from the split flaps, due to a lower certification velocity and a resulting higher sideslip angle. Here, a maximum required $C_{n_{sf}}$ magnitude of $2.4113e-3$ is found.

CS 25.161(d): Lateral and directional trim in OEI situation

Trim also has to be attained in a OEI situation, in this case for a starboard inoperative engine. As an additional constraint, the bank angle can not get larger than 5°. Similarly as for CS 25.161(b), the weight configuration is investigated for MTOW, MLW and ZFW. Here, the ZFW is not a realistic climbing configuration, but it is included to look at the effect of low weight conditions. The trim check results are presented in table 6.4.

Table 6.4: CS 25.161(d): lateral and directional trim in OEI situation

Configuration	OEI	Velocity	α	ϕ	δ_r	δ_{CS1}	δ_{CS2}	δ_{CS3}	$C_{n_{sf}}$
MTOW	Starboard	93.31	11.54	-2.32	20.55	0	0	14.50	0
MLW	Starboard	83.46	11.54	-2.89	25.58	0	0	18.05	0
ZFW	Starboard	73.88	11.54	-3.37	30	0	0	22.65	-7.090e-04

It is observed that these OEI conditions are not critical for the directional control power sizing of the aircraft. Only at low weight conditions, does the rudder go towards the maximum rudder deflection of 30°, but the required additional value is low compared to the coordinated turn and steady sideslip case.

6.1.2. Linear simulations

It is established in the previous section that for some situations, application of split flaps is required for aircraft certification. The most critical magnitude is found as $C_{n_{sf}} = 2.4113e-3$ from the steady heading sideslip requirement. Next, two requirement specifications are to be investigated with the use of the established linear simulation model. As it was shown that these simulations are mostly indicative of nature, the results in this section will only conclude whether the roll or yaw motions are critical for the lateral-directional sizing of the aircraft. For this purpose, it is investigated if these lateral and directional motions are able to be performed well within the limits as prescribed in CS-25, with and without the thus-far critical value of $C_{n_{sf}} = 2.4113e-3$.

CS 25.147(d): Roll capability

It is stated in AMC 25.147(d), it must be possible to roll a OEI aircraft from trim at -30° bank to a 30° bank angle in the other direction within 11 seconds. In terms of inputs, all 3 trailing edge control surfaces (CS1, CS2 and CS3) were used simultaneously as aileron input. The rudder is used to try to minimise the sideslip during the roll motion. The split flap could aid the minimisation of the sideslip through the creation of a yaw rate in the opposite direction of the initial turn.

Several cases are investigated. First and foremost, it is examined whether it is possible to make the bank to bank manoeuvre without the application of split flap deflection. For this, maximum aileron input is given while the split flap influence is set as zero. Figure 6.1 shows the aircraft asymmetric behaviour for a port OEI situation. This is the most adverse OEI situation as the aircraft has to be rolled in the positive roll direction, while the port OEI counteracts this. It is observed in this figure that the bank to bank manoeuvre can be established in 5.20 seconds, well within the constraint of 11 seconds. Even when recognising the uncertainty of these simulations, it is considered that this gives a good indication that the bank to bank requirement can be satisfied. It is however found that negative yaw angles and large positive sideslip angles are created. While CS 25.147(d) does not state specific constraints for these parameters in the adverse OEI situation, it is investigated whether the application of split flaps or a smaller aileron input can create a smoother manoeuvre.

The roll manoeuvre is repeated, now including the application of a split flap with $C_{n_{sf}} = 2.4113e-3$. The roll behaviour is shown in figure 6.2. It is observed that the bank to bank manoeuvre is now completed in 5.27 seconds and that the created sideslip angle is less compared to the case where no split flap deflection was applied. One last repetition is performed, with a lower aileron input. Looking at figure 6.3, it is seen that with only 60% of the maximum aileron input, the roll manoeuvre is still completed well within the 11 second constraint, at a manoeuvre time of 9.50 seconds. The level of created sideslip angle is even further reduced.

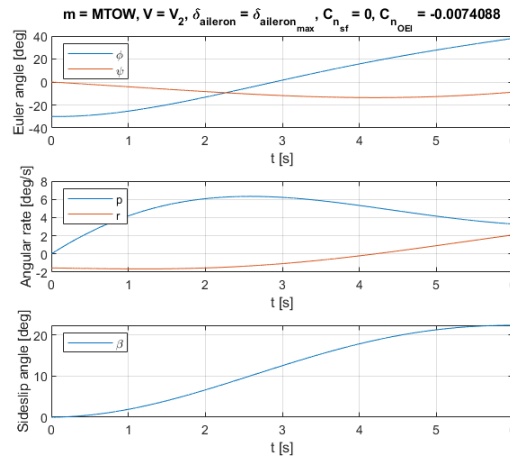


Figure 6.1: OEI bank to bank manoeuvre with full aileron input

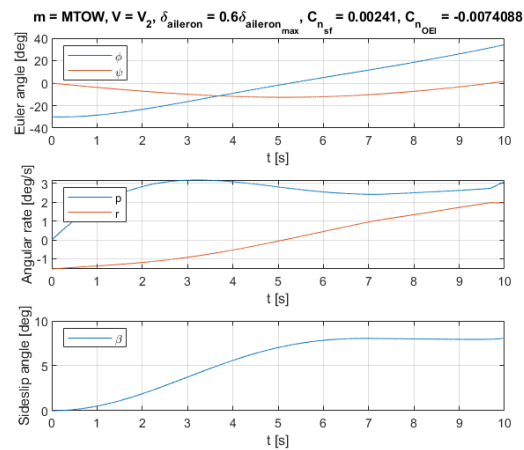
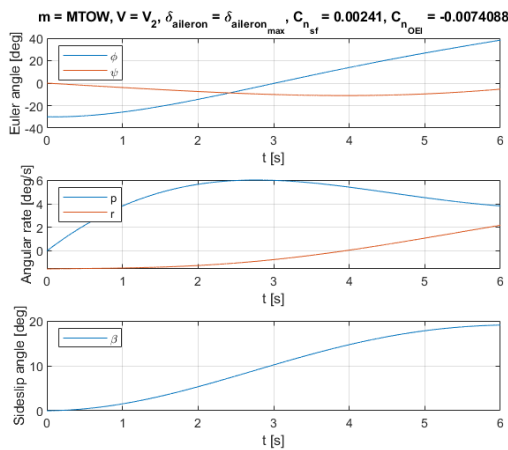


Figure 6.2: OEI bank to bank manoeuvre with full aileron input and split flap input Figure 6.3: OEI bank to bank manoeuvre with 60% aileron input and no split flap input

All in all, a good indication of compliance to the certification requirement CS 25.147(d) is shown, with and without the use of split flaps. This requirement is therefore not deemed critical for the lateral-directional sizing. If wanted, the split flaps and more optimal aileron inputs are shown to help prevent excessive sideslip angles or directional travel.

CS 25.147(a): Directional control

The last motions to be investigated are the OEI yaw manoeuvres prescribed in CS 25.147(a). This requirement is in place to show that the aircraft can be yawed without the additional application of bank angle [20]. The aircraft is trimmed in straight flight with a OEI situation, after which a maximum rudder input is given to try and establish a 15° yaw angle, without invoking a rolling motion. This has been done with and against the operative engine, and for either $C_{n_{sf}} = 0$ and $C_{n_{sf}} = 2.4113e-3$. The ailerons are used to the extent necessary to minimise the roll rate.

The positive yaw motion with the advantageous starboard OEI is shown in figure 6.4 and figure 6.5. Here it is observed that without split flaps, it is possible to increase the yaw angle to 15° in 3.23 seconds. When split flaps are incorporated this manoeuvre is completed in 2.92 seconds. CS 25.147(a) is not specific about the time constraint of the manoeuvre, it only

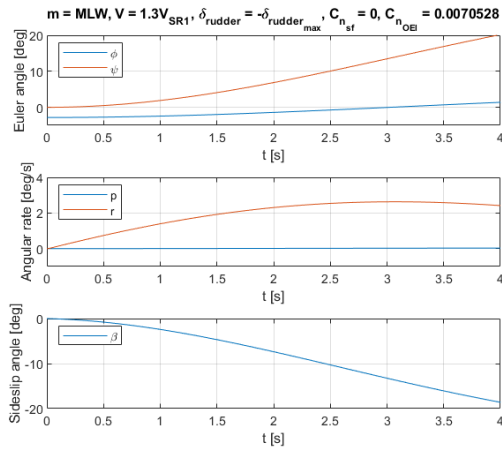


Figure 6.4: OEI yaw manoeuvre with the operative engine

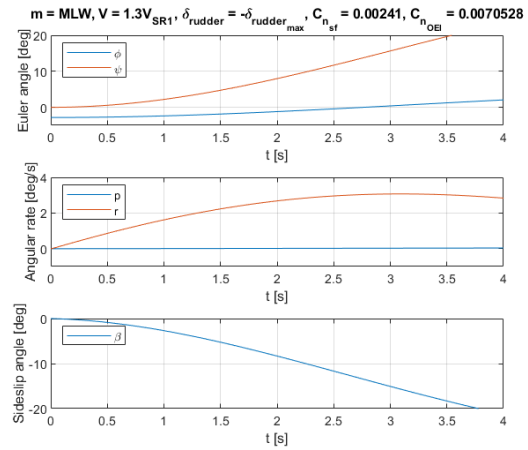


Figure 6.5: OEI yaw manoeuvre with the operative engine, including split flap input

states that it should be possible to 'make a reasonably sudden change in the heading of up to 15° '. Either indicated value is considered to be 'reasonably sudden' as they are faster than a rate-one turn of 3° per second. It is concluded that the requirement is not critical for the split flap sizing, as the rudder alone can induce a quick manoeuvre.

Lastly, CS 25.147(a) also states that 'it must be possible to yaw into the operative engine'. This again seems like an ambiguous requirement as no time limitation or required yaw angle is given. It is believed that the requirement is just in place to make sure the directional control can overcome the most adverse OEI situation without the application of large bank angles. Figure 6.6 and figure 6.7 show the behaviour of full yawing power against the operating engine, with and without the split flaps. It is observed that when no split flaps are used, it would possibly be very hard to yaw into the operative engine without further application of bank angle. When a potential split flap with $C_{n_{sf}} = 2.4515e-3$ is added, it can be seen that the yaw rate is significantly increased. Creating a substantial yaw angle is still a slow procedure, but at least now a clearly observable yaw rate can be attained. Further increasing $C_{n_{sf}}$ would accelerate the motion, however it is not specifically needed in the current explanation of CS 25.147(a). Keeping the uncertainty of the simulation in mind, it is concluded that the application of the split flaps is preferable to show a good indication of compliance with CS 25.147(a). However, due to the ambiguity of the requirement, it is not considered as critical for the sizing. It might be wise however to take this requirement into account during future lateral-directional control studies.

6.1.3. Sensitivity analysis

It can be concluded from section 6.1.1 and section 6.1.2 that the most critical CS-25 requirements in terms of the aircraft directional control power are the 30° coordinated turn against the operative engine and the trim during a steady heading sideslip. Here additional $C_{n_{sf}}$ values of $2.2178e-3$ or $2.4113e-3$ are required, respectively. For both calculations, a sensitivity analysis is performed to analyse the effect of changing conditions or assumptions. Ultimately, this will provide a sense of the certainty of the calculated $C_{n_{sf}}$, based on the uncertainty of the input parameters. The values of $2.2178e-3$ or $2.4113e-3$ will be taken as reference yawing moment values.

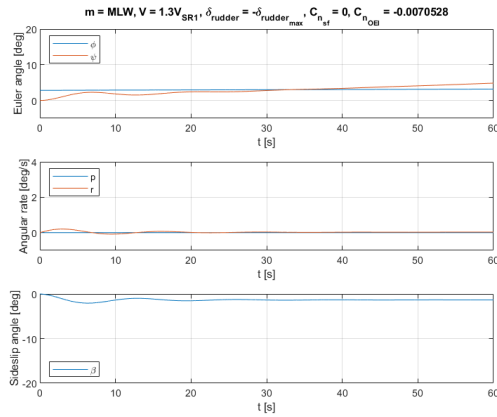


Figure 6.6: OEI yaw manoeuvre against the operative engine

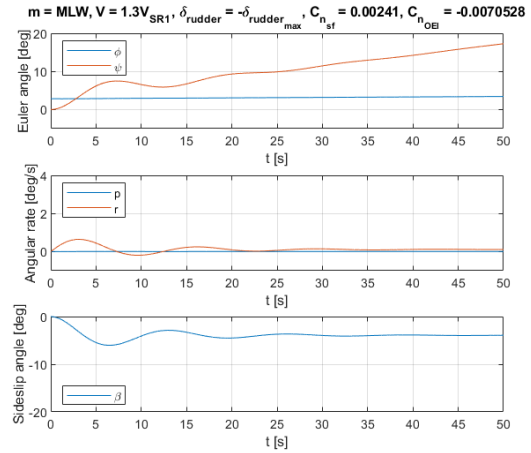


Figure 6.7: OEI yaw manoeuvre against the operative engine, including split flap

Sensitivity of coordinated turn condition

The sensitivity of all investigated parameters on the coordinated turn requirement is presented in figures 6.8 and 6.9. Here, the percentile change of the required $C_{n_{sf}}$ is plotted versus the percentile change of the parameter. The percentile change in required split flap yawing moment is calculated as:

$$\Delta C_{n_{sf}} = 100 \cdot [C_{n_{sf_{new}}} - C_{n_{sf_{ref}}}] / C_{n_{sf_{ref}}} \quad (6.1)$$

For the coordinated turn, it can be seen in figure 6.8 that the parameters with respect to the yaw rate r are the most influential. This is logical for the coordinated turn case, as the yaw rate is substantial in a coordinated turn. Especially changes in C_{n_r} would influence the required split flap performance. It is expected that due to the used flight mechanics calculations, the yaw rate is slightly overestimated. This would thus result in a conservative value of $C_{n_{sf}}$.

Next, the sensitivity of the control derivatives for the critical case is presented in figure 6.9. Here, the contributions of CS1, CS2 and CS3 are taken as one, under the subscript 'CS', as it is imagined that they have similar uncertainties due to Reynolds effects. For total evaluation, a combined sensitivity of the derivative in sideforce, roll and yaw is performed for both the rudder and the CS surfaces. It is observed that changes to the rudder control derivatives are most influential, especially $C_{n_{\delta_r}}$, which was to be expected. Considering that the rudder will probably have an increase in efficiency due to Reynolds effects [38], the final full-size $C_{n_{sf}}$ will probably decrease. This makes the outcome split flap, discussed in the next section, somewhat conservative.

Sensitivity of steady heading sideslip condition

In a similar fashion as for the coordinated turn condition, the sensitivity for the steady heading sideslip requirement is investigated. The sensitivity of varying the stability derivatives and control derivatives is presented in figure 6.10 and figure 6.11.

The graphs basically follows a similar logic as the sensitivity of the coordinated turn requirement, but now the outcome is sensitive to changes with respect to β . In the case of steady sideslip, the required value of $C_{n_{sf}}$ is especially sensitive to the yaw stability $C_{n_{\beta}}$ of the aircraft. This is logical, as the parameter wants to return the aircraft to a state of zero sideslip, for which a counteracting yaw control should be created. In terms of the control derivatives, again a high sensitivity with the rudder is seen. Similar as before, a higher rudder power

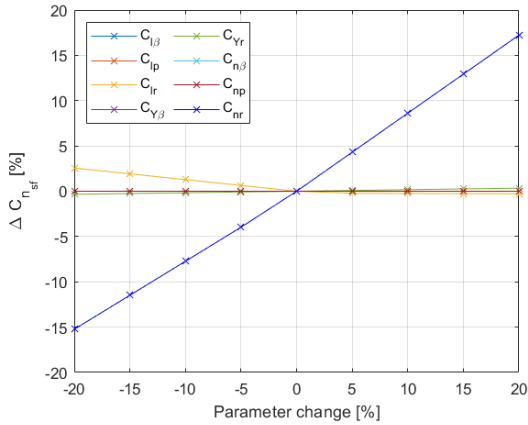


Figure 6.8: Sensitivity of stability derivatives for the coordinated turn design case

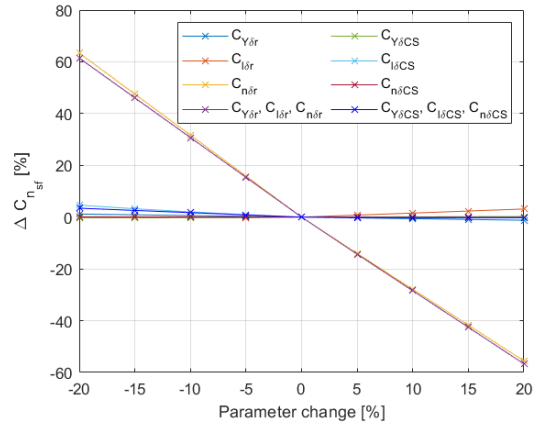


Figure 6.9: Sensitivity of control derivatives for the coordinated turn design case

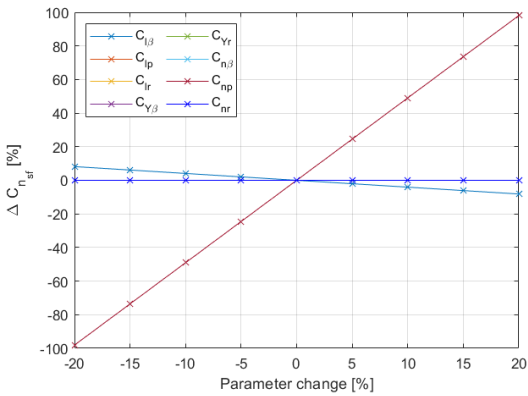


Figure 6.10: Sensitivity of stability derivatives for the steady heading sideslip design case

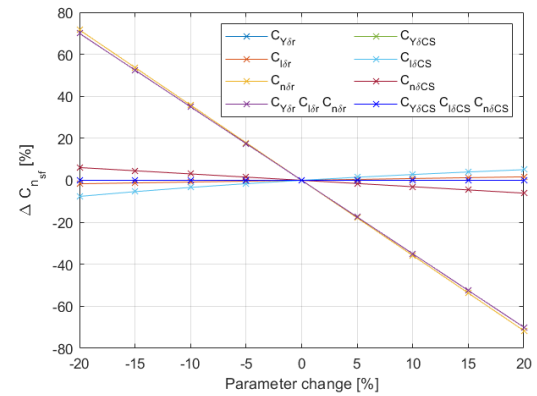


Figure 6.11: Sensitivity of control derivatives for the steady heading sideslip design case

would alleviate the amount of control needed from the split flaps. Expecting a higher control power from the full-size rudders, the value of $C_{n_{sf}}$ would again be somewhat conservative.

6.2. Split flap sizing

Now that the critical value for $C_{n_{sf}}$ is estimated, it can finally be determined if this converts to a feasible split flap geometry. This section will first give a recommended split flap geometry for $\delta_{sf_{max}} = 60^\circ$, after which the consequence of varying split flap deflection angles is discussed. The estimated sizes will give another insight into whether split flaps are a feasible addition to the Flying V. The section will close by showing the projected performance of the split flap, with respect to the current winglet rudders.

6.2.1. Recommended split flap geometry

It is shown from section 6.1.1 and section 6.1.2 that the most demanding CS-25 requirements in terms of the aircraft directional control power are the 30° coordinated turn against the operating engine and the steady heading sideslip requirements. Here an estimated $C_{n_{sf}}$ of $2.2178e-3$ and $2.4113e-3$ are required. As the created $C_{n_{sf}}$ is dependent on the angle of attack α , both requirements are investigated for the sizing.

The generalised $C_{n_{sf}}/S_{sf}$ behaviour with varying angle of attack is taken from averaging

Table 6.5: Final sizing summary for $\delta_{sf_{max}} = 60^\circ$

Critical requirement	$C_{n_{sf}}$ [-]	α [°]	$C_{n_{sf}}/S_{sf}(\alpha)$ [mm^{-2}]	S_{sf} [mm^2]	b_{sf} [mm]
CS 25.143(h)	2.2178e-3	15.17	2.1036e-7	1.0543e4	109.72
CS 25.161(b)	2.4113e-3	11.54	2.2404e-07	1.0763e4	111.87

their respective values found from SF10, SF15 and SF20 for a deflection angle of $\delta_{sf} = \delta_{sf_{max}}$, which is taken as 60° . Combining $C_{n_{sf}}/S_{sf}$ and the calculated $C_{n_{sf}}$, a required sub-scale split flap area S_{sf} is found, which leads to the needed sub-scale width of the split flap. The results of these steps are summarised in table 6.5.

It is seen that a minimum (sub-scale) split flap width of 111.87 mm is needed to fulfil all need of high directional control power. Such a flap would span 50.85% of the current CS3 surface. Now to get into terms of the full-scale aircraft, use is made of the 4.6% scale factor of the experimental model. For now, it is assumed that the split flap effectiveness would not significantly change between sub-scale and full-scale. A full-size split flap width b_{sf} of 2.431 meters is then found. It should explicitly be noted here that this is just a first order estimation of the required split flap size. Based on the discussion of varying Reynolds number and the sensitivity, such a split flap is probably a conservative estimate. More elaborate full-scale split flap testing and simulations have to be performed for an optimal final split flap sizing, for which this split flap geometry could be a good starting point.

The final split flap geometry applied on a plain Flying V model is presented in figure 6.12. Here, the surfaces in red represent the split flaps, of which the left wing part has been deflected to the maximum of $\delta_{sf} = 60^\circ$.

6.2.2. Varying maximum split flap deflection

The previous results are under the assumption that it is possible to create a split flap with a maximum deflection $\delta_{sf_{max}}$ of 60° . Considering that it might be impossible to create such large deflections due to structural or complexity issues, the resulting size is investigated for smaller maximum values of $\delta_{sf_{max}}$. This will show the sensitivity of the split flap width with set $\delta_{sf_{max}}$. The results are presented in figure 6.13, where the required sub-scale split flap width is calculated for various values of maximum attainable split flap deflection. A $\delta_{sf_{max}}$ of 10 degrees is not included here, as it would lead to an infeasible required width. A clear parabolic relation can be seen, which is due to the relation of the surface area with the width (see equation (3.16)).

Looking at the tables in section 6.1.1, there is no need for high roll power during the situations where high yaw power is required. On top of this, as the split flap is only used for yaw on one side of the wing, it is envisioned that the flap on the other side can aid in creating roll power through mutual upwards or downwards deflection. Additionally, it is shown in section 5.4.2 that when used in split mode, the flaps can be rotated globally to potentially provide both yaw and roll. Figure 6.13 effectively shows that split flaps do not have to be of an unattainable large size to gain enough yaw power for directional control certification. Judging on the fact that the current CS3 surface is about 220mm wide, the designer might choose to fully replace this CS3 surface with split flaps. This would only require a $\delta_{sf_{max}}$ of about 30° . Compared to a case of $\delta_{sf_{max}} = 60^\circ$ this can lead to structural benefits, as the flap panels and hinges would have to withstand a lower concentration of pressure forces. All in all, for the reasons provided above, it is concluded the split flaps are in fact a feasible solution for the aircraft yaw control problems.

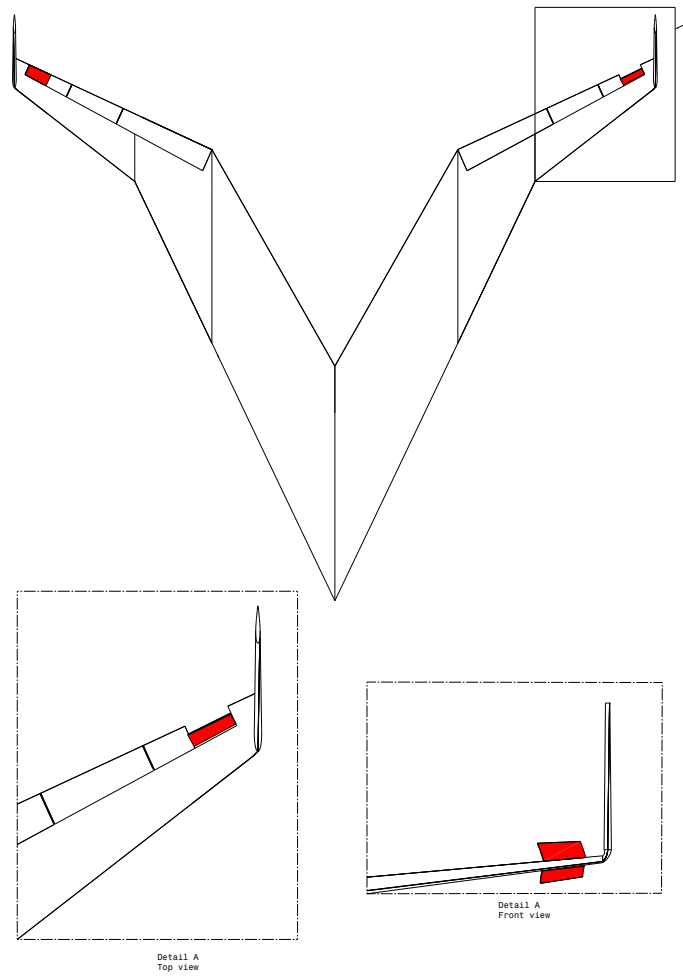


Figure 6.12: Graphic of the final split flap geometry ($b_{sf} = 111.87\text{mm}$) on the Flying V model, including an outboard detail. The surfaces in red represent the split flaps. The left wing split flap has been deflected to $\delta_{sf} = 60^\circ$.

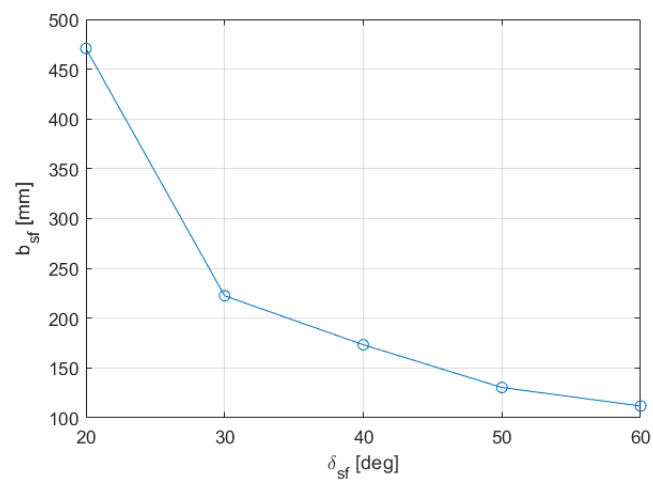


Figure 6.13: Maximum split flap deflection angle versus required (sub-scale) split flap width, for a required $C_{n_{sf}}$ of $2.4113\text{e-}3$ at $\alpha = 11.54^\circ$.

6.2.3. Projected final split flap performance

Now that the final split flap geometry is known, a quick look is taken at its performance in terms of created yaw and drag. This will be done for the recommended split flap geometry presented in figure 6.12. A direct comparison can be made with the current winglet rudders. The addition of the split flaps in terms of ΔC_n is presented in figure 6.14. Also the total projected yaw power of the winglet rudders for positive rudder deflection is presented. Here, it can be seen that at small angles of attack, the split flaps can provide an intermediate addition of yaw power. At $\alpha = 0^\circ$, the total yaw power can be increased by about 38.1% when the rudders and split flaps are used together. However, when the angle of attack is increased, the performance of the winglet rudders decreases drastically, while the split flaps remain relatively constant. This makes that at higher angles of attack, the split flaps can contribute heavily to the available yaw power. At $\alpha = 27.5^\circ$, the available yaw power is even increased by 85.5%.

As previously discussed, the increase in yaw power comes with some drawbacks. The most direct drawback is the large drag penalty associated with the yaw creation. The drag penalty of the split flaps is therefore also compared to the drag penalty of the winglet rudders. It can be seen from figure 6.15 that at low angles of attack, the drag penalty of maximum yaw creation is practically doubled compared to a case where only the winglet rudders are deployed. The yaw control increase of 38.1% is linked to a drag penalty increase of 89.3%, or 47.8 drag counts. At higher angles of attack, the drag penalty compared to the winglet rudders only increases further. The yaw control increase of 85.5% at $\alpha = 27.5^\circ$ will cause a drag penalty increase of 189.3%, or 45.0 drag counts. For now, it is assumed that the drag penalty does not have detrimental consequences for low-speed, low-power flight situations. However, an additional study should be performed on the implications this drag increase has on the available power of the aircraft.

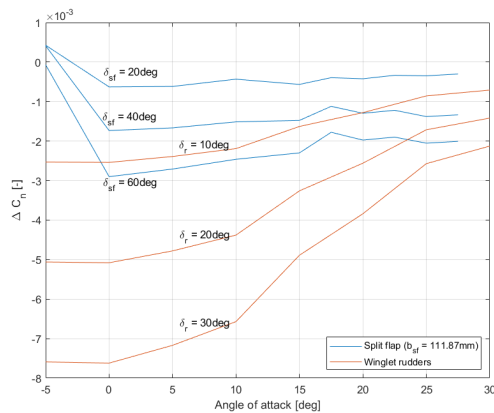


Figure 6.14: Projected final split flap yaw power in comparison with the winglet rudders

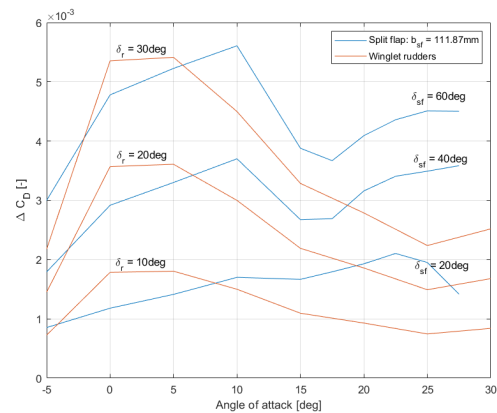


Figure 6.15: Projected final split flap drag penalty in comparison with the winglet rudders

As a final note, the large increase in drag also has one advantage to it. In order to decrease the ground roll at landing, the drag has to be increased, while decreasing the lift coefficient. During the ground roll, the split flaps can be deflected on both wings. Looking at the values in figure 6.15, this would increase the drag with about 95.6 drag counts. Based on the research by Erdinçler, it is expected that this would significantly help in decreasing the aircraft ground roll [33]. The exact decrease of the ground roll is not covered in this thesis however, as it is out of the scope of the study. If an investigation into the ground roll decrease is to be performed, the methods applied by Erdinçler can directly be used.

7

Conclusion and Recommendations

This thesis research consists of an experimental investigation into the addition of split flaps on the outboard wing of the Flying V, in order to identify the aerodynamic behaviour of such yaw devices. Wind tunnel tests have been performed in the OJF facility at the Delft University of Technology with the 4.6% sub-scale half-wing model of the Flying V. In addition, a simple mathematical model is created which was used to perform a conceptual sizing of the split flaps for the Flying V.

7.1. Conclusions

Split flaps on the outboard wing section can effectively increase the directional control over angles of attack between 0° and 30° , at the cost of a significant drag increase. Yaw capability is lost for $\alpha \leq -5^\circ$. The split flaps are most effective at $\alpha = 0$, where the largest yawing moment is created with only a small coupling in pitch and roll. Due to the creation of a leading edge vortex, a large shift is noticed when $\alpha \geq 15^\circ$. The upper split flap becomes ineffective, leading to a decrease in yaw control and an increase in pitch and roll. The minimum yaw effectiveness point is found around $\alpha = 17.5^\circ$.

The created yawing moment is linear with split flap deflection angle, where other aerodynamic properties are non-linear. A linear yaw control derivative was set up for SF10, SF15 and SF20. These all showed similar behaviour with angle of attack, where a maximum effectiveness decrease between 40% and 42% was found at $\alpha = 17.5^\circ$. The split flaps thus retain a substantial amount of yaw power at high angles of attack. Compared to the winglet rudder, which has a continuous effectiveness decrease of up to 70% with increasing angle of attack, it is concluded that the addition of split flaps can become specifically beneficial at higher angles of attack. In terms of yaw per unit surface area, no significant differences were found between the SF10, SF15 and SF20 split flap configurations.

The deflection of split flaps can have a significant effect on rudder yaw power for negative deflection angles. Such a combination of deflected split flap and inboard deflected rudder would not be seen in normal flight operations, as they produce counteracting yaw moments. No interaction was found for positive deflection angles. In terms of interaction with adjacent trailing edge surfaces, the split flaps can cause a significant decrease in created pitching and rolling moments for positive CS2 deflections. Differential deflection between the upper and lower flap can potentially decrease coupling in pitch and roll, while maintaining a certain level of yaw power. For $\alpha < 15$, the upper flap can be set at a slightly lower deflection angle than the lower flap. For $\alpha \geq 15$, the upper flap can be set at a higher deflection angle than the lower flap which could only slightly decrease the coupled moments. For $\alpha < 15$, the split flaps can also be globally rotated trailing edge down to mitigate adverse coupled moments while beneficially increasing the total created yaw. The investigation into global rotation also showed that the split flaps can be used in a dual functionality, as both yaw effector and

roll/pitch effector. To do this effectively, a combination of low to moderate split deflection angles and trailing edge down rotations are required.

It was found that sustaining a steady heading sideslip during crosswind conditions, as well as a 30° coordinated turn into the operative engine, were the most demanding certification specification in terms of directional control. An additional yaw coefficient of 2.4113e-3 has to be provided by the split flaps. Designs with a maximum deflection angle above 30° are deemed feasible, as this would maximally require only the replacement of the current CS3 surfaces. When a maximum deflection of 60° is set by the designer, a sub-scale split flap width of 111.87 mm is needed, which translates to a full-scale split flap of 2.431 m. Based on the sensitivity analysis and projected Reynolds effects, this is considered a conservative design for the full-scale Flying V. The recommended split flap width is considered a sufficient first order estimation of the required split flap size, which can be used as a starting point for followup studies into full-scale split flap integration and performance.

At $\alpha = 0^\circ$, the recommended design of 111.87 mm would increase the maximum directional control power of the Flying V by 38.1%, when both the rudders and split flaps are deployed. This will directly come at the cost of a 47.8 drag count penalty, an increase of 89.3% compared to just the rudders. At $\alpha = 27.5^\circ$, the maximum directional control power can be increased by 85.5%, while increasing the total drag penalty by 189.3%, or 45.0 drag counts.

7.2. Recommendations

The experimental study investigated the general effects of implementing split flaps on the Flying V in order to increase its directional control power. The effectiveness of the split flaps is significantly reduced due to the formation of a leading edge vortex. The addition of a fence, as described by van Uiter [27], should be investigated as method to postpone the point of minimum effectiveness.

The variation of split flap effectiveness with sideslip angle should be investigated, as the split flaps currently have a large hingeline sweep angle. It is proposed to make a full-wing sub-scale model of the Flying V, which can be tested for both varying angle of attack and angle of sideslip. Ruiz Garcia et al. additionally show that significant corrections have to be applied to the half-wing model data [31]. Future wind tunnel tests should therefore include more elaborate wind tunnel corrections, which is more straightforward for dual-wing setups than for half-wing setups.

Additionally, more combinations of split flap placement and deflection angle should be tested. Further inboard placements might be less influenced by the leading edge vortex, and could potentially outperform the current recommended split flaps in terms of created yaw for $\alpha \geq 15^\circ$, at the cost of a generally higher drag increment. Testing various combinations of upper and lower flap deflection with a higher resolution is needed to establish an optimal split flap configuration for each angle of attack.

Instead of additional sub-scale wind tunnel testing, it can also be chosen to investigate additional split flap tests through numerical methods such as Computational Fluid Dynamics (CFD). This can save a lot of time, as the wind tunnel testing is a meticulous and time-consuming process. Additionally, this can eliminate potential systematic errors caused by manual placement and volume behind the split flaps. Attention should be used here to correctly choose turbulence models and boundary conditions, as the split flaps cause large areas of separated flow, which can be difficult to model. If a proper numerical model was to be created, it would be easier to quantify full-scale split flap properties for various different split flap geometries, deflections and locations.

It is proposed that the flight mechanics calculations should be re-iterated with a higher-fidelity flight mechanics model, including a split flap control mode. Special care should be

taken on the requirements on the coordinated turn, the steady heading sideslip and the yaw manoeuvre into the operative engine. Also the consequences for longitudinal control, thrust levels and braking field length should be investigated. The recommended split flap size proposed in the present study can be used as starting point for an iteration of the split flap size. Variations in centre of gravity should be incorporated in the flight mechanics model. Additionally, Reynolds numbers effects on split flap performance and stability & control derivatives have been neglected during the research. A specific study should be performed to investigate and quantify the Reynolds number effects between sub-scale and full-scale Flying V quantities, which can then be used to give better full-scale performance estimations.

Lastly, in order to fully assess the feasibility of adding split flaps to the Flying V, an extensive integration study should be performed. This should include for instance structural feasibility, possible weight penalties, sub-system investigation into actuation and additional flight control design consequences. The effect of added vibrations due to split flap deflection should also be kept in mind. The integration study, together with the more elaborate flight mechanics study, should provide a complete frame in which the designer can decide to implement split flaps on the final Flying V.

Bibliography

- [1] J. D. Anderson, *The Airplane. A History of its Technology* (AIAA, 2002).
- [2] Boeing, *Boeing 747*, <https://www.boeing.com/commercial/747/> (2021), accessed on: 22-03-2021).
- [3] N. E. Antoine and I. M. Kroo, *Framework for aircraft conceptual design and environmental performance studies*, *AIAA Journal* **43**, 2100 (2005).
- [4] J. Benad, *Design of a commercial aircraft for high-subsonic speed as a flying wing configuration*, Report (Airbus, 2015).
- [5] R. M. Wood and S. X. S. Bauer, *Flying wings / flying fuselages*, in *39th AIAA Aerospace Sciences Meeting & Exhibit* (2001).
- [6] N. A. Johnson, *Effect of Winglet Integration and Rudder Deflection on Flying V Aerodynamic Characteristics*, Thesis, Delft University of Technology (2021).
- [7] T. Cappuyns, *Handling Qualities of a Flying V Configuration*, Thesis, Delft University of Technology (2019).
- [8] Delft University of Technology, *Flying-V*, <https://www.tudelft.nl/lr/flying-v> (2022), accessed on: 09-02-2022.
- [9] F. Faggiano, *Aerodynamic Design Optimization of a Flying V Aircraft*, Thesis, Delft University of Technology (2016).
- [10] M. Palermo, *The Longitudinal Static Stability and Control Characteristics of a Flying V Scaled Model: An Experimental and Numerical Investigation*, Thesis, Delft University of Technology (2019).
- [11] K. M. Dorsett and D. R. Mehl, *Innovative Control Effectors*, Report (Lockheed Martin Tactical Aircraft Systems, 1996).
- [12] U.S. Air Force and B. Garcia, *B-2 Spirit*, <https://www.af.mil/About-Us/Fact-Sheets/Display/Article/104482/b-2-spirit/> (2015), accessed on: 02-08-2022.
- [13] N. A. Ratnayake, E. R. Waggoner, and B. R. Taylor, *Lateral-directional parameter estimation on the x-48b aircraft using an abstracted, multi-objective effector model*, in *29th AIAA Applied Aerodynamics Conference* (2011).
- [14] S. Gudmundsson, *General aviation aircraft design: Applied Methods and Procedures* (Butterworth-Heinemann, 2013).
- [15] Y. J. Hasan, J. Flink, S. Freund, T. Klimmek, R. Kuchar, C. M. Liersch, G. Looye, E. Moerland, T. Pfeiffer, M. Schrader, and S. Zenkner, *Stability and control investigations in early stages of aircraft design*, in *2018 Applied Aerodynamics Conference* (2018).
- [16] R. Colgren and R. Loschke, *Effective design of highly maneuverable tailless aircraft*, *Journal of Aircraft* **45**, 1441 (2008).

- [17] P. Lochert, K. C. Huber, C. M. Liersch, and A. Schutte, *Control device studies for yaw control without vertical tail plane on a 53 degrees swept flying wing configuration*, in *2018 Applied Aerodynamics Conference* (2018).
- [18] P. Lochert, K. C. Huber, M. Ghoreyshi, and J. Allen, *Control device effectiveness studies of a 53 degrees swept flying wing configuration. experimental, computational, and modeling considerations*, *Aerospace Science and Technology* **93** (2019), ARTN 105319 10.1016/j.ast.2019.105319.
- [19] C. Breitsamter, *Wake vortex characteristics of transport aircraft*, *Progress in Aerospace Sciences* **47**, 89 (2011).
- [20] European Union Aviation Safety Agency, *Certification Specifications and Acceptable Means of Compliance for Large Aeroplanes CS-25 - Amendment 27*, (2021).
- [21] S. F. Hoerner, *Fluid-dynamic drag*, Hoerner fluid dynamics (1965).
- [22] M. V. Cook, *Flight dynamics principles: a linear systems approach to aircraft stability and control* (Butterworth-Heinemann, 2012).
- [23] J. S. Litt, Y. Liu, T. S. Sowers, A. K. Owen, and T.-H. Guo, *Validation of an integrated airframe and turbofan engine simulation for evaluation of propulsion control modes*, in *53rd AIAA Aerospace Sciences Meeting* (2015) p. 1476.
- [24] EASA, *TYPE-CERTIFICATE DATA SHEET No. EASA E.111 for Engine Trent XWB series engines*, Tech. Rep. (European Union Aviation Safety Agency, 2019).
- [25] Delft University of Technology, *Open Jet Facility*, <https://www.tudelft.nl/lr/organisatie/afdelingen/aerodynamics-wind-energy-flight-performance-and-propulsion/facilities/low-speed-wind-tunnels/open-jet-facility/> (2022), accessed on: 15-02-2022.
- [26] R. A. Viet, *Analysis of the flight characteristics of a highly swept cranked flying wing by means of an experimental test*, Thesis, Delft University of Technology (2019).
- [27] J. J. D. van Uiter, *Experimental Investigation into the Effect of Aerodynamic Add-ons on the Aerodynamic Characteristics of the Flying V*, Thesis, Delft University of Technology (2021).
- [28] B. Ewald, *Wind Tunnel Wall Corrections (la Correction des effets de paroi en soufflerie)*, Report (ADVISORY GROUP FOR AEROSPACE RESEARCH AND DEVELOPMENT NEUILLY-SUR-SEINE (FRANCE), 1998).
- [29] H. C. Garner, E. Rogers, W. Acum, and E. Maskell, *Subsonic wind tunnel wall corrections*, Report (ADVISORY GROUP FOR AEROSPACE RESEARCH AND DEVELOPMENT NEUILLY-SUR-SEINE (FRANCE), 1966).
- [30] J. B. Barlow, W. H. Rae, and A. Pope, *Low-speed wind tunnel testing* (John Wiley & sons, 1999).
- [31] A. Ruiz Garcia, M. Brown, D. Atherstone, N. v. Arnhem, and R. Vos, *Aerodynamic model identification of the flying v from sub-scale flight test data*, in *AIAA SCITECH 2022 Forum* (2022) p. 0713.
- [32] A. Ruiz Garcia, *Aerodynamic Model Identification of the Flying V from Wind Tunnel Data*, Thesis, Delft University of Technology (2019).

- [33] O. Erdinçler, *Aerodynamic and Performance Analysis of Ground Spoilers on the Flying V*, Thesis, Delft University of Technology (2021).
- [34] S. A. van Empelen, *Engine Integration of the Flying V Quantification of Engine Integration Effects using Wind Tunnel Experiments*, Thesis, Delft University of Technology (2020).
- [35] F. M. Dekking, C. Kraaikamp, H. P. Lopuhaä, and L. E. Meester, *A Modern Introduction to Probability and Statistics: Understanding why and how* (Springer Science & Business Media, 2005).
- [36] J. Mulder, W. van Staveren, J. van der Vaart, E. de Weerdt, C. de Visser, A. in 't Veld, and E. Mooij, *Flight Dynamics - Lecture Notes*, Faculty of Aerospace Engineering, Delft University of Technology (2013).
- [37] S. van Overeem, *Modelling, Control, and Handling Quality Analysis of the Flying-V*, Thesis, Delft University of Technology (2022).
- [38] E. Obert, *Aerodynamic Design of Transport Aircraft* (IOS Press, The Netherlands, 2009).
- [39] B. Rubio Pascual, *Engine-Airframe Integration for the Flying-V*, Thesis, Delft University of Technology (2018).
- [40] W. J. Oosterom, *Flying-V Family Design*, Thesis, Delft University of Technology (2021).
- [41] F. Jiang, M. An, and S. Mysko, *Computational analysis of aileron effectiveness characteristics on an advanced wing*, in *18th Applied Aerodynamics Conference* (2000) p. 4324.
- [42] J. Xie, I. Chakraborty, S. I. Briceno, and D. N. Mavris, *Development of a certification module for early aircraft design*, in *AIAA Aviation 2019 Forum* (2019) p. 3576.
- [43] Y. Tian, S. Liu, L. Liu, and P. Xiang, *Optimization of international roughness index model parameters for sustainable runway*, *Sustainability* **13**, 2184 (2021).
- [44] M. Drela and H. Youngren, *AVL 3.36 User Primer*, (2017).



Test matrix summary

The table on the following page summarises the used test settings and combinations.

Table A.1: Summary of the test matrix used throughout the wind tunnel campaigns

Configuration	δ_{sf} (upper/lower) [°]	V [m/s]	α [°]	δ_r [%]	δ_{CS2} [%]	δ_{CS3} [%]	Tufts
clean	-	[15, 20, 25, 30]	[-10:35:2.5]	-	-	-	-
clean	-	20	[-10, -5, 0, 5, 10, 15, 17.5, 20, 22.5, 25, 27.5, 30]	[-100, 0, 100]	[-100, 0, 100]	-	-
SF15	[20/20, 40/40, 60/60]	[15, 20, 25, 30]	[-10:35:2.5]	-	-	-	-
SF15	[10/10, 20/20, 30/30, 40/40, 50/50, 60/60]	20	[-10, -5, 0, 5, 10, 15, 17.5, 20, 22.5, 25, 27.5, 30]	[-100, 0, 100]	[-100, 0, 100]	-	-
SF10	[10/10, 20/20, 30/30, 40/40, 50/50, 60/60]	20	[-10, -5, 0, 5, 10, 15, 17.5, 20, 22.5, 25, 27.5, 30]	[-100, 0, 100]	[-100, 0, 100]	-	-
SF20	[10/10, 20/20, 30/30, 40/40, 50/50, 60/60]	20	[-10, -5, 0, 5, 10, 15, 17.5, 20, 22.5, 25, 27.5, 30]	[-100, 0, 100]	[-100, 0, 100]	-	-
SF22	[10/10, 20/20, 40/40, 60/60]	20	[-10, -5, 0, 5, 10, 15, 17.5, 20, 22.5, 25, 27.5, 30]	-	-	[-100, -50, 0, 50, 100]	-
SF15	[(0, 20, 40, 60) / (0, 20, 40, 60)]	20	[-10, -5, 0, 5, 10, 15, 17.5, 20, 22.5, 25, 27.5, 30]	-	-	-	-
clean	-	20	[-10:30:2.5]	-	-	-	yes
SF15	[20/20, 40/40, 60/60]	20	[-10:30:2.5]	-	-	-	yes